DEVELOPMENT OF AN IN-CYLINDER HEAT TRANSFER MODEL WITH VARIABLE DENSITY EFFECTS ON THERMAL BOUNDARY LAYERS

by

Hee Jun Park

A dissertation submitted in partial fulfillment
of the requirements for the degree of
Doctor of Philosophy
(Mechanical Engineering)
in The university of the Michigan
2009

Doctoral Committee:

Professor Dionissios N. Assanis, Co-Chair
Assistant Professor Dohoy Jung, Co-Chair
Professor Margaret S. Wooldridge
Assistant Professor Matthias Ihme
Assistant Research Scientist Aristotelis Babajimopoulos
Visiting Research Scientist George A. Lavoie

DEDICATION

To my parents,

To my wife and son

ACKNOWLEDGEMENTS

I would like to express sincere appreciation to Professor Assanis for his encouragement, guidance and support. Thanks to him, I had the valuable opportunity to study in the W.E Lay Automotive Laboratory at the University of the Michigan. It is a great honor for me to study in W.E Lay Automotive Laboratory and achieve a doctoral degree. I would also like to express deep appreciation to Professor Dohoy Jung. He guided me with valuable advice through this research.

I also truly appreciate my dissertation committee, Professor Wooldridge and Professor Ihme for their helpful advices.

I also express special appreciation to Dr. Babajimopoulos and Dr. Lavoie. Their advice was truly valuable for me to complete this research.

This research has been supported by a University Consortium on Low Temperature Combustion for High-Efficiency, Ultra-low Emission Engines, funded by Department of Energy.

PREFACE

This theoretical and numerical study addresses in-cylinder heat transfer modeling and its applications to a spark-ignition engine and a Homogeneous Charge Compression Ignition (HCCI) engine. Accurate prediction of in-cylinder heat transfer is critical because engine operating parameters such as in-cylinder temperature and pressure are affected by heat transfer. To improve the prediction of heat transfer, variable density effects are introduced into the new heat transfer model which is named VDHT (Variable Density Heat Transfer) model. The density, dynamic viscosity variation and variable density effects on turbulent Prandtl number and eddy viscosity ratio variation in thermal boundary layers are employed in the VDHT model with a power-law approximation. This approximation yields a model constant. The basis of the VDHT model is thoroughly investigated through quantification of critical parameter effects on in-cylinder heat transfer modeling. The model constant of VDHT model is found by matching experimental heat flux measurements in a spark-ignition engine. The VDHT model with this constant is then applied to an HCCI engine and the effect of turbulence modeling on thermal conditions is investigated through the analysis of the probability density function of the charge temperature.

TABLE OF CONTENTS

LIST OF TABLES

LIST OF FIGURES

LIST OF ABBREVIATIONS

ATDC	After Top Dead Center
BTDC	Before Top Dead Center
VDHT	Variable Density Heat Transfer Model with laminar thermal conductivity effects and turbulent Prandtl number variation
EVO	Exhaust Valve Opening
IHT	Incompressible Heat Transfer Model without laminar thermal conductivity effects and turbulent Prandtl number variation
IVC	Intake Valve Closing
Pr	Prandtl number
k	Thermal conductivity
q	Heat flux
u^*	Frictional velocity
y	Wall normal direction
y^+	Dimensionless turbulence wall unit=yu^*/v

μ	Laminar dynamic viscosity
v	Laminar kinematic viscosity
v_t	Eddy kinematic viscosity
v^+	Eddy viscosity ratio = v_t / v

Subscript

c	Denotes height of cell adjacent to wall
w	Denotes wall quantities

CHAPTER 1

INTRODUCTION

1.1 Background

Heat transfer is one of the important issues in the study of internal combustion engines because it affects critical engine operating parameters such as in-cylinder temperature and pressure. However, analysis and modeling of engine heat transfer are among the most complex engineering subjects because of the turbulence in the cylinder charges, the combustion process and piston motion within a combustion chamber of complex shape. All of these factors contribute to strong unsteadiness and local changes in in-cylinder heat transfer. Therefore, the details of turbulence, combustion and piston motion must be investigated before discussing the development of in-cylinder heat transfer modeling.

Turbulence develops in the in-cylinder charge under typical operating conditions of internal combustion engines as the Reynolds number is sufficiently high. Furthermore, when the air-fuel mixture is introduced into the cylinder chamber, complex motions such as tumbling and swirling flows are created. Due to the unsteadiness and local changes caused by turbulence, tumbling, swirling motions and interactions with valve motions, engine heat transfer undergoes unsteadiness and local changes.

The combustion process also has a significant impact on engine heat transfer because it increases density, pressure and temperature in the cylinder rapidly. In particular, in spark ignition engines, flame propagation separates the cylinder charge into burning and unburned zones, thus creating a strong local change in heat transfer. Furthermore, the flame interacts with turbulence flows, which also adds to the complexity of engine heat transfer.

The compression and expansion of the piston affects in-cylinder heat transfer as well. Furthermore, the position of the piston at ignition has strong effects on combustion processes. Turbulence is also affected by piston speed because the Reynolds number is directly proportional to piston speed. Thus understanding these influential factors is a prerequisite to modeling of engine heat transfer.

Heat transfer modeling is an important issue in the numerical study of internal combustion engines. Inaccurate predictions of heat transfer cause inaccurate predictions of thermal conditions and inaccurate predictions of cylinder thermal conditions have adverse effects on the predictions of combustion processes and engine performance. Therefore, the accurate prediction of heat transfer is a prerequisite for an accurate prediction of engine performance.

Furthermore, heat transfer has a strong influence on exhaust emissions because temperature has a strong effect on emissions [1-7]. For example, the formation of nitric oxides (NO_x) has an exponential dependence on temperature. A reduction in the peak combustion temperature of 25-50 K can halve the NO_x emissions [7]. Furthermore, the wall temperature is important for emissions because in spark ignition engines, NO_x

emissions increase significantly with increasing surface temperatures [1]. Therefore, the accurate prediction of heat transfer is important for the accurate prediction of emissions.

In Homogeneous Charge Compression Ignition (HCCI) engines, the accurate prediction of thermal conditions is critical because thermal conditions strongly affect the combustion process [8 - 11]. For example, the wall temperature strongly influences the heat-release rate. Specifically, the enhanced thermal stratification caused by the lowered wall temperatures decreases the peak heat release rate significantly [9]. Another experimental study [10] shows that the increase of thermal stratification delays the pressure rise rates during combustion. As discussed in the study of Dec and Sjöberg [12], intake temperatures have strong influences on CO (Carbon Oxide) emissions in an HCCI engine. In their study, as intake temperatures are increased, the CO emissions are decreased significantly. For these reasons, reliable heat transfer models are the basis for the accurate prediction of engine performance and emissions in HCCI engines.

In engine design, the analysis of heat transfer is also important. For example, accurate prediction of heat flux is essential for the analysis of thermal stress limits for cylinder materials. In particular, the accurate prediction of heat flux is also useful for the determination of the cylinder chamber geometry to minimize emissions.

1.2 Review of in-cylinder heat transfer models

In-cylinder heat transfer models were categorized as global, zonal, one-dimensional and multi-dimensional by Borman and Nishiwaki [13], based on their spatial resolution. This categorization is based on the core region resolution. In strict meaning,

both one-dimensional and multi-dimensional models by Borman and Nishiwaki are one-dimensional models because a simplified one-dimensional equation of the thermal boundary layer is solved for these models. Therefore, in this study, one-dimensional models and multi-dimensional models by Borman and Nishiwaki definition are referred to as one-dimensional heat transfer models.

Global [14-21] and zonal models [22-24] are empirical correlations with dimensionless numbers as parameters. Global and zonal models use correlations to calculate the overall heat transfer coefficient *h*.

To investigate the procedure of heat flux calculation in global and zonal models, the representative correlation and heat flux equation are examined.

$$NU \equiv {hl}/{k} = C\,\mathrm{Re}^{n} \tag{1.1}$$

$$q = h(T_g - T_w) \tag{1.2}$$

Eq. (1.1) shows the typical correlation in global heat transfer models, where NU denotes the Nusselt number, which is non-dimensional and represents the heat transfer coefficient divided by the thermal conductivity *k* and the length scale *l*. Re denotes the Reynolds number and C and n denote model constants. From the known model constants and the Reynolds number, an overall heat transfer coefficient can be obtained from Eq. (1.1).

Eq. (1.2) is the heat flux equation for global and zonal models. Heat flux q is calculated from the overall heat transfer coefficient h, the temperature of the global core region T_g and the wall temperature T_w.

Figure 1. 1 shows a schematic of a global heat transfer model and Figure 1. 2 shows a schematic of a two-zone heat transfer model as an example of zonal heat transfer models. In two-zonal models [22, 23], the cylinder was divided into an unburned and a burned zone. Each unburned and burned zone has its own history of the heat transfer coefficient for the calculation of heat flux of each zone. Therefore, this model can consider the effects of heat transfer variation caused by the flame propagation.

However, these global and zonal models do not yield specific local information of heat transfer. Moreover, this type of model requires ad-hoc parameter tuning and is strongly dependent on empirical constants. Thus their applicability is limited to the operating range from which the correlation is derived. Because the detailed spatial variation of heat-flux, temperature and flow field is not available from these approaches, these models are applied to engineering applications that require only global quantities.

In one-dimensional heat transfer models [25-31], the wall heat flux is calculated directly by solving an energy equation of thermal boundary layers without using the heat transfer coefficient. Figure 1. 3 shows a schematic of one-dimensional heat transfer models with a global core zone. For one-dimensional heat transfer models, the near-wall region and the core region are distinguished. For the near-wall region, the elaborated solution based on the assumptions of thermal boundary layers is calculated. The core region is considered a global region with uniform properties without spatial distinction or multi-dimensional core regions. Compared to global and zonal models, one-dimensional heat transfer models can consider the physics of thermal boundary layers because an energy equation of thermal boundary layers is directly solved with modeling assumptions.

An interesting approach in heat transfer modeling was made by a two-zone HCCI model [32], which is based on a boundary layer heat transfer model [33]. This two-zone model calculated the overall heat transfer coefficient based on the energy equation of thermal boundary layers unlike previous approaches where the overall heat transfer coefficient was obtained from empirical correlations.

In internal combustion engine flows, the core region cannot be considered globally because there are local changes in the core region due to turbulence, swirling, tumbling motions and combustion effects with the flame propagation. Therefore, one-dimensional heat transfer models with multi-dimensional core regions are required for a detailed and an advanced analysis of heat transfer.

In multi-dimensional approaches, the three dimensional governing equations of mass, momentum and energy conservation are solved for core regions. For near-wall regions, two approaches are available. The first one is to solve wall-layer regions with full governing equations. In other words, without distinction between core regions and near-wall regions, the full governing equations of whole regions are solved. In DNS (Direct numerical Simulation), the full governing equations are solved without any modeling. To solve near-wall regions without modeling, all turbulent length and time scales need to be resolved. As is well known, a huge amount of calculation time is required to resolve all turbulent length and time scales for practical high Reynolds number flows. Because of the huge amount of computational cost at near-wall regions, it is not practical to solve the wall-layer without modeling for turbulent flows.

To bypass the huge amount of computational cost at near-wall region, a zonal approach was adopted by Jennings and Morel [34] where the core region is solved using full governing equation and the wall-layer is solved using two-dimensional parabolized governing equations. However, this approach has the disadvantage of additional computational effort for wall-layer solving and the difficulty of matching solutions in wall regions to the outer-layer solutions. At high Reynolds number flows, this approach still requires a huge amount of computational cost. Therefore, this method is only applicable to low Reynolds number flows.

The second approach is the wall-layer modeling. Figure 1. 4 shows the schematic of a one-dimensional heat transfer model with multi-dimensional core regions. For the near-wall layer region, a heat flux solution based on the assumptions of thermal boundary layers is used without solving the full governing equation numerically. The representative wall-layer modeling is the law of the wall. The law of the wall was developed based on experimental results and dimensional analysis for the steady, incompressible and fully-developed turbulent flows. The near-wall region consists of viscous sub-layers and log-layers. Therefore, without solving near wall-regions, the solutions of viscous sub-layers and log-layers are used to avoid the huge amount of computational cost of the near-wall resolution. However, this law of the wall was derived from incompressible, steady, fully-developed turbulent flows. Therefore, the law of the wall has inherent drawbacks and limits when this wall treatment is applied to internal combustion engine flows that have wall-bounded turbulent flows with strong density variable effects caused by temperature variation.

One of the main issues in in-cylinder heat transfer modeling is to improve the heat flux wall-layer modeling from the classical wall-layer modeling based on the assumptions of incompressible flows.

Each category of in-cylinder heat transfer model has its own role to play. In fact, heat transfer correlations are used as a simplified model for practical application where time-consuming detailed approaches are not required. Multi-zone approaches can be used as a compromise between global and one-dimensional heat transfer models. However, only one-dimensional heat transfer models with multi-dimensional core regions offer the detailed spatial information of heat transfer. The results of one-dimensional heat transfer models with multi-dimensional core regions can be used as a good comparison to analyze experiment data and its parametric study can be used for advanced heat transfer correlations.

In particular, the detailed spatial information of thermal conditions is important because details of emissions, thermal stresses distribution can be investigated based on detailed spatial thermal information. Furthermore, for an HCCI engine, the thermal distribution itself has a strong influence on combustion processes [9]. Thermal stratification has strong effects on the peak heat-release rates and knocking intensity in an HCCI engine. Therefore, a reliable heat transfer model is a prerequisite for the study of HCCI engines. In this study, a one-dimensional in-cylinder heat transfer model is developed to improve the predictions of in-cylinder heat transfer and the resulting temperature field.

The details of in-cylinder heat transfer models based on the thermal boundary layer equation are discussed. Essentially, in-cylinder heat transfer modeling is the wall-layer modeling for thermal boundary layers. As discussed before, the classical law of the wall of incompressible flows is not applicable to internal combustion engine flows because of the disparity between incompressible boundary layers and in-cylinder boundary layers.

Compressible turbulent boundary layers can be divided into two categories: turbulent boundary layers with compressibility effects and turbulent boundary layers with variable density effects. The effects associated with the density change of the fluid in response to pressure change caused by high Mach number are compressibility effects and the effects associated with the density change of the fluid from temperature change are variable density effects.

Unlike the classical incompressible boundary layers, in-cylinder boundary layers have strong thermal effects which involve variable density effects on boundary layers.

The importance of variable density effects on turbulent boundary layers were discussed in previous studies [7, 35, 36]. Nijeweme et al. [7] emphasized that variable density effects of the boundary layer are important parameters, these effects needs to be considered for in-cylinder heat transfer modeling. DNS results [35] show variable density effects change the law of the wall of compressible boundary layers. White and Christoph show that variable density effects change the law of the wall of compressible boundary layers using momentum integral methods [36].

Various attempts have been made to develop in-cylinder heat transfer models. The earlier studies focused on the laminar thermal boundary layers [25-27] derived heat transfer equations for laminar thermal boundary layers under time dependent pressure with simplified assumptions of isentropic compression and thermal conductivity proportional to temperature. In this ideal case, the wall heat loss is the summation of thermal energy defect in the boundary layers and the work done in compressing boundary layers. The thermal energy defect means the energy stored in thermal displacement thickness which is defined as the change in the thermal boundary layer thickness by compression. However, these laminar heat transfer model is not applicable to real turbulent engine flows.

Yang and Martin [28] proposed an improved thermal boundary layer model by employing turbulent conductivity k_t. In their model, a linearized thermal boundary layer equation is solved using the empirical correlation for turbulent thermal conductivity. The wall-unit correlations based on incompressible flows are adopted for this model. This result was compared to the motored experimental data and showed good performance. However, their turbulent conductivity involves the characteristic length which is the function of friction velocity u^*. Therefore, their solution is strongly dependent on the choice of u^*. By tuning u^*, the results of this model were matched to experimental data. Furthermore, Han and Reitz [31] showed the effect of this unsteady solution is negligible for the firing conditions of a spark ignition engine.

The heat transfer model built in KIVA 3V [30] is most widely used. This model considers the turbulent conductivity effects. However, this model is based on the assumptions of incompressible flows. Density and viscosity are assumed to be constant

across thermal boundary layers. Laminar thermal conductivity and turbulent Prandtl number variation are not considered. The Han and Reitz [31] model considered density variation. On the other hand, this model assumes kinematic viscosity is constant and adopts the wall unit correlations of incompressible flows and curve fitting of wall unit function shows a step increase, which denotes the wall unit function is arbitrarily tuned. In other words, there is a contradiction because one part adopts partial variable density effects and other parts adopt assumptions of incompressible flows, which is also pointed out by the previous study [7]. Thus, full variable density effects on thermal boundary layers are not employed thoroughly. Table 1. 1 summarizes the drawbacks of the previous heat transfer models.

Table 1. 1 Summary of assumptions of previous heat transfer models

	KIVA 3V	Han and Reitz [31]
Density	Constant	Variable
Kinematic Viscosity	Constant	Constant
Law of the wall	Incompressible flow correlation	Incompressible flow correlation with wrong curve-fitting

To date, full variable density effects on in-cylinder heat transfer modeling have not been employed and the quantitative importance of variable density effects has not been investigated. Furthermore, heat transfer modeling is expected to be affected by

turbulence modeling because a heat flux equation of heat transfer modeling is a function of turbulent quantities. However, the effects of turbulence modeling on engine heat transfer and thermal conditions have not been investigated.

HCCI combustion processes are significantly influenced by thermal conditions. Therefore, heat transfer has a direct effect on HCCI combustion. However, the effects of one-dimensional heat transfer modeling with multi-dimensional core regions on the prediction of HCCI combustion processes have not been examined.

In this study, variable density effects on in-cylinder heat transfer modeling, turbulence modeling effects on the prediction of heat transfer and in-cylinder heat transfer modeling effects on the prediction of HCCI combustion process are investigated. As will be shown, these issues can be investigated through the development of an improved heat transfer model and application of this model to an HCCI combustion engine.

To develop advanced in-cylinder heat transfer models, various influential factors on heat transfer need to be investigated, as shown in Figure 1. 5. First, it should be noticed that various phenomena such as combustion, turbulent motions and piston motions are present in internal combustion engines. For turbulent motions, a reliable turbulence model needs to be adopted for the solution of turbulence variables. For turbulent combustion, a reliable turbulent combustion model needs to be adopted. Additionally, the grid and time step can have an effect on heat transfer predictions. Therefore, grid and time-step independency need to be investigated for heat transfer

predictions. The effects of operation range from motoring to high-load firing conditions on heat transfer predictions need to be examined.

Ultimately, an improved in-cylinder heat transfer model needs to be developed and validated against a wide range of experimental measurements with the combination of turbulence modeling, combustion modeling and grid and time-step independency study. In this study, an advanced heat transfer model is presented by employing variable density effects on kinematic viscosity, turbulent Prandtl number and eddy viscosity ratio variation using a power law approximation. This model is compared to the heat transfer model built in KIVA 3V which is based on the assumptions of incompressible flows.

1.3 Objectives and Study Overview

The objective of this study is the improvement of predictions of in-cylinder heat transfer by developing an advanced heat transfer model. To develop an advanced heat transfer model, the physics of in-cylinder thermal boundary layers need to be thoroughly investigated. Through the sensitivity studies of parameter effects, the details of in-cylinder thermal boundary layers are examined. Based on this analysis, the new heat transfer model was developed. This new heat transfer model is named as VDHT (Variable Density Heat Transfer) model [37].

The model constant of VDHT model is determined by applying this heat transfer model to a spark-ignition engine. Subsequently, the VDHT model with the model constant determined from a spark-ignition engine is applied to an HCCI engine and the effects of heat transfer models on the prediction of an HCCI engine are investigated in

detail. The effects of turbulence models are also investigated by the analysis of probability density function of the charge temperature and the prediction of heat transfer.

The detailed study overview is summarized as follows.

Turbulence and Combustion modeling

Before discussing in-cylinder heat transfer modeling, turbulence modeling, wall-layer modeling and turbulent combustion models need to be reviewed because heat transfer modeling is closely related to turbulence modeling, wall-layer modeling and turbulent combustion models. A reliable turbulence model and combustion model are necessary as prerequisites for heat transfer modeling study.

The concept of wall-layer modeling is also explained because the concept of wall-layer modeling is fundamental to the heat transfer modeling.

Development of an advanced in-cylinder heat transfer model

In-cylinder heat transfer modeling is closely related to the physics of thermal boundary layers. Various heat transfer models can be developed based on whether physical parameters are considered or not. For example, the conductivity and turbulent Prandtl number variation inside thermal boundary layers are important parameters. In particular, variable density effects on thermal boundary layers are important issues in in-cylinder heat transfer modeling as discussed by previous studies [7, 31]. First, the heat transfer model built in KIVA3V is investigated through the examination of model derivation and its assumptions. And then, the VDHT model is derived.

Although variable density effects are important parameters in in-cylinder heat transfer modeling, variable density effects on thermal boundary layers have not been investigated thoroughly before this study. Based on physics of thermal boundary layers, it is found that variable density effects are present in density, viscosity, turbulent Prandtl number and eddy viscosity variation. In the present study, full variable density effects on thermal boundary layers are employed using a power law assumption based on dimensional analysis. Fundamentally, this VDHT model is an innovatively different model compared to previous heat transfer models. Nevertheless, this model employs a constant, which is inevitably required to model variable density effects on thermal boundary layers. This modeling approach with a model constant is similar to the turbulence modeling in turbulent k-ε models where model constants were adopted for eddy viscosity modeling.

Quantification of parameter effects on in-cylinder heat transfer modeling

Although effects of laminar conductivity, turbulent Prandtl number variation and variable density are main factors in in-cylinder heat transfer modeling, systematic and quantified analysis is not available. To quantify the effects of laminar thermal conductivity and turbulent Prandtl number variation, three in-cylinder heat transfer models based on the assumptions of incompressible flows are defined.

The first model does not consider laminar thermal conductivity and turbulent Prandtl number variation. This model is named as IHT (Incompressible Heat Transfer model without laminar thermal conductivity and turbulent Prandtl number variation)

model. The second model considers only laminar thermal conductivity and is named as Intermediate I model. The third model considers both laminar thermal conductivity and turbulent Prandtl number variation and is named as Intermediate II model. By comparing IHT model, Intermediate I and Intermediate II model, the effects of laminar thermal conductivity and turbulent Prandtl number variation can be studied. The heat transfer model built in KIVA3V is compared to these three models and the results are discussed.

To quantify the effects of density variation and dynamic viscosity variation, two in-cylinder heat transfer models are defined. The first model is defined as Intermediate II model with density variation and is named as Intermediate III model. The second model is defined as Intermediate II model with dynamic viscosity variation and is named as Intermediate IV model. By comparing Intermediate III, Intermediate IV model and Intermediate II model, variable density effects on density and dynamic viscosity variation can be studied. The effects of conductivity, turbulent Prandtl number variation and density and dynamic viscosity variation are summarized through classification and quantifications of in-cylinder heat transfer models.

These sensitivity studies of various parameters clearly reveal the quantitative importance of effects of laminar thermal conductivity, density variation and dynamic viscosity variation. Furthermore, sensitivity studies of various parameters offer the quantitative information of heat flux predicted by various heat transfer models. In particular, quantification of parameters effects on in-cylinder heat transfer modeling offers the basis of VDHT model.

Determination of the VDHT model constant

To determine the model constant in VDHT model, VDHT model is applied to premixed spark ignition experimental data. The heat transfer model built in KIVA 3V is also applied to this spark ignition engine for the comparison with VDHT model. Heat flux measurements of four test conditions of the spark ignition engine are used for this study.

For premixed combustion, the CFM 2-b model is chosen among various coherent flamelet turbulent combustion models and the RNG k-ε model is adopted in this study because these models show better agreement with experimental data compared to other models. Through error analysis, the model constant of VDHT model is determined and the details of the heat flux predicted by each heat transfer are discussed.

Application to an HCCI engine

For HCCI engines, thermal conditions are critical in combustion processes because chemical kinetics has dominant influences on HCCI combustion. Therefore, heat transfer has strong effects on combustion processes. A reliable heat transfer model is essential for accurate predictions of HCCI combustion process. However, the detailed numerical study of heat transfer effects on HCCI engines is not available.

First, VDHT model and the heat transfer model built in KIVA 3V are applied to motoring conditions of an HCCI engine because accurate predictions of motoring conditions are fundamentals for upcoming ignition and combustion processes. The effects

of heat transfer and turbulence models on the predictions of pressure trace, temperature are investigated for three operating conditions based on different coolant temperatures and swirling conditions. Through the comparisons of probability density function of temperature, the effects of heat transfer and turbulence models on thermal stratification are investigated.

Finally, heat transfer models are applied to firing conditions and the details of effects of heat transfer modeling on HCCI combustion processes are investigated through the comparisons of the predicted pressure trace, heat flux and mean charge temperature by the VDHT model and the heat transfer model built in KIVA 3V.

CHAPTER 2

TURBULENCE AND COMBUSTION MODELING

2.1 Turbulence modeling

Turbulent modeling is required to solve practical engineering flows in high Reynolds number. Turbulent flows have a wide range of length scales from mean flows to the smallest scale which is known as the Kolmogorov scale. To solve turbulent flows thoroughly, all length scales as well as time scales should be resolved.

Numerical approaches in turbulent flows can be divided into three categories; Direct Numerical Simulation (DNS), Large Eddy Simulation (LES) and Reynolds Averaged Navier-Stokes (RANS) [38]. DNS resolves all turbulent scales without any modeling. However, as Reynolds number increases, the ratio of the Kolmogorov scale to large scales is increased. The required grid resolutions are exponentially proportional to the Reynolds number. Therefore, in high Reynolds number flows, even for moderate Reynolds number flows, the computational requirement of DNS is very intensive so that the application of DNS to real engineering turbulent flows is impractical. The application of DNS is limited to low Reynolds number flows and used for academic purposes.

As an alternative, LES has been used to reduce the amount of computational time because this approach resolves only large scale flows with modeling of small scale flows.

The philosophy of LES comes from the distinction between turbulent small scales and large scales. According to experimental analysis and turbulent physics, turbulent small scales have universal structures while turbulent large scales are specific to boundary conditions. Therefore, small scales can be modeled, while large scales should be solved. In LES, filtered governing equations are used. This filtering operation is a low-pass filtering. In other words, low wave number quantities which are related to large scale flows are maintained while high wave number quantities which are related to small scale flows are suppressed or set to zero. This filtering operation on governing equations introduces unknown filtered turbulent stress terms, thus creating closure problems for the governing equations. Turbulence modeling in LES is to solve this closure problem, which results from unknown filtered turbulent stresses. This LES resolves the unsteady three dimensional large scales in turbulent flows. Therefore, the performance of LES is expected to be prominently better for unsteady, complex turbulent flows. However, rigorous LES is still expensive because of near-wall layer resolution. Therefore, rigorous LES is not applicable to high Reynolds number flows with near-wall layers. Furthermore, applications of DNS and LES to complex geometry and moving boundary layers are not developed well. Therefore, the application and validation of LES to internal engine flows are still not developed well.

To avoid this huge amount of computational requirement, in classical engineering applications, RANS has been widely used. In RANS approaches, governing equations are ensemble-averaged. Therefore, RANS approaches directly solve mean flows. By introducing ensemble-average operation into nonlinear terms (convection terms) of the Navier-Stokes equation, unknown Reynolds stress terms are introduced, thus making

governing equations closure problems. Turbulence modeling in RANS approaches is required to solve this closure problem, which results from unknown Reynolds stresses. Based on the method for modeling Reynolds stress terms, the turbulence modeling can be classified. The most popular turbulence models are eddy viscosity models.

The representative eddy viscosity models are algebraic, one-equation and two-equation models. Among various models, k-ε models are the most widely used. In k-ε models, the transportation of turbulent kinetic energy k and dissipation rate ε are solved and the eddy viscosity is calculated from k and ε. Various engineering problems are applied with this type of models. For the numerical simulation of internal combustion engine, the standard k-ε models and the RNG k-ε model are widely used.

For RANS approaches, core-regions are solved using full mass, momentum, energy and species equations with turbulence modeling. One the other hand, wall-layers are modeled with the solution of one-dimensional boundary layer equation to bypass the huge amount of computational cost.

The details of wall-layer modeling and the previous study of turbulence modeling for the simulation of internal combustion engine are discussed.

2.1.1 Wall-layer modeling

In multi-dimensional approaches, wall-layer modeling is applied to velocity boundary layers and thermal boundary layers. Wall-layer modeling can be easily explained with Figure 2. 1 and Figure 2. 2.

At normal cells, full governing equations are solved after temporal and spatial discretization of governing equations. In case of cells adjacent to wall, wall-layer modeling is applied to alleviate the huge amount of computational cost. In other words, the friction and heat flux at the wall is expressed using known quantities based on modeling.

First, wall-layer modeling for velocity boundary layers is reviewed. Although turbulent thermal boundary layers have dominant effects on in-cylinder heat transfer prediction, turbulent velocity boundary layers are also important because the velocity boundary layers affect the thermal boundary layers through the turbulent conduction term which involves friction velocity u^*. For the velocity boundary layer modeling, the law of the wall is most widely used because this model is robust and easy to implement. The frictional velocity is defined in two ways.

$$u^* = \sqrt{\frac{\tau_w}{\rho}} \tag{2.1}$$

$$u^* = c_\mu^{1/4} K^{1/2} \tag{2.2}$$

The choice of u^* definition is important because u^* is closely related to turbulent thermal boundary layers. KIVA II adopted Eq. (2.1) and KIVA3V adopted Eq. (2.2). Previous numerical studies [39, 40] showed that u^* predicted by Eq. (2.2) improves the in-cylinder heat transfer prediction. Physically, the superiority of Eq. (2.2) to Eq. (2.1)

can be explained. Frictional velocity defined by Eq. (2.1) is based on incompressible boundary layers. Instead, well-developed dimensional analysis can be applied without constraint of geometry. The preliminary comparison between the KIVA II and the KIVA3V heat transfer model showed the superiority of u^* definition by Eq. (2.2). Therefore, for u^*, Eq. (2.2) is adopted in this study.

In case of thermal boundary layers, the wall heat flux needs to be modeled using known quantities of cells adjacent to wall and wall quantities. For example, density, temperature, viscosity of cells adjacent to wall and wall temperature are important parameters for heat transfer modeling.

2.1.2 Turbulent modeling for core regions

As mentioned earlier, k-ε turbulence models are widely used in various engineering applications. However, a reliable turbulence model for internal combustion engine flows needs to be investigated. Even with an improved heat transfer model, without a reliable turbulence model, accurate estimation of a heat transfer model is not possible. The dedicated research on turbulence modeling of internal combustion engine flows is available in a previous study [41].

LES, linear k-ε and non-liner k-ε models [42] were applied to internal combustion engine flows. LES and non-linear k-ε models require huge amount of computational time compared to linear models. Specifically, for LES, a compressible version of the Dynamic Smagorinsky Model [43] was applied and a quadratic version of the non-linear standard k-ε and the RNG k-ε turbulence model were applied. The performance of non-linear

turbulence model is worse than linear k-ε models for the prediction of mean velocity profiles and recirculation length for a backward facing step. Non-liner models also showed high grid dependency for confined coflow jets. Moreover, for direct injection in a stratified charge engine, nonlinear models were incapable of converging the energy equation. The performance of LES is overwhelmed by the numerical diffusion produced by the finite difference scheme. In fact, LES was first developed using spectral scheme where the order of accuracy is very high. However, this spectral scheme is applicable to simple geometry because of the nature of spectral numerical method. In fact, periodicity of spectral methods requires simple geometry. Therefore, application of LES to complex geometry with finite difference method is not developed well.

On the other hand, the linear RNG k-ε model [44] showed the best performance for the prediction of re-circulating flows for a backward facing step. Moreover, the RNG k-ε model showed a better trend in capturing the details of the velocity field in the mid-section of the combustion chamber for direct injection in a stratified charge engine. Therefore, the linear RNG k-ε model is adopted throughout this study for combustion simulations.

2.2 Combustion modeling

Another important factor in heat transfer modeling is turbulent combustion modeling. Turbulent combustion modeling has direct effects on the engine heat transfer. Even with a reliable turbulence and heat transfer models, without a reliable turbulent combustion model, accurate predictions of heat transfer cannot be achieved. In this study,

combustion modeling of two combustion modes is discussed. The first one is spark-ignition combustion and the second is HCCI combustion. Each combustion mode has quite different mechanism for ignition and combustion processes. The details of combustion models of each combustion mode are reviewed.

2.2.1 Spark ignition combustion

The dedicated research of turbulence combustion modeling on spark ignition combustion is available from a previous study [45]. Brief review of turbulent combustion modeling is as follows. The KIVA combustion model is a chemistry-controlled global reaction model. This model is incapable of producing proper amount of turbulent combustion heat-release rates without ad-hoc tunings. Fundamentally, this model excludes the effects of turbulence. Therefore, applicability of this model is limited.

Among various turbulent combustion models [46-50], the coherent flamelet model (CFM) was successfully applied to spark ignition engines. The coherent flamelet model represents the chemical reaction as an ensemble of wrinkled laminar flame surfaces. Therefore, the local reaction rate is determined by the flame surface density which is defined as the flame sheet per unit volume. The flame surface density transport equation is solved. And based on the solution of the flame surface density, the combustion reaction source term is determined. Based on the definition of production and destruction term in the flame surface density transport equation, various CFM models are available.

Among various CFM models, the CFM1 [49], the CFM 2a and the CFM 2b model are most-popular models. The performance of CFM models for premixed turbulent combustion cases was investigated by previous studies [45, 51]. Among them, the CFM 2b model [50] showed the best performance in numerical studies [45, 51]. As shown in the numerical study [50, 52, 53], the CFM 2b model showed the best agreement with experimental data. Therefore, the CFM 2b model is adopted as a turbulent combustion model throughout this study.

Coherent flamelet combustion models are embedded in the KIVA 3V code by Vanzieleghem [45]. This CFM code is used for this study. The heat transfer model part of the original coherent flamelet code was modified to employ the new heat transfer model. In addition, this original CFM combustion code was developed for a gasoline fuel. In this study, propane is used as an engine fuel. Therefore, burning velocity and pressure exponents for the original CFM code need to be changed. Burning velocity and pressure exponents were modified for propane fuel based on curve fitting data from experiment results [54].

2.2.2 HCCI combustion

It is well known that HCCI is essentially controlled by chemical kinetics with little direct effect of turbulence [55]. Spectroscopic and imaging investigations of HCCI verified that simultaneous multi-point ignition occurs with no flame propagation, which supports that heat release is dominated by chemical kinetics [56-59]. Therefore, HCCI combustion can be calculated accurately by fully integrating a computational fluid

dynamics code with a detailed chemical kinetics code. In this case, very fine grids are required to resolve the temperature distribution in the cylinder (10^4-10^5). However, calculation of both fluid dynamics and detailed chemical kinetics with this resolution is impractical due to huge amount of computational time.

To reduce the computational time, a sequential multi-zone modeling approach [60-62] was introduced. In this approach, decoupling of the turbulent mixing process and chemistry are assumed. The limitation of the sequential method is that once the chemistry calculation begins, the detailed information from the CFD (Computational Fluid Dynamics) code is lost and there is no mixing between zones. These models under-predict the CO emissions by an order of magnitude. To overcome the limitation of sequential method, a coupled CFD / multi-zone model was developed by Flowers et al [63]. In their approach, CFD cells are grouped based on the temperature in a similar range for mapping between CFD cells and multi-zone for detailed chemical kinetics. This method improved the HC and CO emissions compared to sequential multi-zone method. However, under certain conditions, the effect of composition stratification cannot be captured by this model because multi-zones are defined only by temperature ranges.

As an improved model, a fully coupled CFD and multi-zone model is developed by Babajimopoulos et al. [55]. In this approach, the fluid dynamics are solved at the CFD cells with fine grids in KIVA 3V and the detailed chemical kinetics are solved at multi-zones with coarse grids to reduce computational time. The composition of the cell is mapped back and forth between KIVA 3V CFD cells and the multi-zone cells. For mapping, CFD cells are grouped based on the temperature and equivalence ratio in the similar range.

This approach offers a computational efficiency while maintaining good agreement with the detailed solution. The HCCI combustion code developed by Babajimopoulos is adopted in this study.

CHAPTER 3

DERIVATION OF IN-CYLINDER HEAT TRANSFER MODELS

3.1 Parameters related to in-cylinder heat transfer modeling

In-cylinder heat transfer modeling is closely related to the physics of thermal boundary layers. There are important parameters, which are closely related to the physics of thermal boundary layers. For example, thermal conductivity and turbulent Prandtl number variation inside thermal boundary layers are important parameters. In particular, variable density effects on thermal boundary layers are important issues in multi-dimensional in-cylinder heat transfer modeling as discussed in previous studies [7, 31]. Although variable density effects are important parameters, detailed analysis of variable density effects on thermal boundary layers is not available. Therefore, the employment of full variable density effects on in-cylinder heat transfer modeling has not been suggested. Based on physics of thermal boundary layers, it is found that variable density effects are present in viscosity, turbulent Prandtl number and eddy viscosity variation.

In this section, two in-cylinder heat transfer models are investigated in detail. The first one is a heat transfer model with assumptions of incompressible flows. The second one is a heat transfer model with full variable density effects. The heat transfer model built in KIVA 3V corresponds to the heat transfer model with assumptions of incompressible flows. First, the detailed derivation of the heat transfer model built in

KIVA 3V is investigated in this section because this model is widely used and offers good comparisons with newly developed in-cylinder heat transfer models for the following chapters of quantification of parameter effects on in-cylinder heat transfer modeling and numerical applications.

A heat transfer model with full variable density effects corresponds to a new in-cylinder heat transfer model which is named as VDHT (Variable Density Heat Transfer) model. Full variable density effects on thermal boundary layers are employed using a power law assumption. Fundamentally, this VDHT model is an innovatively different model compared to previous heat transfer models because this model has a model constant, which is inevitably required to model variable density effects on thermal boundary layers. This modeling approach with a model constant is a general approach in turbulence modeling such as turbulent k-ε models, where model constants are introduced for the unknown turbulent stress terms and these model constants are found by matching predicted turbulent quantities with experimental data or theory.

After derivation of each heat transfer model, the detailed difference between VDHT model and the heat transfer model built in KIVA3V is examined. The basis of VDHT model is also discussed in chapter 4 through the quantification of parameter effects on in-cylinder heat transfer modeling. And the heat transfer model built in KIVA 3V is classified based on the results of quantification study of parameter effects.

3.2 Eddy viscosity ratio and turbulent Prandtl number correlations

To derive the in-cylinder heat transfer models, correlations of wall unit y^+ are required for eddy viscosity ratio and turbulent Prandtl number variation. These correlations need to be integrated to obtain a heat flux equation. However, the integration of these correlations is not an easy task because of a complex functional shape and integration of correlations needs to be expressed in closed form equation for a final heat flux equation. Using the curve-fitting technique with polynomial equations, the integration of correlations is facilitated. In this section, the curve-fitting technique with polynomial equations is investigated.

3.2.1 Eddy viscosity ratio correlation

Eddy viscosity ratio is defined as eddy viscosity divided by laminar viscosity. For boundary layers of incompressible flows, an eddy viscosity ratio v^+ correlation based on the experimental data is available from Reynolds [64].

$$\nu^+ = 1 + \kappa y^+ [1 - \exp(-y^{+2} / A^2)] \qquad (3.2.1\text{-}1)$$

Von-karman constant κ is 0.41 and A is 26 in Eq. (3.2.1-1)

Figure 3. 1 shows an eddy viscosity ratio correlation based on Eq. (3.2.1-1). As can be seen in Eq. (3.2.1-1), direct integration is not an easy task. Moreover, although integrated value can be obtained by numerical integration, this integrated value does not offer the equation in closed form. Therefore, a polynomial curve-fitting technique is introduced because polynomial formulation is easy to be integrated and the integrated results can be expressed in a closed form of equation.

Polynomial curve-fitting formulation is defined as

$$\nu^+ = 1 - 0.0495y^+ + 0.01055y^{+2} \qquad \text{for } y^+ < 40,$$

$$\nu^+ = 0.42y^+ \qquad \text{for } y^+ \geq 40 \qquad (3.2.1\text{-}2)$$

For $y^+ < 40$, a quadratic polynomial equation is used and for $y^+ \geq 40$, a linear equation is used. As can be seen in Figure 3. 2, the correlation and the curve-fitting equation show a good agreement. For the derivation of heat transfer modeling, the inverse of Eq. (3.2.1-2) is integrated. This Eq. (3.2.1-2) is used for the derivation of various heat transfer models, where turbulent Prandtl number is assumed to be constant.

3.2.2 Turbulent Prandtl number and eddy viscosity ratio correlation

A Pr_t/ν^+ correlation is available by combining two correlations. Reynolds [64] and Yakhot and Orszag [65] are used for Pr_t/ν^+ correlation. The Pr_t/ν^+ correlation is obtained by combining these two correlations and the shape of Pr_t/ν^+ correlation is a function of wall unit y^+. Figure 3. 3 shows the shape of Pr_t/ν^+ by Han and Reitz [31] using Reynolds [64] and Yakhot and Orszag [65] correlations.

Polynomial curve-fitting formulation is defined as

$$\mathrm{Pr}_t/\nu^+ = 0.1 + 0.025y^+ + 0.013y^{+2} \qquad \text{for } y^+ < 45,$$

$$\mathrm{Pr}_t/\nu^+ = 0.59y^+ \qquad \text{for } y^+ \geq 45 \qquad (3.2.1\text{-}3)$$

For $y^+ < 45$, a quadratic polynomial equation is used and for $y^+ \geq 45$ a linear equation is used. As can be seen in Figure 3. 4, the correlation and the curve-fitting

equations show a good agreement. This Eq. (3.2.1-3) is used for the derivation of various heat transfer models in chapter 4, where turbulent Prandtl number variation is considered.

3.3 The heat transfer model built in KIVA 3V

The heat transfer model built in KIVA 3V is derived based on assumptions of incompressible flows with perturbation theory [29]. In KIVA 3V, thermal boundary layers are modeled as a one-dimensional flow based on following assumptions.

- The flow is quasi-steady.
- The fluid velocity is directed parallel to a flat wall and varies only in the direction normal to the wall.
- There are no streamwise pressure gradients.
- There are no chemical reactions in the gas or on the wall surface.
- There is no spray source.
- The dimensionless wall heat loss is small compared to unity.
- Reynolds number is large and laminar viscosity is very smaller than eddy viscosity.
- Mach number is small, so that dissipation of turbulent kinetic energy is a negligible source to the internal energy.

Based on above assumptions, energy equation is given as

$$q_w = (k + k_t)\frac{dT}{dy} \tag{3.3.1}$$

By the assumption that turbulent thermal conductivity is considerably larger than laminar thermal conductivity, laminar thermal conductivity k is neglected.

$$q_w = (k_t)\frac{dT}{dy} \tag{3.3.2}$$

From the definition of k_t and the closure definition of k-ε model eddy viscosity

$$k_t = \frac{c_p \mu_t}{\mathrm{Pr}_t}, \quad \mu_t = c_\mu \rho \frac{K^2}{\varepsilon} \tag{3.3.3}$$

Combination Eq. (3.3.2) with Eq. (3.3.3) and normalization of T by T_w, K by u^{*2}, ε by u^{*3}/y and ρ by ρ_w give

$$c_\mu \rho^+ \frac{k^2}{\varepsilon} y \frac{dT^+}{dy} = \frac{q_w \mathrm{Pr}_t u^*}{c_p \tau_w T_w} = \varsigma \tag{3.3.4}$$

From a steady one-dimensional momentum boundary layer equation without unsteady, convective, pressure gradient, other source terms,

$$\mu_t \frac{du}{dy} = \tau_w \tag{3.3.5}$$

Normalization of u by u^* with using definition of eddy viscosity of Eq. (3.3.3)

$$c_\mu \rho^+ \frac{k^2}{\varepsilon} y \frac{du^+}{dy} = 1 \tag{3.3.6}$$

Application of perturbation theory to Eq. (3.3.4) and Eq. (3.3.6) gives

$$u^+ = u_0 + u_1 \varsigma + ... \tag{3.3.7}$$

$$T^+ = T_0 + T_1\varsigma + \text{.....} \tag{3.3.8}$$

From Eq. (3.3.7) and Eq. (3.3.8)

$$\frac{dT^+}{dy} \Big/ \frac{du^+}{dy} = \varsigma \tag{3.3.9}$$

From Eq. (3.3.9),

$$\frac{dT_0}{dy} = 0 \text{ and } \quad \frac{dT_{i+1}}{dy} = \frac{du_i}{dy}$$

For the first-order perturbation solution,

$$T^+ = T_0 + (u_0^+ + c_0)\varsigma \tag{3.3.10}$$

If ζ goes to zero, boundary layers become isothermal thermal boundary layer conditions, Therefore, T_0=1.

$$T^+ = 1 + (u_0^+ + c_0)\varsigma \tag{3.3.11}$$

$$u_0^+ = \frac{u_0}{u*} \tag{3.3.12}$$

By dimensionalization of Eq. (3.3.11) and arrangement gives

$$\frac{T}{T_w} = 1 + \frac{q_w \,\mathrm{Pr}_t \, u*}{c_p \tau_w T_w}\left(\frac{u}{u*} + c_o\right) \tag{3.3.13}$$

Therefore, heat flux is given as

$$q_w = \frac{(T - T_w) C_p \rho u^*}{\mathrm{Pr}_t}\left(\frac{u_0}{u^*} + C\right)^{-1} \tag{3.3.14}$$

and constant C is given as

$$C = 11.05\left(\frac{\mathrm{Pr}}{\mathrm{Pr}_t} - 1\right) \tag{3.3.15}$$

C is obtained by matching temperature profiles of logarithmic regions with temperature profiles of viscous sub-layer regions based on assumptions that linear temperature profiles for viscous sub-layer regions (y^+<11.05).

Therefore, for log layer regions (y^+>11.05) with law of the wall of incompressible flows and with Pr=0.74 and Pr_t=0.90,

$$\frac{u}{u*} + C = 2.32558\ln(y+) + 3.52647 \tag{3.3.16}$$

For viscous sub-layer regions, based on liner temperature profiles assumptions,

$$q_w = \frac{(T - T_w)C_p \rho \nu}{\Pr y} \tag{3.3.17}$$

Finally, rearrangement gives the heat flux equation of the heat transfer model built in KIVA 3V as

$$q_w = \frac{(T_c - T_w)C_P \rho_c u*}{\Gamma} \tag{3.3.18}$$

$$\Gamma = 0.74 y^+ \qquad \text{for } y^+ < 11.05,$$

$$\Gamma = 2.093\ln(y^+) + 3.173 \quad \text{for } y^+ \geq 11.05 \tag{3.3.19}$$

As shown in the derivation of the built-in KIVA 3V heat transfer model, the law of the wall of incompressible flows is employed. Laminar thermal conductivity is neglected with constant turbulent Prandtl number with 0.9.

Laminar thermal conductivity effects are considered indirectly by linear temperature profiles for viscous sub-layer regions. As can be seen later, incompressible heat transfer model has the formation of the common numerator part of Eq. (3.3.18) with a different denominator part.

3.4 Derivation of VDHT model

In this section, VDHT model is developed. Full variable density is employed in this in-cylinder heat transfer model. Variable density effects on thermal boundary layers are important issues in one-dimensional in-cylinder heat transfer modeling as discussed in previous studies [7, 31]. However, the understanding of variable density effects on thermal boundary layers was not sufficient. Therefore, variable density effects on in-cylinder heat transfer modeling were not employed rigorously. Based on the physics of thermal boundary layers, variable density effects can be divided into three categories; Density, dynamic viscosity and turbulent Prandtl number and eddy viscosity ratio variation.

By the Sutherland law, variable density effects on viscosity are employed. VDHT model employs variable density effects on turbulent Prandtl number and eddy viscosity ratio variation by a power approximation based on dimensional analysis. Because variable density effects on turbulent Prandtl number and eddy viscosity ratio variation is unknown, inevitably, in-cylinder heat transfer modeling needs to come up with a model constant. This modeling approach with a model constant is a similar approach in turbulence modeling. For example, the optimal model constant c_μ and c_ε for turbulent k-ε models were found by matching experimental data or theory. This concept of using model constant distinguishes this VDHT model from previous in-cylinder heat transfer models.

In this modeling approach, the quasi-steady assumption is adopted. Engine wall heat transfer is unsteady in nature. However, Greif el al. [26] showed that the unsteady effects on wall temperature are small when the temperature change of wall is small compared to core region temperature change. In typical metal engine conditions, the wall temperature cyclic swing is less than 10 K. On the other hand, core region temperature change is higher than 2000 K. Moreover, Han and Reitz [31] showed that the unsteady effects on the amount of heat transfer prediction are negligible and variable density effects on thermal boundary layer have dominant effects on the magnitude on heat transfer prediction.

From the energy equation of compressible flows by neglecting viscous dissipation based on assumption of low Mach number flows,

$$\rho \frac{Dh}{Dt} = \frac{DP}{Dt} + div(q) + s \tag{3.5.1}$$

Thermal boundary layers are modeled as a one-dimensional flow based on following assumptions.

- The flow is quasi-steady.
- The direction of fluid velocity is parallel to the wall.
- The pressure is assumed to be uniform in space.
- Variables are only function of wall-normal direction.
- Chemical reaction effects are negligible in the near wall region.

where heat flux q is given as

$$q = -(k + k_t)\nabla T \tag{3.5.2}$$

After applying thermal boundary layers assumptions to equation (1), the integration of equation (1) from the wall gives the magnitude of wall heat flux as

$$q_w = (k + k_t)\frac{dT}{dy} \tag{3.5.3}$$

This Eq. (3.5.3) is a widely used formulation for one-dimensional heat transfer modeling with multi-dimensional core regions [30, 31].

Substitution k and k_t with

$$k = \frac{C_p \mu}{\Pr} \tag{3.5.4}$$

$$k_t = \frac{C_p \mu_t}{\Pr_t} \tag{3.5.5}$$

and introduction of u^* give

$$\frac{C_p}{q_w}\rho u^* dT = \frac{1}{\frac{\nu}{\Pr} + \frac{\nu_t}{\Pr_t}} d(yu^*) \tag{3.5.6}$$

VDHT model employs the density variation, variable density effects on kinematic viscosity, turbulent Prandtl number and eddy viscosity ratio. The right hand side of Eq. (3.5.6) is normalized by introducing eddy viscosity ratio v^+ and the turbulence wall unit y^+ is introduced.

$$\frac{C_p}{q_w}\frac{u^*}{\nu_w}\rho \nu dT = \frac{1}{\frac{1}{\Pr} + \frac{\nu^+}{\Pr_t}} d(y^+) \tag{3.5.7}$$

Kinematic viscosity is not the constant across thermal boundary layers. By introducing the Sutherland law, kinematic viscosity variation is considered.

$$\nu = \frac{a_1 T^{3/2}}{T + a_2} \Big/ \rho \tag{3.5.8}$$

Eq. (3.5.8) shows the Sutherland law for kinematic viscosity. For the Sutherland law constant a_1 and a_2, air constants are used and Eq. (3.5.8) is integrated. The integral form of Eq. (3.5.8) from the wall to the wall unit at the height of the cell adjacent to the wall is

$$\int_{T_w}^{T_c} \frac{C_p}{q_w} \frac{u*}{\nu_w} \frac{a_1 T^{3/2}}{T + a_2} dT = \int_0^{y^+} \frac{1}{\frac{1}{\mathrm{Pr}} + \frac{\nu^+}{\mathrm{Pr}_t}} d(y^+) \tag{3.5.9}$$

The left hand side consists of a temperature function with constants such as u^*, C_P, ν_w, which are not the function of position. First, the left hand side is integrated.

$$\int_{T_w}^{T_c} \frac{C_p}{q_w} \frac{u*}{\nu_w} \frac{a_1 T^{3/2}}{T + a_2} dT = \frac{u* C_P a_1}{q_w \nu_w} \times$$
$$\left[2 \tan^{-1} \frac{\sqrt{T}}{\sqrt{a_2}} a_2^{3/2} - 2\sqrt{T} a_2 + \frac{2}{3} T^{3/2} \right]_{T_w}^{T_c} \tag{3.5.10}$$

For the wall kinematic viscosity ν_w calculation, based on low Mach number assumptions, pressure is assumed to be uniform. With ideal gas law, the relation between temperature and density becomes reciprocal.

Therefore, wall density can be calculated as

$$\rho_w = \frac{\rho_c T_c}{T_w} \tag{3.5.11}$$

Therefore,

$$\nu_w = \frac{a_1 T_w^{3/2}}{T_w + a_2} / \rho_w \tag{3.5.12}$$

By employing Eqs. (3.5.10), (3.5.11) and (3.5.12), variable density effects on dynamic viscosity and density variation across boundary layer are considered in Eq. (3.5.9).

The right hand side of Eq. (3.5.9) is a wall unit function. Fundamentally, this non-dimensional wall unit function part is not derivable. Instead, this wall unit function part needs to be obtained by experimental data. For incompressible flows, experimental data for v^+/Pr_t is available. Previous models [29-31] calculated this wall unit function part based on incompressible flow data because compressible flow data is not available. Because variable density effects on v^+/Pr_t are unknown, no previous in-cylinder heat transfer model employed full variable density effects. The new heat transfer model employs the variable density effect on this right hand side of Eq. (3.5.9) with a power law approximation.

The basis of a power law approximation is as follows. First, the right hand side of Eq. (3.5.9) is non-dimensional. Based on dimensional analysis, a non-dimensional term which can represent the variable density effects is introduced. Variable density effects are directly related to density variation inside boundary layers and density variations inside the boundary layers are strongly dependent on temperature variation. Based on the assumption of low Mach number flows, density and temperature are in reciprocal relation. Therefore, only a non-dimensional temperature term is sufficient to define variable density effects. Non-dimensional variable density effects can be introduced by normalized temperature with wall temperature. For the normalized temperature, two temperatures are available for multi-dimensional approaches; the wall temperature and

the temperature at the height of cell adjacent to the wall. With these two temperatures, normalized temperature is defined as

$$\pi_1 = T_c/T_w \tag{3.5.13}$$

The right hand side of Eq. (3.5.9) needs to satisfy three conditions. First is the constraint that the right hand side of Eq. (3.5.9) reaches the formulation derived by the eddy viscosity and turbulent Prandtl number variation based on incompressible flow data asymptotically when the difference between T_c and T_w becomes negligible. Second is the difference between the right hand side of Eq. (3.5.9) and the formulation derived by the eddy viscosity and turbulent Prandtl number based on incompressible flow data is increased when the difference between T_c and T_w becomes larger. Third, the right hand side of Eq. (3.5.9) is a function of π_1. Various shapes of function can satisfy these three conditions.

A power law approximation is chosen for variable density effects because power law function can cover wide range of increasing or decreasing shape of functions with one simple exponent parameter.

$$\left.\int_0^{y^+} \frac{1}{\frac{1}{\mathrm{Pr}}+\frac{\nu^+}{\mathrm{Pr}_t}}\,d(y^+)\right|_{comp.} \sim \left(\frac{T_c}{T_w}\right)^M \left.\int_0^{y^+} \frac{1}{\frac{1}{\mathrm{Pr}}+\frac{\nu^+}{\mathrm{Pr}_t}}\,d(y^+)\right|_{incomp.} \tag{3.5.14}$$

Based on Eq. (3.2.1-3) with Pr=0.7, incompressible data for right hand side of equation (3.5.9) is calculated.

$$\Gamma = (\frac{T_c}{T_w})^M \times (7.12196\tan^{-1}(0.0925855y^+ + 0.0890245) - 0.632362) \text{ for } y+<45,$$

$$\Gamma = (\frac{T_c}{T_w})^M (1.69492 \ln(y^+) + 2.4589) \quad \text{for } y+ \geq 45. \quad (3.5.15)$$

The constant *M* should be found by matching the predicted heat transfer rate with experimental data.

Finally, the heat flux equation of the VDHT model is given as

$$q_w = \frac{u^* C_P a_1}{\nu_w} \times \left[2\tan^{-1} \frac{\sqrt{T}}{\sqrt{a_2}} a_2^{3/2} - 2\sqrt{T} a_2 + \frac{2}{3} T^{3/2} \right]_{T_w}^{T_c} / \Gamma \quad (3.5.16)$$

3.5 Model Comparison

Detailed derivation of heat transfer models is investigated. The heat transfer model built in KIVA 3V is representative of the heat transfer models based on the assumptions of incompressible flows. VDHT model is developed by employing variable density effects on kinematic viscosity, turbulent Prandtl number and eddy viscosity ratio variation with a power law approximation.

This VDHT model suggests a totally different approach compared to previous in-cylinder heat transfer models. Because variable density effects on Prandtl number and eddy viscosity ratio are unknown, inevitably, in-cylinder heat transfer modeling needs to come up with a matching constant. This modeling approach with a model constant is a general approach in turbulence modeling. For example, the optimal model constant c_μ and c_ε for turbulent *k*-ε models were found by matching the predicted turbulent quantities

with experimental data. Because eddy viscosity is unknown, turbulence k-ε model introduced the c_μ and c_ε.

This concept of using a model constant distinguishes this new heat transfer model from previous in-cylinder heat transfer models. The model constant which can yield accurate match with the experimental data should be found.

CHAPTER 4

QUANTIFICATION OF EFFECTS OF MODELING PARAMETERS ON IN-CYLINDER HEAT TRANSFER PREDICTION

4.1 Outline

As can be seen in the derivation of the previous chapter, turbulent Prandtl number, thermal conductivity and variable density effects are important parameters in in-cylinder heat transfer modeling. However, a systematic and quantitative analysis of the effects of these modeling parameters on in-cylinder heat transfer predictions is not available. In this work, the effects of laminar thermal conductivity, turbulent Prandtl number variation, density variation and dynamic viscosity variation on in-cylinder heat transfer modeling are investigated. Furthermore, various heat transfer models are classified systematically based on these parameters.

The following five heat transfer models are defined for comparisons.

- IHT model is Incompressible Heat Transfer Model without laminar thermal conductivity and turbulent Prandtl number variation.
- Intermediate I model is defined as IHT model with laminar thermal conductivity effects.

- Intermediate II model is defined as Intermediate I model with turbulent Prandtl number variation.

- Intermediate III model is defined as Intermediate II model with density variation.

- Intermediate IV model is defined as Intermediate II model with dynamic viscosity variation.

The first three models are compared to the heat transfer model built in KIVA 3V, where, laminar thermal conductivity effects are considered indirectly by the introduction of linear temperature profiles for viscous sub-layer regions. Because the IHT model, the Intermediate I and II models, the heat transfer model built in KIVA 3V are based on the assumptions of incompressible flows, the numerator part of these heat transfer model equations is identical and only the denominator part is different.

The last two models are compared to Intermediate II model. The Intermediate II, III and IV model have the same modeling assumptions for laminar thermal conductivity and turbulent Prandtl number variation. For these models, the denominator part of the wall unit function is identical. But other parts of the heat transfer equation are different. Therefore, by comparing these models, the effects of density variation and dynamic viscosity variation can be quantified.

4.2 Effects of laminar conductivity and turbulent Prandtl number variation

To clarify the quantitative effects of laminar thermal conductivity and turbulent Prandlt number variation, four heat transfer models based the on assumptions of incompressible flows are analyzed and compared. The first three models are newly

defined models (IHT, Intermediate I and Intermediate II model) and the other model is the heat transfer model built in KIVA 3V. The detailed derivation of the IHT, Intermediate I and II models is presented first, and then these models are compared to the heat transfer model built in KIVA 3V through the quantification of the denominator part of each heat transfer model.

4.2.1 IHT model derivation

The IHT model is a basic heat transfer model because laminar conductivity, turbulent Prandtl number variation and variable density effects are not considered. By adding the effects of each parameter to the IHT model, various heat transfer models can be defined. By comparing newly defined heat transfer models with the IHT model, assumptions and parameter effects can be quantified. As discussed in the derivation of heat transfer models in chapter 3, based on the assumptions of thermal boundary layer, the integration of the energy equation gives the magnitude of heat flux as

$$q_w = (k + k_t)\frac{dT}{dy} \tag{4.2.1-1}$$

From Eq. (4.2.1-1), neglecting laminar thermal conductivity *k*, using Eq. (3.5.5) and introducing *u** gives

$$\frac{C_p}{q_w}\rho u^* dT = \frac{\mathrm{Pr}_t}{\nu_t} d(yu^*) \tag{4.2.1-2}$$

Based on the assumptions of incompressible flows, the right hand side of Eq. (4.2.1-2) is normalized by *ν*.

$$\frac{C_p}{q_w}\rho u^* dT = \frac{\mathrm{Pr}_t}{\nu^+} d(y^+) \tag{4.2.1-3}$$

Each side of Eq. (4.2.1-3) is integrated. A constant value 0.9 is used for Pr_t. For the wall unit function of v^+, an experimental correlation [64] is used. The curve-fitted polynomial formulation of Eq. (4.1.2-2) is used.

Finally, re-arrangement gives the IHT model formulation.

$$q_w = \frac{(T_c - T_w) C_P \rho_c u^*}{\Gamma} \tag{4.2.1-4}$$

The denominator part Γ is defined as

$$\Gamma = -9.02829 \times \tan^{-1}(0.248278 - 0.105832 y^+) + 2.1971 \qquad \text{for } y^+ < 40$$

$$\Gamma = 2.14286 \ln(y^+) + 6.25422 \qquad \text{for } y^+ \geq 40 \tag{4.2.1-5}$$

Thus, the IHT model has no variable density effects and neglects laminar thermal conductivity and turbulent Prandtl number variation.

4.2.2 Intermediate I model derivation

The Intermediate I model has the same modeling assumptions with the IHT model except for the inclusion of laminar thermal conductivity. Therefore, by comparing the IHT model with the Intermediate I model, the effects of laminar thermal conductivity can be investigated.

As shown in the derivation of the IHT model, the application of thermal boundary layer assumptions to energy equation and integration gives the magnitude of heat flux as

$$q_w = (k + k_t) \frac{dT}{dy} \tag{4.2.2-1}$$

In Eq. (4.2.2-1), Eq. (3.5.4) and Eq. (3.5.5) are introduced for thermal conductivity replacement. Introduction of u^* gives

$$\frac{C_p}{q_w}\rho u^* dT = \frac{1}{\frac{\nu}{\mathrm{Pr}} + \frac{\nu_t}{\mathrm{Pr}_t}} d(yu^*) \tag{4.2.2-2}$$

Based on the assumptions of incompressible flows, the right hand side of Eq. (4.2.2-2) is normalized by v.

$$\frac{C_p}{q_w}\rho u^* dT = \frac{1}{\frac{1}{\mathrm{Pr}} + \frac{\nu^+}{\mathrm{Pr}_t}} d(y^+) \tag{4.2.2-3}$$

Each side of equation (4.2.2-3) is integrated. A constant value 0.9 is used for Pr_t. A xonstant value of 0.7 is used for Pr. For the wall unit function of v^+, the experimental correlation [64] is used. The curve-fitted polynomial formulation of Eq. (3.1.2-2) is used.

Finally, re-arrangement gives the Intermediate I model formulation.

$$q_w = \frac{(T_c - T_w)C_P \rho_c u^*}{\Gamma} \tag{4.2.2-4}$$

The denominator part Γ is defined as

$$\Gamma = -5.87074 \tan^{-1}(0.16144 - 0.06881 y^+) + 0.9396 \qquad \text{for } y^+ < 40$$

$$\Gamma = 2.14286 \ln(y^+) + 0.094479 \qquad \text{for } y^+ \geq 40 \tag{4.2.2-5}$$

4.2.3 Intermediate II model derivation

The Intermediate II model has the same modeling assumptions with Intermediate I except for the inclusion of the turbulent Prandtl number variation. Therefore, by

comparing the IHT model with the Intermediate I and II heat transfer models, the turbulent Prandtl number variation can be investigated.

As shown in the derivation of the IHT model, the application of thermal boundary layer assumptions to the energy equation and integration gives the magnitude of heat flux as

$$q_w = (k + k_t)\frac{dT}{dy} \tag{4.2.3-1}$$

Introducing Eq. (3.5.4) and Eq. (3.5.5) into Eq. (4.2.3-1) for thermal conductivity replacement and using u^* gives

$$\frac{C_p}{q_w}\rho u^* dT = \frac{1}{\frac{\nu}{\mathrm{Pr}} + \frac{\nu_t}{\mathrm{Pr}_t}} d(yu^*) \tag{4.2.3-2}$$

Based on the assumptions of incompressible flows, the right hand side of Eq. (4.2.3-2) is normalized by ν.

$$\frac{C_p}{q_w}\rho u^* dT = \frac{1}{\frac{1}{\mathrm{Pr}} + \frac{\nu^+}{\mathrm{Pr}_t}} d(y^+) \tag{4.2.3-3}$$

Each side of Eq. (4.2.3-3) is integrated. For the wall unit function of ν^+/Pr_t variation in Eq. (4.2.3-3), the experimental correlation [64,65] is used. A polynomial curve fitting formulation of Eq. (3.2.1-3) is used for ν^+/Pr_t correlations to facilitate integration. For Prandtl number, 0.7 is used.

Finally, re-arrangement gives the Intermediate II model formulation.

$$q_w = \frac{(T_c - T_w)C_P \rho_c u^*}{\Gamma} \tag{4.2.3-4}$$

The denominator part Γ is defined as

$$\Gamma = 7.12196 \times \tan^{-1}(0.0925855 y^{+} + 0.0890245) - 0.632362 \quad \text{for } y^{+}<45$$

$$\Gamma = 1.69492 \ln(y^{+}) + 2.4589 \quad \text{for } y^{+}\geq 45 \quad (4.2.3\text{-}5)$$

4.2.4 Quantification of effects of laminar conductivity and turbulent Prandtl number variation

Three newly derived in-cylinder heat transfer models (IHT, Intermediate I and Intermediate II) are compared to the heat transfer model built in KIVA 3V. These models are all built based on assumptions of incompressible flows. Density and viscosity are considered constant across the thermal boundary layers. For the correlations of eddy viscosity ratio and turbulent Prandtl number variation, correlations based on incompressible flows are used. As can be seen in each heat transfer model equation, these heat transfer models have the same numerator formulation given as

$$(T_c - T_w) C_P \rho_c u^{*} \quad (4.2.4\text{-}1)$$

On the other hand, the denominator part of the heat flux equation is different because each model has different assumptions for laminar conductivity and turbulent Prandtl number variation. The denominator part of these heat transfer model is the turbulence wall unit function. The effects of laminar conductivity and turbulent Prandtl number variation influence the wall unit function part for heat transfer models based on incompressible flow assumptions. By comparing the denominator part of each heat transfer equation, the effects of laminar conductivity and turbulent Prandtl variation can

be investigated. This is the main idea of quantification of parameter effects on in-cylinder heat transfer modeling.

In case of the IHT model, Intermediate I and II models, the modeling assumptions about laminar thermal conductivity and turbulent Prandtl variation are clear. However, in the case of the heat transfer model built in KIVA 3V, the modeling assumption about laminar thermal conductivity and turbulent Prandtl variation is not clear because these effects are considered indirectly by the assumption of linear temperature profile for viscous sub-layer regions. Quantification analysis can offer useful information about the assumption of linear temperature profile of the heat transfer model built in KIVA 3V, which is not easy to understand because of indirect introduction of laminar thermal conductivity and turbulent Prandtl number variation.

From wall unit range of $1 \leq y^+ \leq 100$, the denominator function Γ of each model can be directly compared. Figure 4. 1 shows the denominator function of each model.

To quantify the effects of laminar thermal conductivity and turbulent Prandtl number variation, a relative magnitude e and a relative predicted heat flux are defined as

$$e = \frac{\sum_{y^+=1}^{100} \frac{\Gamma_{Model}(y^+)}{\Gamma_{IHT}(y^+)}}{n} \tag{4.2.4-2}$$

$$q_{rel} = \frac{(q_{w\_Model} - q_{w\_IHT})}{q_{w\_IHT}} \tag{4.2.4-3}$$

Over the range of $1 \leq y^+ \leq 100$, the relative magnitude e is defined. The range of y^+ less than 100 is chosen, because this range is typical of the y^+ value for multi-dimensional

approaches. *n* is the number of samples used to compute the relative magnitude *e*. In this case, *n*=100 is used. Every integer value is sampled.

Table 4. 1 Relative magnitude and predicted heat flux comparison

	IHT	KIVA 3V	Intermediate I	Intermediate II
e	1	0.786	0.561	0.618
q_{rel}	1	0.27	0.78	0.62

Table 4. 1 shows the relative magnitude and predicted heat flux results. Because the relative magnitude *e* is related to the denominator value, the inverse value of e needs to be used for relative heat flux. The IHT model neglects the laminar thermal conductivity *k* with constant turbulent Prandtl number. The Intermediate I model considers the laminar thermal conductivity *k* and prediction of heat flux is increased by 78 %. By considering the Pr_t variation (Intermediate II), prediction of heat flux is decreased by 16 %.

This quantification of parameters effects on in-cylinder heat transfer modeling shows that the importance of laminar thermal conductivity *k* effects is strong compared to turbulent Prandtl number variation. In case of the heat transfer model built in KIVA 3V, the linear temperature profile assumption for viscous sub-layers corresponds to the intermediate assumption between IHT and Intermediate I model.

4.3 Density variation and dynamic viscosity variation effects

As discussed before, variable density effects can be divided into three categories; Density, Viscosity and Turbulent Prandtl number, and Eddy viscosity ratio variation. For incompressible flows, density is constant. However, for internal combustion engine flows, density and viscosity are variable. The wall unit function of v^+/Pr_t for internal combustion engine flows for boundary layers has different shape than the wall unit function of v^+/Pr_t for incompressible flow because of variable density effects. The effects of density and viscosity variation can be quantified. However, as discussed before, this effect cannot be quantified because variable density effects on v^+/Pr_t are unknown.

To clarify the quantitative effects of density and dynamic viscosity variation, the Intermediate III and IV models are derived and compared to Intermediate II model.

4.3.1 Intermediate III model derivation

Intermediate III heat transfer model is defined with partial variable density effects. For Intermediate III model, density variation is considered across the thermal boundary layers and the correlation of incompressible flows is used for non-dimensional y^+ functions for eddy viscosity ratio and turbulent Prandtl number.

As shown in the derivation of Intermediate II model, application of thermal boundary layer assumptions to the energy equation and integration gives the magnitude of heat flux as

$$q_w = (k + k_t)\frac{dT}{dy} \tag{4.3.1-1}$$

Combing Eq. (4.3.1-1) with Eq. (3.5.4) and Eq. (3.5.5) and introducing u^* gives

$$\frac{C_p}{q_w}\rho u^* dT = \frac{1}{\frac{\nu}{\mathrm{Pr}} + \frac{\nu_t}{\mathrm{Pr}_t}} d(yu^*) \tag{4.3.1-2}$$

Based on incompressible flow assumptions, the right hand side of Eq. (4.3.1-2) is normalized by ν.

$$\frac{C_p}{q_w}\rho u^* dT = \frac{1}{\frac{1}{\mathrm{Pr}} + \frac{\nu^+}{\mathrm{Pr}_t}} d(y^+) \tag{4.3.1-3}$$

The right hand side of Eq. (4.3.1-3) is integrated based on incompressible assumptions with experimental correlation [64, 65] and polynomial curve-fitting results given by Eq. (4.2.3-5). The left had side of Eq. (4.3.1-3) is integrated by considering density variation.

Using a low Mach number assumption, the spatial variation of pressure is negligible inside boundary layers. And with ideal gas law, the integration of the right hand side of Eq. (4.3.1-3) is given as Eq. (3.4.9)

Finally, the heat flux equation is given as

$$q_w = \frac{T_c \ln(T_c / T_w) C_p \rho u^*}{\Gamma} \tag{4.3.1-4}$$

The denominator part Γ is defined as

$$\Gamma = 7.12196 \times \tan^{-1}(0.0925855 y^+ + 0.0890245) - 0.632362 \quad \text{for } y^+ < 45$$

$$\Gamma = 1.69492 \ln(y^+) + 2.4589 \quad \text{for } y^+ \geq 45 \tag{4.3.1-5}$$

4.3.2 Intermediate IV model derivation

Intermediate IV heat transfer model is defined with partial variable density effects. For Intermediate IV model, dynamic viscosity variation is considered for temperature variation and incompressible assumptions are used for non-dimensional y^+ functions of eddy viscosity ratio and turbulent Prandtl number variation.

As shown in the derivation of Intermediate II model, application of thermal boundary layer assumptions to energy equation and integration gives the magnitude of heat flux as

$$q_w = (k + k_t)\frac{dT}{dy} \tag{4.3.2-1}$$

Combing Eq. (4.3.1-1) with Eq. (3.5.4) and Eq. (3.5.5) and introducing u^* gives

$$\frac{C_p}{q_w}\rho u^* dT = \frac{1}{\frac{\nu}{\mathrm{Pr}} + \frac{\nu_t}{\mathrm{Pr}_t}} d(yu^*) \tag{4.3.2-2}$$

The right hand side of Eq. (4.3.2-2) is normalized by introducing the eddy viscosity ratio v^+ and wall unit y^+ is as follows:

$$\frac{C_p}{q_w}\frac{u^*}{\nu_w}\rho\nu dT = \frac{1}{\frac{1}{\mathrm{Pr}} + \frac{\nu^+}{\mathrm{Pr}_t}} d(y^+) \tag{4.3.2-4}$$

The right hand side of Eq. (4.3.2-4) is integrated based on incompressible assumptions with experimental correlation [64,65] and polynomial curve-fitting results given by Eq. (4.2.3-5).

The left hand side of Eq. (4.3.2-4) is integrated with the Sutherland law.

$$\int_{T_w}^{T_c} \frac{C_p u^* \rho \nu}{q_w \nu_w} dT = \frac{C_p u^* \rho}{q_w \nu_w} \int_{T_w}^{T_c} \frac{a_1 T^{2/3}}{T + a_2} dT = \frac{C_p u^* \rho}{q_w} \frac{T_w + a_2}{T_w^{3/2}} \times \left[2\tan^{-1}\left(\frac{\sqrt{T}}{\sqrt{a_2}} \right) a_2^{3/2} - 2\sqrt{T} a_2 + \frac{2}{3} T^{3/2} \right]_{T_w}^{T_c} \quad (4.3.2\text{-}5)$$

Finally, the heat flux equation is given as

$$q_w = \frac{C_p \rho u^*}{\Gamma} F(T) \quad (4.3.2\text{-}6)$$

F(T) is given as

$$F(T) = \frac{T_w + a_2}{T_w^{3/2}} \times \left[2\tan^{-1}\left(\frac{\sqrt{T}}{\sqrt{a_2}} \right) a_2^{3/2} - 2\sqrt{T} a_2 + \frac{2}{3} T^{3/2} \right]_{T_w}^{T_c} \quad (4.3.2\text{-}7)$$

The denominator part Γ is defined as

$$\Gamma = 7.12196 \times \tan^{-1}(0.0925855 y^+ + 0.0890245) - 0.632362 \quad \text{for } y^+ < 45$$

$$\Gamma = 1.69492 \ln(y^+) + 2.4589 \quad \text{for } y^+ \geq 45 \quad (4.3.2\text{-}8)$$

4.3.3 Quantification of density and dynamic viscosity variation effects

In fact, the variable density effect of each category is not separable. In case of Pr_t and k effects, each effect can be considered independently based on modeling assumptions. However, in case of variable density effects, density, viscosity and v^+/Pr_t need to be considered because a model with partial variable density effects becomes a contradictory model. In this case, for the purpose of investigating parameter effects, Intermediate III and Intermediate IV models were introduced hypothetically.

Based on previous model derivations, a temperature function *F(T)* can be defined for each heat transfer model. This temperature function is closely related to variable density effects. By comparing different temperature functions *F(T)*, the effects of density and dynamic viscosity variation can be investigated.

Eq. (4.3.3-1) is the temperature function for incompressible heat transfer models. As shown in section 4.2, all incompressible heat transfer models have Eq. (4.3.3-1).

$$F(T) = (T_c - T_w) \tag{4.3.3-1}$$

As shown in Eq. (4.3.3-1), function shape of incompressible heat transfer model is simply difference between T_c and T_w.

When density variation is considered, temperature function *F(T)* is given below:

$$F(T) = T_c \ln(\frac{T_c}{T_w}) \tag{4.3.3-2}$$

When dynamic viscosity variation is considered, the temperature function *F(T)* is given by Eq. (4.3.3-3).

$$F(T) = \frac{T_w + a_2}{T_w^{3/2}} \times \left[2\tan^{-1}\left(\frac{\sqrt{T}}{\sqrt{a_2}}\right) a_2^{3/2} - 2\sqrt{T}a_2 + \frac{2}{3}T^{3/2} \right]_{T_w}^{T_c} \tag{4.3.3-3}$$

By comparing each temperature function, density and dynamic viscosity variation effects can be investigated. To quantify density and dynamic viscosity variation effects, an average wall temperature needs to be defined. Based on experimental data [67], 420 K is chosen as wall temperatures. The temperature function defined as *F(T)* is calculated from the wall temperatures to 2000 K. Figure 4. 2 show the temperature function from

the wall temperature to 2000 K. As can be seen, the difference of *F(T)* between incompressible conditions and density or dynamic viscosity variation is higher at the higher core temperature region.

The relative magnitude is defined as

$$e = \frac{\sum_{T=T_w}^{2000} \frac{F(T)_{Model}}{F(T)_{Incompressible}}}{n} \quad (4.3.3\text{-}4)$$

n is the number of samples for relative magnitude *e*.

Table 4. 2 Quantification of density and dynamic viscosity variation effects for wall temperature 420 K

T_w=420 K	Incompressible conditions	Density variation	Dynamic viscosity variation
Relative magnitude e	1	1.72	1.64
q_{rel}	1	0.72	0.64

Table 4. 2 show the quantification of density variation and dynamic viscosity variation effects for two different wall temperature cases. Based on quantification of parameter effects on in-cylinder heat transfer modeling results, it can be concluded that variable density effects are more important at higher core temperature. Density variation and dynamic viscosity variation show similar quantitative effects.

4.4 Summary of quantification of parameter effects on in-cylinder heat transfer modeling

In this chapter, the effects of laminar thermal conductivity, turbulent Prandtl number variation, density and dynamic viscosity variation are quantified by defining various heat transfer models and comparing predictions of these models.

Figure 4. 3 shows the quantification of heat transfer models based on sensitivity study of each parameter. Predicted heat flux by the Intermediate III and IV models can be about three times higher than that of the IHT model. The combined effects of laminar thermal conductivity, turbulent Prandtl number variation and density, and dynamic viscosity variation can cause a difference in heat flux prediction as large as 180 %. This result clearly shows the importance of these parameters. However, because variable density effects on turbulent Prandtl number and eddy viscosity ratio variation are unknown, these effects cannot be quantified. Fundamentally, these variable density effects on turbulent Prandtl number and eddy viscosity ratio variation needs to be modeled, and hence the need for the introduction of a model constant.

Figure 4. 4 show the summary of important parameters and classification of various heat transfer models. Four heat transfer models with assumptions of incompressible flows (IHT, Intermediate I, II model and the heat transfer model built in KIVA3V) are classified by laminar thermal conductivity and turbulent Prandtl number variation and three heat transfer models (Intermediate III, IV and the new heat transfer model) are classified based on variable density effects.

This systematic quantification of parameter effects on in-cylinder heat transfer predictions suggests a new approach to analyze heat transfer models through sensitivity

studies. These systematic and quantitative results offer useful information to the issues about variable density effects.

Furthermore, this quantification of parameter effects on in-cylinder heat transfer predictions clearly shows why a model constant needs to be introduced for in-cylinder heat transfer modeling. This feature distinguishes the VDHT model from previous heat transfer models.

CHAPTER 5

VDHT MODEL CONSTANT

5.1 Experimental data

To determine the model constant *M* of the VDHT model and compare the predicted heat flux with the heat transfer model built in KIVA 3V, experimental heat flux data from a spark ignition engine reported by Alkidas [67] and Alkidas & Myers [68] are chosen. This experimental data covers various operating conditions with a simple, disk-shaped cylinder chamber, and hence is suitable to evaluate heat transfer models for spark ignition combustion.

In this numerical study, heat flux measurement data at four operating conditions based on different volumetric efficiencies and equivalence ratios are compared to numerical results. The details of experimental setup are available from the experimental studies [67, 68].

The operating conditions and parameters for the test cases are summarized in the following three tables. Table 5. 1 shows the specification of the spark ignition engine. Table 5. 2 shows the operating condition of each test case, i.e. equivalence ratio and volumetric efficiency. Table 5. 3 shows the residual gas fraction for each test case. Heat

flux measurements at the point located 18 mm from head center are compared with experimental data.

Table 5. 1 Specification of a spark ignition engine

Bore	10.5 Cm
Stroke	9.53 Cm
Compression ratio	8.56
Engine Speed	1500 RPM
Spark timing	27 BTDC
IVC	117 BTDC
Heat flux measurement location	18.7 mm from head center
Fuel	Propane

Table 5. 2 Test case summary

Case	Volumetric Efficiency	Equivalence Ratio
Case 1	40 %	0.87
Case 2	40 %	0.98
Case 3	50 %	0.87
Case 4	60 %	0.87

Table 5. 3 Residual gas fraction

Case	Residual gas fraction
Case 1	12 %
Case 2	14 %
Case 3	10 %
Case 4	12 %

5.2 Numerical conditions

The averaged wall temperature is 420 K based on experimental data. Grief et al. [26] showed that the difference of heat-flux predictions between the transient wall temperature and the averaged wall temperature is negligible when the variations of wall temperature are small compared to the variations in the core region temperature. In this case, the wall temperature change is less than 10 K. On the other hand, the temperature change of the core regions is larger than 2000 K.

The initial gas temperature, pressure and species distributions are assumed to be uniform throughout the chamber. The initial temperature is calculated from the known trapped mass, species composition information and experimental pressure trace. The trapped mass is calculated from volumetric efficiency and residual gas fraction. The initial swirl ratio is set to zero based on a previous study [31]. Initial turbulence kinetic energy and dissipation rate are defined according to the following correlation [69].

$$K_o = 0.61(\eta_v rpm)^2 \quad (5.2.1)$$

$$\varepsilon_o = 0.305(\eta_v rpm)^3 \quad (5.2.2)$$

K_o denotes the initial turbulent kinetic energy and ε_o denotes the initial turbulent kinetic dissipation energy. This correlation is based on the experimental data which has very similar operating conditions with Alkidas' data. The baseline experimental data for this correlation is based on the same chamber shape and RPM and a similar range of compression ratio, equivalence ratio with Alkidas' data. This correlation is widely used for the initialization of turbulent conditions of pancake chamber simulations.

The CFM 2b combustion code implemented into KIVA 3V [45] and the RNG *k*-*ε* model are used for all simulations.

As discussed in the experimental study [67], during scavenging, the level of heat flux is comparatively very low and large errors may occur in the calculation of heat flux from experimental surface temperature measurements. Therefore, only closed cycle simulations were executed for all test cases. Simulations start from IVC and end at EVO.

5.3 Grid and time step independency

In numerical studies, it is important to investigate the grid and time-step independency of the computations. When grid and time-step independency are achieved, numerical results can be compared with experimental data. Grid and time-step independency study was examined for case 1.

5.3.1 Grid independency

If the grid resolution is not dense enough, grid effects on numerical solution are not negligible. Therefore, by grid independency study, optimal grid resolution needs to be found and then numerical results based on the optimal resolution can be compared to experimental data. To determine a basis grid resolution, the thermal boundary layer thickness value can be used. In principle, the first grid cell needs to be located inside the boundary layer region for turbulent wall-layer modeling.

For internal combustion engine flows, the determination of boundary layer thickness is not an easy task because it depends on the operating conditions and piston crank-angle position. A reference value of the thermal boundary layer thickness is available from experimental data [70, 71]. The basis boundary layer thickness in internal combustion engine flows is around 3 mm. Therefore, as a basis grid resolution, the first grid point needs to be located inside 3 mm from the wall. Because of axi-symmetric geometry, a two-dimensional uniform mesh is used for this numerical study. Figure 5. 1 shows the grid used for SI combustion simulations at TDC. To investigate the grid effects on heat transfer prediction, predicted heat flux is examined for different sets of grid resolution.

Six grid resolution sets are simulated for each heat transfer model to examine grid effects on heat flux prediction. The resolution in the x-direction (radial direction) is 60 and the resolutions in the z direction (axis direction) are 30, 50, 60, 70, 80 and 90 respectively. These resolutions of grid sets are typical for spark ignition simulation. The resolution in the x direction is fixed because the heat flux location is fixed in the x direction. Grid independency results are shown in Figure 5. 2 for each heat transfer model.

For the coarsest resolution (60*30), the predicted peak heat flux by the heat transfer model built in KIVA 3V is slightly different from the predicted heat flux at denser resolution. As resolution increases, the difference in the peak heat flux position is negligible for each resolution. The difference in the magnitude of the peak heat flux and its location at higher resolution is negligible for all heat transfer models. Overall. The predicted heat flux shows a similar trend for higher resolutions (60*50-60*90). As shown in chapters 3 and 4, each heat transfer model has the curve-fitting the splitting point for wall unit function. In these grid resolutions, y^+ ranges from a value higher than splitting point to a value lower than the splitting point. Moreover, at these grids sets, the minimum y^+ is in the viscous sub-layer range. Therefore, resolution in the range from 60*50 to 60*90 is dense enough because the lowest y^+ is within the viscous sub-layer range.

At higher resolution, each heat transfer model shows an abrupt change in heat flux at the flame arrival region. Because of flame arrival at the mesh point, and region, the predicted heat flux is changed severely. Therefore, at flame arrival range, the predicted heat flux shows a large change compared to other regions. However, this local change of heat flux by the flame arrival has negligible effects on the prediction of mean temperature. Based on grid independency results, the overall trend of heat flux predicted by each grid set is consistent. Therefore, the effects of grid resolution on the prediction of heat flux are small. Grid resolution of 60*60 is chosen for this study.

At BDC, the distance between the cylinder wall and the cell adjacent to the wall is 0.87 mm, and the distance between the head and piston surfaces and the cell adjacent to the wall is 1.79 mm, which is smaller than the basis thermal boundary layer thickness of 3 mm. At TDC, the distance between the cylinder wall and the cell adjacent to the wall is

0.87 mm ,and the distance between head and piston surface and cell adjacent to the wall is 0.6 mm,

5.3.2 Time step independency

In KIVA 3V, by imposing an allowable maximum time step, the numerical time step can be controlled. In principle, a small allowable maximum time step is desirable for accurate numerical simulations. However, a small allowable maximum time step requires high computational costs. For optimal numerical simulations, time-step independency needs to be clarified. Three time steps are tested in this study. Time-step sets of 0.01 msec, 0.05 msec and 0.1 msec are tested for each heat transfer model.

As shown in Figure 5. 3 for three time-steps, the predictions of heat flux by each heat transfer models are almost identical. Therefore, it can be concluded that the effects of time-step is negligible for the prediction of heat flux. 0.05 msec is used as a maximum time step.

Based on grid and time-step independency, it can be concluded that the effects of grid and time-step on the prediction of heat flux are small.

5.4 Results

Eq. (5.4.1) shows the production term of the CFM 2-b model in the transport equation of surface flame density. The production term S is a function of flame surface density Σ,

turbulent kinetic energy K, dissipation rate ε, tuning constant α and the correction function $\Gamma_{\bar{k}}$ used.

For the CFM 2-b model, the tuning constant α of the production term was adjusted to match net heat release rate and pressure trace with experimental data.

$$S = \alpha \frac{\varepsilon}{\kappa} \Gamma_{\bar{k}} \Sigma \tag{5.4.1}$$

When numerical predictions of the net heat releaser rate match experimental data as closely as possible, numerical heat flux results can be compared to experimental measurements. M value of the VDHT model is set to minimize heat flux error with experimental data. Hence, M ranging from 1.10 to 1.16 is used for this study. The heat transfer model built in KIVA 3V and the VDHT model are compared in this numerical study.

Figure 5. 4 - Figure 5. 11 compare the predicted pressure and net heat release rates against experimental data for four cases. Predicted pressure and net heat release rate show good agreements with experimental data for all test cases. Figure 5. 12- Figure 5. 15 shows the heat flux comparison between each heat transfer model and experimental data for all cases.

For all cases, the heat transfer model built in KIVA 3V under predicts the heat flux, which shows that a heat transfer model based on the assumptions of incompressible flows under-predicts heat flux. In particular, at the peak heat flux region, the under-prediction of heat flux by the heat transfer model built in KIVA 3V is more pronounced. At the peak heat flux region, strong variable density effects are present in the thermal boundary layer because core regions have higher temperatures.

For the given range of *M*, the predicted heat flux by the VDHT model matches the heat flux measurements well compared to the KIVA 3V heat transfer model.

The heat flux prediction near the flame arrival region needs to be discussed. Numerical results and measurements show slight differences in the flame arrival time. The flame propagation is affected by the flame interaction with turbulence. Although reliable turbulence and combustion models are used, exact match of the local flame propagation is not achieved because of the complexity involved with modeling of the flame and turbulence interaction. However, the predicted heat fluxes are still valid enough to evaluate heat transfer models when the complexity of numerical modeling of flame interaction with turbulence is considered.

The predicted heat flux shows the sudden increase at the flame arrival. This sudden increase results from the sudden increase of numerical cell temperature and density by the flame arrival. This local sudden change has negligible effects on the mean temperature prediction as discussed before.

Error analysis is carried-out to assess the various heat transfer models. The first error criterion considers magnitude difference with phase difference of heat flux.

$$E_1 = \frac{\int \left| q_{\exp} - q_{Numerical} \right| d(CA)}{\left(\int q(CA) \right)_{\exp}} \tag{5.4.1}$$

The main source of error for the VDHT model results from the phase difference caused by the flame arrival prediction and the sudden increase of heat flux by sudden increase of numerical cell temperature and density associated with the flame arrival. In this case, a second error criterion based on peak value error is also useful.

The peak heat flux error is defined as

$$E_2 = \frac{\left|(q_{\exp})_{peak} - (q_{numerical})_{peak}\right|}{(q_{\exp})_{peak}} \tag{5.4.2}$$

Table 5. 4 Average error for heat flux prediction

Model	Average Error E_1	Average Error E_2
KIVA3V	44.72 %	47.70 %
M=1.10	20.38 %	4.74 %
M=1.12	19.58 %	4.58 %
M=1.14	19.64 %	5.36 %
M=1.16	19.91 %	6.94 %

Table 5. 4 summarizes the averaged errors for each heat transfer model. Based on averaged error, it can be estimated that the heat transfer model built in KIVA3V under-predicts heat flux by 44.7 % and 47.7 % depending on each error definition used. The difference in average error for each value of *M* is small. Therefore, the sensitivity of values of M on the heat flux prediction is small for the given range of values of *M*. Based on the averaged error, a value of *M* set at 1.12 minimizes error.

The assumptions of the heat transfer model built in KIVA 3V are significantly different from those of the VDHT model. The heat transfer model built in KIVA 3V assumes density, viscosity and turbulent Prandtl number are constant across the thermal boundary layer. The laminar thermal conductivity *k* was neglected and linear temperature profile is used for the viscous-sub layers. For the wall-unit function, the law of the wall

for incompressible flow is used. Basically, no variable density effects were considered in the heat transfer model built in KIVA 3V. The difference in modeling assumptions for each heat transfer model yields the difference in the heat flux prediction. Based on numerical results, it can be concluded that the variable density effects increase the magnitude of heat flux prediction.

Finally, the predicted mean temperature of each heat transfer model is examined. Figure 5. 16 - Figure 5. 19 show the mean temperature predicted by each heat transfer model. The difference in mean temperature predicted by each heat transfer model is as large as 100 K.

For spark ignition cases, the pressure trace can be matched by re-tuning the production terms of the surface flame density for each heat transfer model. However, even if the pressure trace is predicted well, due to difference in the prediction of heat transfer, the predicted mean temperature can be different significantly. As discussed before, these inaccurate predictions of temperature yield inaccurate prediction of emissions. This example clearly shows the importance of heat transfer model on the prediction of thermal conditions.

CHAPTER 6

APPLICATION TO AN HCCI ENGINE

6.1 Introduction

Homogeneous Charge Compression Ignition (HCCI) has the potential to achieve both the higher efficiency and low NO_x and soot emissions [72-78]. The HCCI combustion process is strongly dependent on thermal conditions because chemical kinetics has dominant effects on HCCI combustion. Thus, heat transfer influences the combustion processes directly. Nevertheless, the effects of one-dimensional heat transfer modeling on the prediction of HCCI combustion processes have not been investigated. In this study, the VDHT model and the heat transfer model built in KIVA 3V are applied to an HCCI engine, and their effects on the prediction of HCCI combustion processes are investigated. Furthermore, the effects of turbulence modeling on the prediction of thermal conditions are also investigated by comparing the numerical results obtained by the RNG k-ε and the standard k-ε model.

6.2 Experimental data

To apply the VDHT model and the heat transfer model built in KIVA 3V to HCCI combustion, experimental data from an HCCI engine where the effects of coolant

temperatures on heat release rates were studied [9] are chosen as a test case. Specifically, three test conditions based on different coolant temperatures and swirling ratios are used to investigate the effects of thermal stratification on the heat release rates. Table 6. 1 shows the specification of an HCCI engine and Table 6. 2 shows three test conditions.

Table 6. 1 Specification of an HCCI engine

Bore	102 mm
Stroke	120 mm
Nominal geometric compression ratio	18:1
Engine speed	1200 RPM
IVC	205 BTDC
Equivalence Ratio	0.381
Fuel	Isooctane

Table 6. 2 Test conditions

Test Case	Coolant Temperature	Swirl Ratio
Case 1	100 ℃	0.9
Case 2	50 ℃	0.9
Case 3	50 ℃	3.6

6.3 Numerical Conditions

To apply alternative heat transfer models to HCCI combustion, a reliable combustion model is necessary. The multi-zone / CFD (Computational Fluid Dynamics)

HCCI combustion model developed by Babajimopoulos [55] is adopted in this study. For the calculation of HCCI combustion, fine meshes are required that are dense enough to capture temperature variations near wall regions. These fine meshes require a high computational cost. Moreover, the calculation of chemical kinetics is also time-consuming.

In multi-zone / CFD approaches, the fluid dynamics are solved at the CFD cells with fine grids and the chemical kinetics are solved at a much smaller number of zones to reduce computational time. Based on the temperature and equivalence ratio occurrences in the similar range, CFD cells are grouped into zones. The computed composition of each zone is mapped back and forth to/from the KIVA 3V CFD cells.

Initial value of pressure is available from experimental data. The initial temperature and wall temperatures are based on the correlation of Sjöberg and Dec [79]. Turbulent conditions are available from a previous study [9] where the combustion chamber was represented by an axisymmetric two-dimensional grid. Figure 6. 1 shows the grid used for this study. The mesh was refined near the walls, in order to resolve the cold temperature variation near the wall region and also included the topland crevice. The cell size was about 65 μm close to the piston and the head and 30 μm in the crevice region and near the cylinder liner. The number of cells is 35,760 at BDC and 9,240 at TDC. This grid from Sandia National Lab is used in this study. The actually measured compression ratio is 17.6. The compression ratio grid is slightly reduced to 17.32 by neglecting head gasket volume.

To investigate the grid effects on the numerical results, three grid sets are used. The base grid has 35,760 cells at BDC [9]. The fine grid set has 60,502 cells at BDC and the coarse grid set has 17,486 cells at BDC. The fine and coarse grid sets are made by increasing or decreasing the grid number of the base grid in the x and z direction by 30 %. These grid sets have the wall grid size ranging from 0.1 mm ~ 0.02 mm. This range of wall grid size is typical in the numerical study of HCCI combustion. As shown in Figure 6. 2, the effect of grid sets on the prediction of pressure trace is small.

6.4 Results

The numerical results can be divided into two parts. The first one is a motoring result for each test case and the second one is an HCCI combustion result for each test case.

6.4.1 Motoring cases

To investigate the pure effects of heat transfer models and turbulence models on the prediction of thermal conditions without complication from the combustion processes, the results of motoring cases are discussed first. For turbulence models, the standard k-ε and the RNG k-ε model are used for this study and for heat transfer models, the heat transfer model built in KIVA3V and VDHT model with M=1.12 are used. As shown in Figure 6. 3, the sensitivity of M value on numerical results is negligible.

Both the standard k-ε and the RNG k-ε model are two-equation turbulence models. The model constants of the RNG k-ε model are different from those of the standard k-ε

model because model constants of the RNG *k*-*ε* model are based on the Renormalized Normalized Group (RNG) theory and the rapid distortion theory [41].

Figure 6. 4 - Figure 6. 9 show the pressure traces for each test case. The upper figures show the pressure trace for the entire computation and the bottom figures show the pressure trace near the TDC region. For motoring cases, when the standard *k*-*ε* model is used, each heat transfer model over-predicts pressure near the TDC region compared to experimental measurements. Compared to the predicted pressure trace by the heat transfer model built in KIVA 3V, the VDHT model improves the prediction of pressure trace. When the RNG *k*-*ε* model is used, the prediction of pressure trace is improved significantly for each heat transfer model. These results clearly show the importance of the turbulence model used on the prediction of pressure trace. As discussed in Chapters 2 and 5, the RNG *k*-*ε* model was chosen for spark-ignition cases as a reliable turbulence model.

Turbulence modeling effects on heat transfer prediction can be investigated directly with the results of heat flux prediction. Figure 6. 10 - Figure 6. 12 show the prediction of averaged heat flux on the head surface for each test case. For the given turbulence modeling, the heat flux predicted by the VDHT model is higher than the heat flux predicted by the heat transfer model built in KIVA 3V. Compared to the standard *k*-*ε* model cases, the predicted heat flux is increased significantly when the RNG *k*-*ε* model is used. As shown by the difference in the prediction of heat flux between test cases 1 and 2, by lowering the coolant temperature, the predicted heat flux is increased slightly. As shown by the difference in the prediction of heat flux between test cases 2 and 3, by increasing swirl ratio, the predicted heat flux is increased slightly.

The effects of turbulence models and heat transfer models on thermal stratification can be clearly investigated through the PDF (Probability Density Function) of the charge temperature. The crank angle of 5 ATDC is chosen to investigate the temperature distribution before combustion. Figure 6. 13 - Figure 6. 15 show the PDF of the charge temperature predicted by each turbulence and heat transfer models. As shown in Figure 6. 13 and Figure 6. 14, for the standard k-ε model, the PDF of the high core temperature region shows a narrow and sharp shape. On the other hand, for the RNG k-ε model, the PDF of the high temperature region shows a wide and flat shape. These results clearly show that turbulence modeling affects the temperature distribution of core regions with high temperatures. As shown in Figure 6. 15, PDF shape of the high temperature regions still shows the same tendency with previous cases. However, the difference in the PDF shape of the high temperature region is small compared to previous cases for this high swirl ratio case. The PDF of the high temperature region is shifted to the lower temperature direction when the RNG k-ε model is used. The PDF of the high temperature region is also shifted to the lower temperature direction when the VDHT model is used. These results clearly show that turbulence modeling significantly influences the prediction of thermal conditions.

Figure 6. 16 - Figure 6. 18 show the cumulative probability of the charge temperature predicted by each turbulence and heat transfer model. Cumulative probability results clearly show that the charge temperature distribution is affected by the heat transfer models and turbulence models used. The VDHT model shifts the cumulative probability of the charge temperature to lower temperature regions compared to the heat transfer model built-in KIVA3V. The RNG k-ε model also shifts the cumulative

probability of the charge temperature to lower temperature regions compared to the standard k-ε model.

Based on the study of Papageorgakis [41] and our motoring results, the RNG k-ε model is adopted for the following HCCI combustion study.

To investigate the effects of turbulence models and heat transfer models on the in-cylinder thermal condition, the mean charge temperatures are compared for each test case. Figure 6. 19 - Figure 6. 21 show the comparison of mean charge temperature by each turbulence model and heat transfer model. For the motoring cases, the temperature difference caused by each heat transfer model is as high as 30 K.

As discussed in chapter 2, heat transfer modeling is wall-layer modeling for thermal boundary layers. Therefore, the energy transfer at core regions is not directly affected by the heat transfer models. Instead, turbulence models have an important role in energy transfer in core regions because the convection and mixing of turbulent flows are dominant factors to transfer energy in core regions. Furthermore, heat transfer modeling is expected to be affected by turbulence modeling because the heat flux equation in heat transfer modeling is a function of turbulent quantities. Therefore, to predict the heat transfer accurately, both reliable heat transfer modeling and turbulence modeling need to be considered.

Finally, in order to explore the effects of heat transfer modeling on the prediction of near-wall regions, temperature profiles are investigated. Figure 6. 22 - Figure 6. 24 show the temperature profiles at the location 3 mm below the cylinder head. In order to investigate the temperature profile before combustion, 5 ATDC is chosen. Because the

heat transfer model built in KIVA3V under-predicts the heat flux, temperature profiles predicted by this model show the higher temperature distribution compared to the temperature profiles by the VDHT model.

6.4.2 Firing cases

For firing cases, the reduced mechanism by Chen et al. [80] is used for isooctane. This reduced mechanism showed good agreement with the results of a detailed mechanism.

Before discussing the details of firing case results, the shape of the predicted heat flux is compared to experimental data [81]. As shown in Figure 6. 25, the shape of the predicted heat flux results shows good agreement with experimental measurements. The predicted peak heat flux before ignition occurs prior to TDC. Experimental measurements also show that the peak heat flux under motoring conditions occurs prior to TDC. Because the crank angle of occurrence of the peak turbulent kinetic energy is less than TDC, the crank angle of peak heat flux under motoring conditions is less than TDC.

The HCCI combustion process is sensitive to the initial charge temperature. In order to investigate the effects of heat transfer models on the prediction of pressure trace, the same initial charge temperature is applied to each heat transfer model. Figure 6. 26 exhibits large difference in the pressure traces. This clearly shows that heat transfer modeling strongly influences the HCCI combustion processes.

The initial charge temperature is slightly adjusted to match the start of combustion with the experimental measurements for each test case. Unlike the coherent flamelet models in spark ignition cases, for HCCI combustion, no tuning parameter is available for the HCCI combustion model. Only the start of combustion can be matched with experimental data. After ignition, the entire combustion processes is dictated by thermal conditions. Therefore, by comparing pressure traces, the effects of heat transfer models on HCCI combustion can be investigated clearly.

Figure 6. 27 shows a comparison of pressure traces for test case 1. The heat transfer model built in KIVA3V over-predicts the pressure trace compared to the experimental data. The pressure trace predicted by the VDHT model shows a good agreement with the experiment data. Figure 6. 28 shows the comparison of the averaged heat flux into the head surface for test case 1. Because thermal conditions are dominant factors in HCCI combustion, the alternative heat transfer models have direct effects on the pressure trace. As shown in the quantification of parameter effects on in-cylinder heat transfer modeling, spark ignition combustion and motoring results, the heat transfer model built in KIVA 3V under-predicts heat flux. The over-prediction of pressure trace by the heat transfer model built in KIVA 3V under HCCI combustion results from under-prediction of heat flux by this model. On the other hand, the VDHT model predicts the pressure trace accurately, which reveals that the VDHT model predicts heat flux accurately during HCCI combustion.

As shown in Figure 6. 29 - Figure 6. 32, the peak pressure trace is slightly decreased as the coolant temperature is decreased and swirling ratio is increased. For test

cases 2 and 3, the VDHT model predicts pressure trace accurately, while the heat transfer model built in KIVA 3V over-predicts the pressure trace.

Finally, the mean temperature is compared for each heat transfer model in Figure 6. 33 - Figure 6. 35. The difference in the mean temperature is as large as 70 K. As compared to spark-ignition results, the difference in mean temperature is decreased. HCCI combustion is low temperature combustion compared to spark ignition. In this case, the peak mean temperature is 1900 K. On the other hand, the peak mean temperature is 2500 K for spark ignition cases.

To investigate the effects of heat transfer models on the prediction of emissions, the predicted CO (Carbon monoxide) emissions are compared. As shown in Figure 6. 36, the predicted CO emissions by the VDHT model are higher than those by the heat transfer model built-in KIVA3V. Previously, the multi-zone / CFD combustion model [55] with the heat transfer model built in KIVA 3V under-predicted CO emissions [82, 83]. In fact, the VDHT model increases the overall heat transfer and changes the temperature distribution at the near-wall region. As shown in Figure 6. 37, temperature contours at the near-wall region by each transfer model show different temperature distribution. The temperature contour by the VDHT model shows a wider low temperature region at the near-wall region compared to the heat transfer model built in KIVA 3V. Due to different temperature distributions by different heat transfer models, the predicted CO emissions by each heat transfer model show differences. Figure 6. 38 shows the CO distribution in terms of mole fraction at 10 ATDC. Due to the wider low temperature region at the near-wall region computed by the VDHT model, the predicted CO emissions are increased. This results show that the VDHT model has the potential to

improve the CO emission prediction compared to the heat transfer model built in KIVA3V.

Based on the reported results, it can be concluded that the VDHT model improves the prediction of pressure trace and mean temperature through more accurate prediction of heat flux. On the other hand, the heat transfer model built in KIVA 3V over-predicts the pressure and mean temperature by under-prediction of heat flux. As a result, HCCI combustion processes can be more accurately predicted with the VDHT model and the RNG k-ε model.

CHAPTER 7

SUMMARY, CONCLUSIONS AND FUTURE SUGGESTION

7.1 Summary

A comprehensive study of in-cylinder heat transfer modeling has been conducted with emphasis on variable density effects in order to improve the prediction of heat transfer in internal combustion engines.

The VDHT (Variable Density Heat Transfer) model was developed based on the employment of variable density effects on thermal boundary layers. Specifically, the density variation, dynamic viscosity variation and variable density effects on turbulent Prandtl number and eddy viscosity ratio variation are employed in VDHT model. To employ the variable density effects on turbulent Prandtl number and eddy viscosity ratio variation, the power-law approximation with the model constant is introduced.

Based on the sensitivity study of various parameters, the importance of parameters for in-cylinder heat transfer modeling is investigated through the quantification and the classification of heat transfer models. Five heat transfer models are defined for the quantification of parameter effects on in-cylinder heat transfer modeling. By comparing these heat transfer models, the effects of laminar thermal conductivity, turbulent Prandtl number variation, density variation and dynamic viscosity variation are

quantified. This quantification of parameter effects on in-cylinder heat transfer modeling offers the basis of VDHT model. Because the variable density effects on turbulent Prandtl number and eddy viscosity variation are unknown, these effects need to be modeled with a model constant.

VDHT model and the heat transfer model built in KIVA 3V are applied to a spark-ignition engine to determine the model constant of VDHT model and compare the predicted heat flux by two models. These two heat transfer models are also applied to an HCCI engine. As shown in the classification of heat transfer models, VDHT model is characterized by the full variable density effects with laminar conductivity and turbulent Prandtl number variation. On the other hand, the heat transfer model built in KIVA 3V is based on the assumptions of incompressible flows.

In a spark-ignition engine, the CFM 2-b combustion model was used for the premixed SI combustion simulation. Four test cases with different volumetric efficiencies and equivalence ratios were simulated. The model constant of VDHT model is determined for spark-ignition cases to be in the rage 1.10 -1.16. The predicted heat flux and mean temperature of each heat transfer model are investigated.

In an HCCI engine, the CFD / Multi-zone combustion model was used for the HCCI combustion simulation. Three test cases based on different coolant temperatures and swirl ratios were used. To investigate the pure effects of heat transfer models and turbulence models on the prediction of thermal conditions without complication of combustion processes, motoring results are analyzed. The predicted pressure trace, heat

flux, mean temperature and probability density function of the charge temperature were compared for each heat transfer model and turbulence model.

The results of HCCI combustion cases are analyzed. The predicted heat flux, pressure trace and mean temperature by each heat transfer model are investigated.

7.2 Conclusions

- The laminar thermal conductivity effects on in-cylinder heat transfer modeling are more important than the effects of turbulent Prandtl number variation.
- The combined effects of laminar thermal conductivity, turbulent Prandtl number, density and dynamic viscosity variation can increase the heat flux prediction by 180 % compared to the predicted heat flux by IHT model.
- The heat transfer model built in KIVA 3V is classified as an intermediate model between IHT and Intermediate I, II model based on the quantification of parameter effects on in-cylinder heat transfer modeling.
- The power-law approximation with the model constant M was introduced to employ the variable density effects on turbulent Prandtl number and eddy viscosity variation. The model constant M of 1.12 for the power-law approximation was found through the spark-ignition heat flux measurements. For spark-ignition cases, the main benefit of VDHT model is the accurate prediction of the mean temperature. The difference in the mean temperature predicted by each heat transfer model is as high as 100 K.

- Based on the probability density function and cumulative probability of the charge temperature, turbulence modeling strongly influences the predictions of temperature distribution. Based on the prediction of heat flux, the RNG k-ε model improves the prediction of pressure trace. These results clearly confirm that a reliable turbulence model is a pre-requisite to the accurate heat flux prediction.

- VDHT model improves the prediction of the pressure trace and the mean temperature by the accurate prediction of heat transfer in HCCI combustion cases. On the other hand, the heat transfer model built in KIVA 3V over-predicts pressure trace and mean temperature by under-predicting the heat flux. The difference in the mean temperature predicted by each heat transfer model is as high as 70 K.

7.3 Summary of Accomplishments

Three unexplored issues are investigated. The following lists present a summary of the accomplishments regarding these issues.

- The variable density effects on in-cylinder heat transfer modeling are thoroughly investigated through quantification and classification of in-cylinder heat transfer models. These systematic and quantified results offer useful information to the issues about variable density effects.

- The effects of turbulence modeling on the prediction of thermal conditions are investigated. Previous studies only focused on in-cylinder heat transfer

modeling to improve the prediction of heat transfer. However, these results clearly show that both turbulence modeling and heat transfer modeling are important to improve the prediction of heat transfer.

- The effects of one-dimensional in-cylinder heat transfer modeling with multi-dimensional core regions on the prediction of HCCI combustion are investigated for the first time.

7.4 Suggestions for Future Work

In this study, the new heat transfer model which can improve the prediction of heat flux for SI combustion and HCCI combustion is presented. With a reliable heat transfer model, the following research topics can be investigated further.

- Conduct a parametric study to investigate the effects of wall temperatures and intake temperatures on HCCI combustion processes.

- The accurate prediction of emissions is an important issue in internal combustion engines. The main benefit of the accurate heat transfer model is the accurate prediction of in-cylinder temperature. Because emissions are strongly dependent on in-cylinder temperature, a parametric study of effects of wall temperature on HCCI emissions should be conducted using the VDHT model.

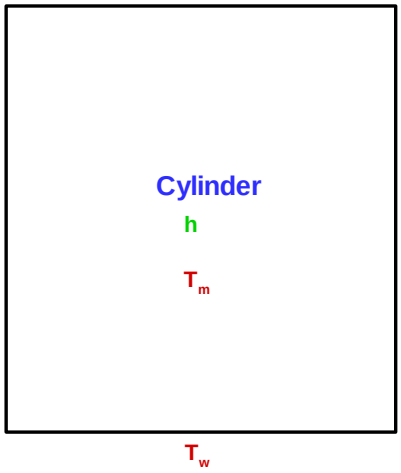

Figure 1. 1 A global heat transfer model

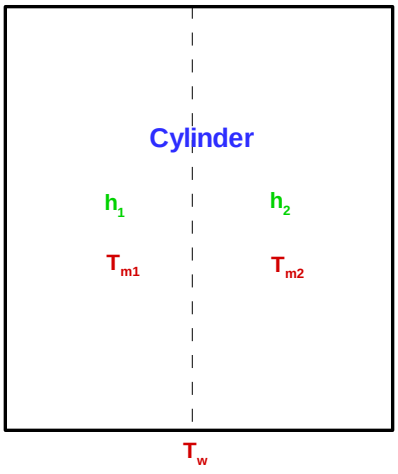

Figure 1. 2 A two-zone heat transfer model

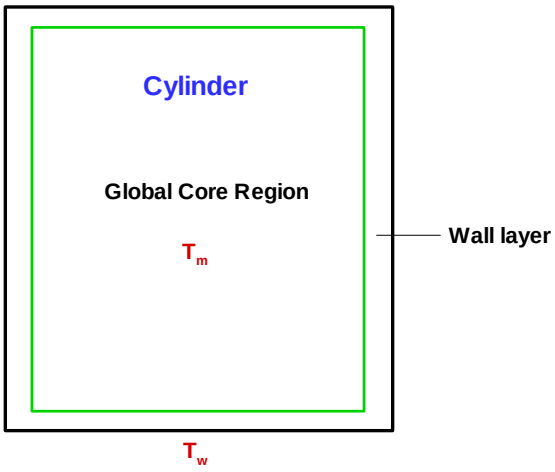

Figure 1. 3 A one-dimensional heat transfer model with a global core region

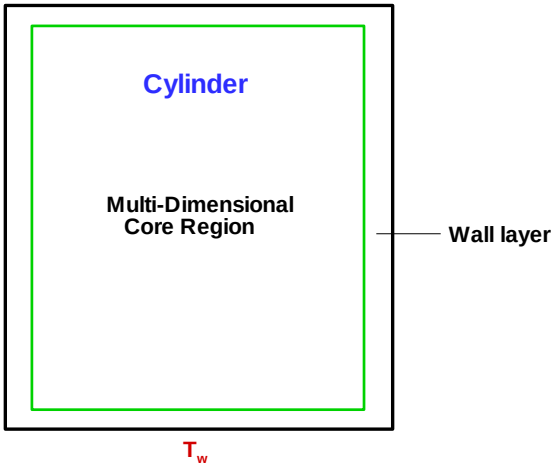

Figure 1. 4 A one-dimensional heat transfer model with a multi-dimensional core region

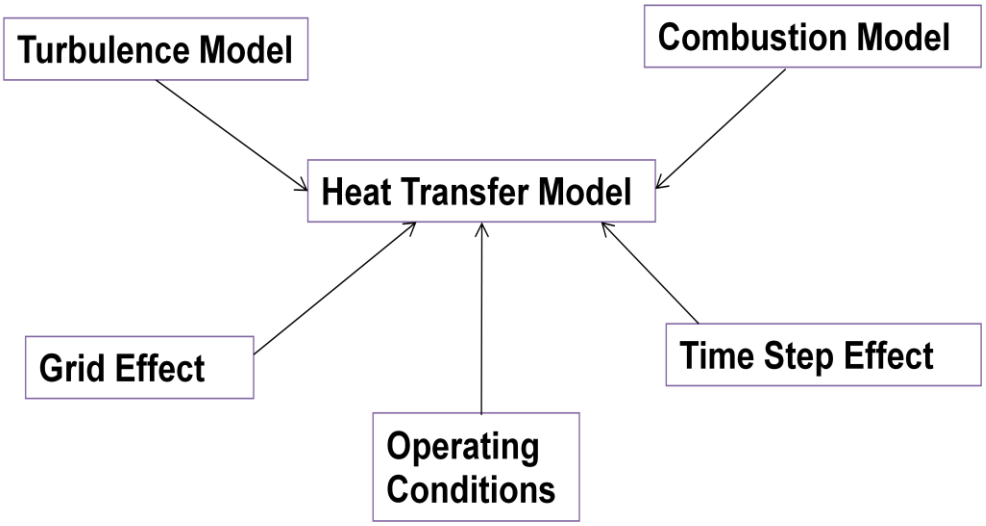

Figure 1. 5 Various influential factors on heat transfer modeling

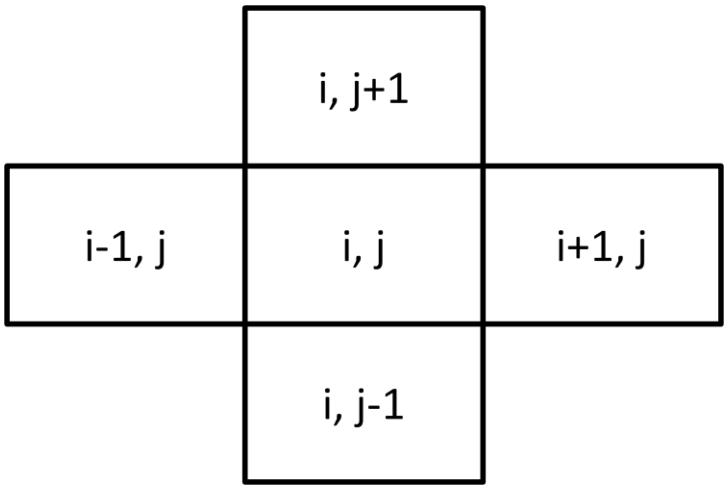

(a) Normal cell

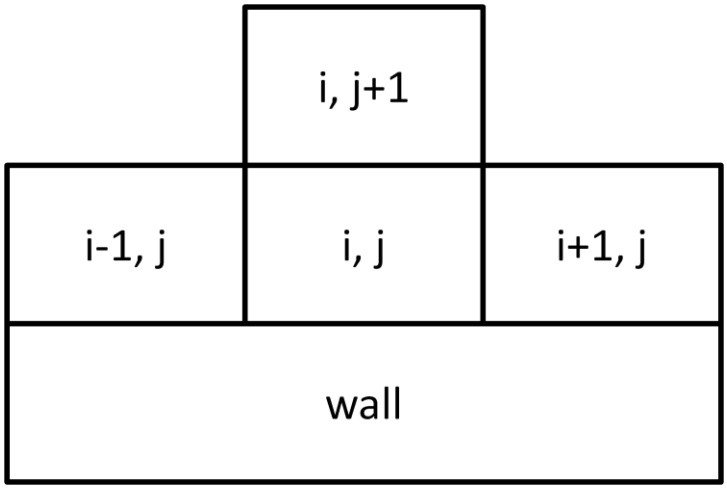

(b) Cell adjacent to wall

Figure 2. 1 Cell structure for multi-dimensional method

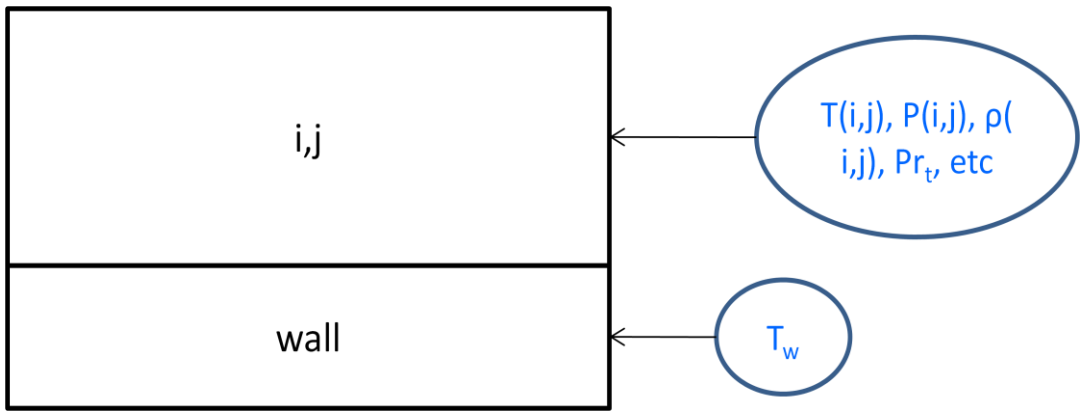

Figure 2. 2 Wall-layer modeling parameters

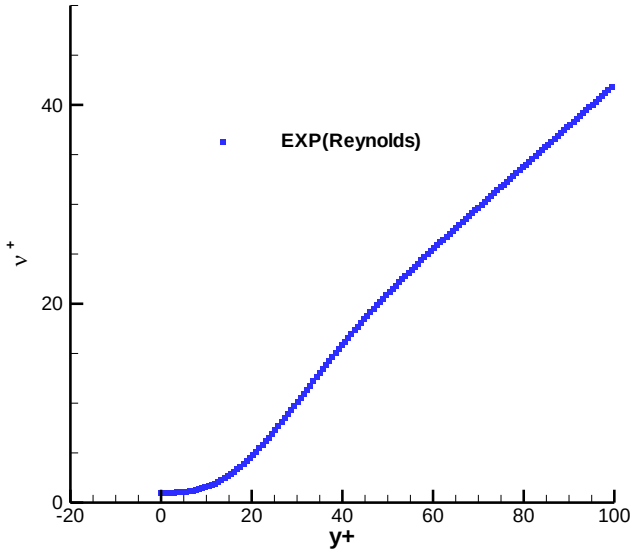

Figure 3. 1 An eddy viscosity ratio correlation [64]

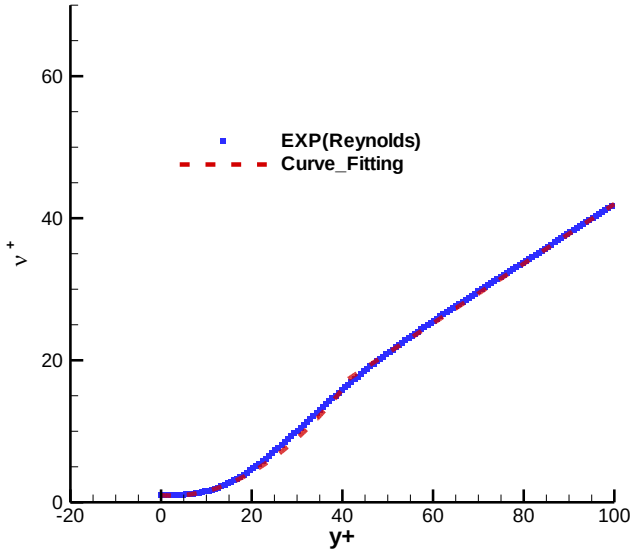

Figure 3. 2 Match between experimental correlation and the curve-fitting formula for eddy viscosity ratio

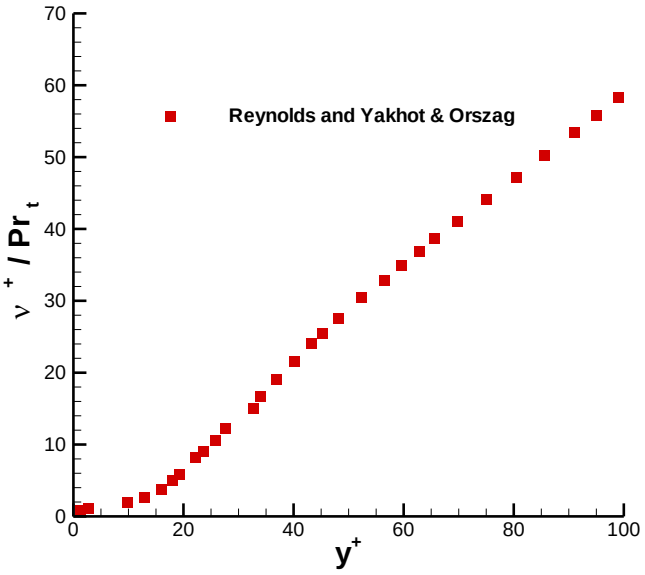

Figure 3. 3 A turbulent Prandtl and eddy viscosity ratio correlation

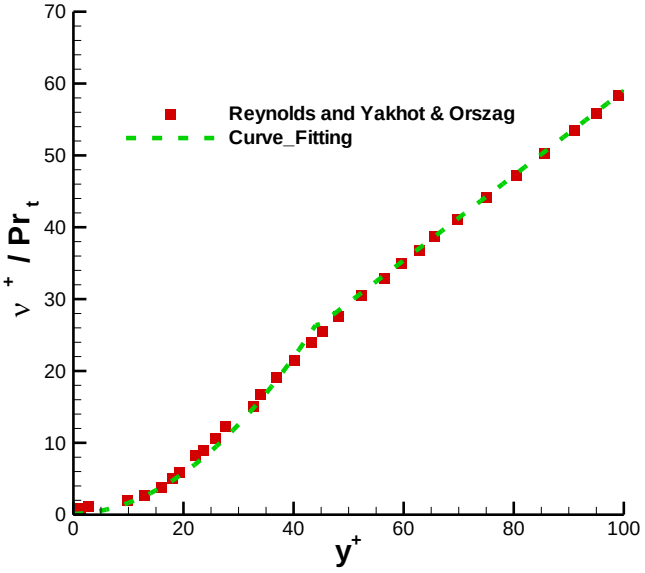

Figure 3. 4 Match between experimental correlation and the curve-fitting formula for turbulent Prandtl number and eddy viscosity ratio

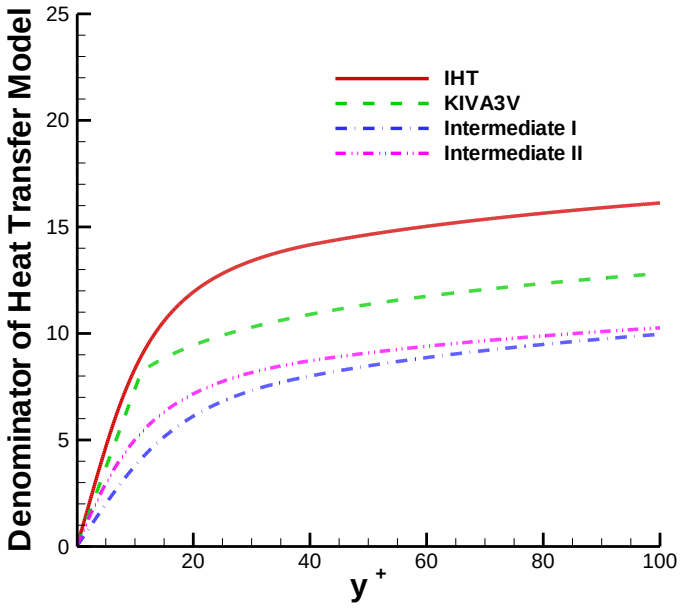

Figure 4. 1 Comparison of denominator part of heat transfer models

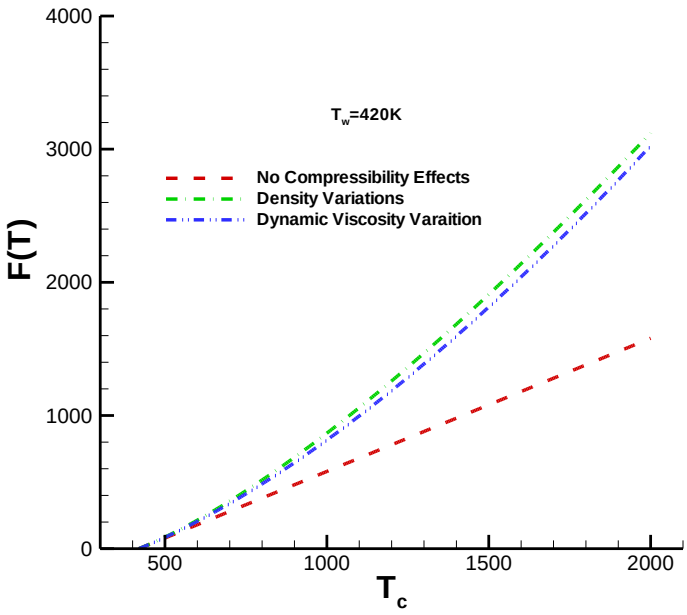

Figure 4. 2 Comparison of temperature function F(T) at T_w=420 K

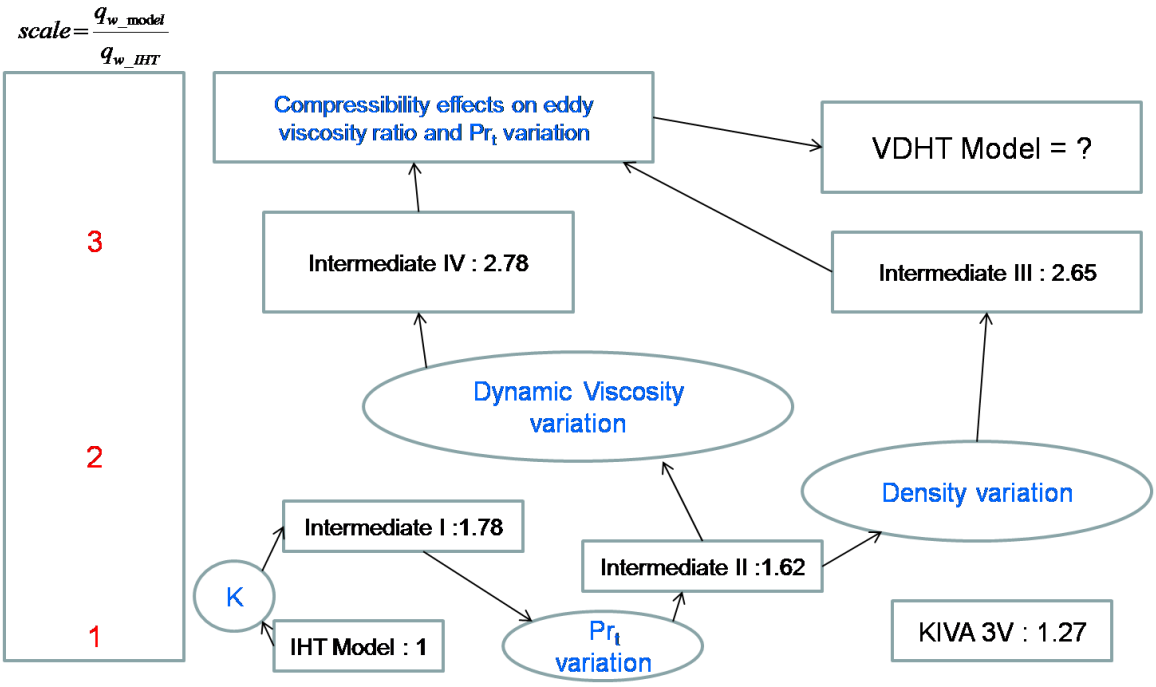

Figure 4. 3 Quantification of in-cylinder heat transfer models

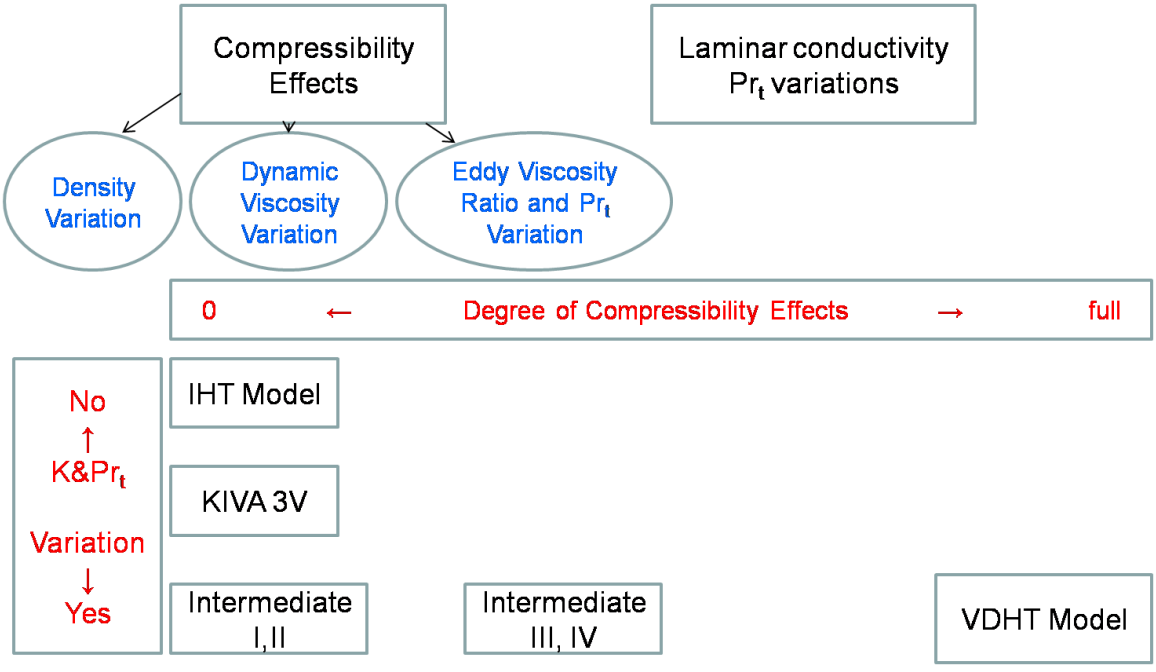

Figure 4. 4 Classification of in-cylinder heat transfer models

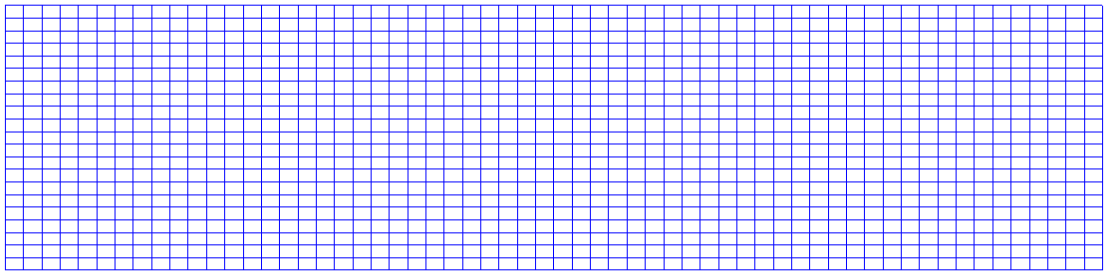

Figure 5. 1 Two dimensional axis-symmetric grids used for SI combustion simulation at TDC

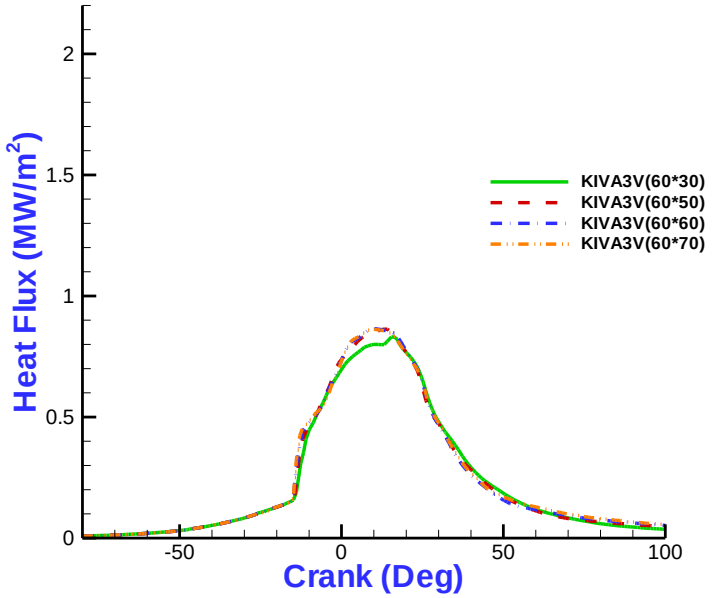

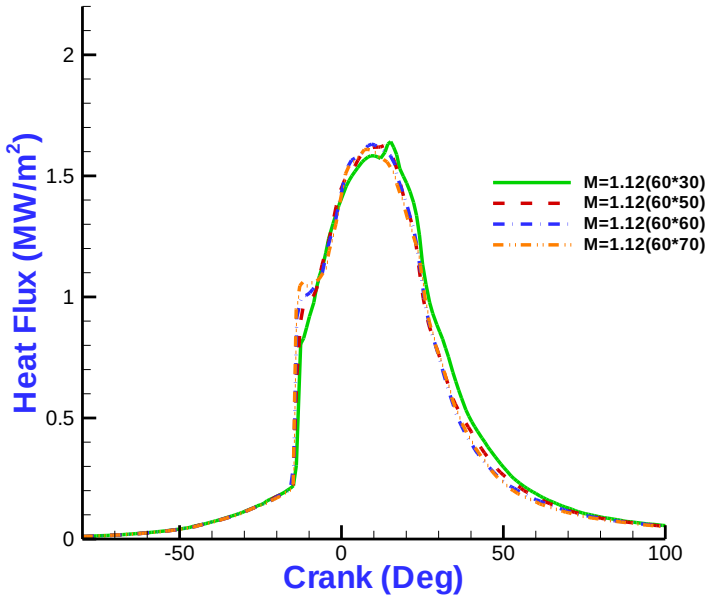

Figure 5. 2 Heat flux prediction for different grid sets

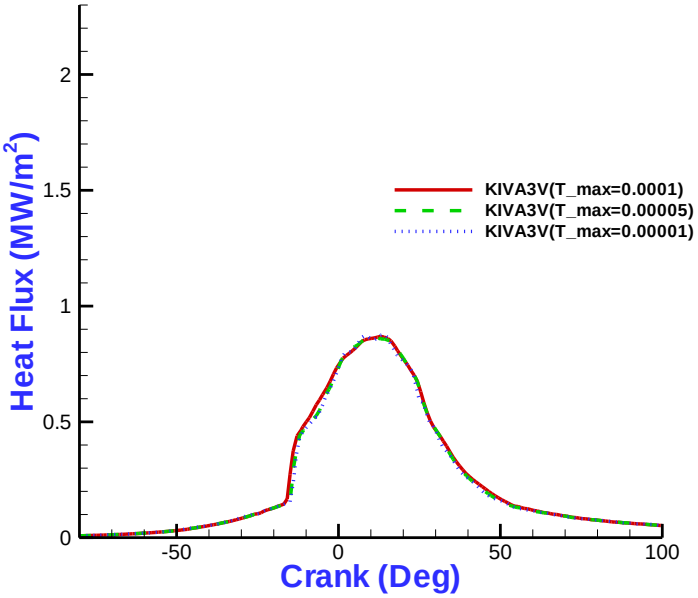

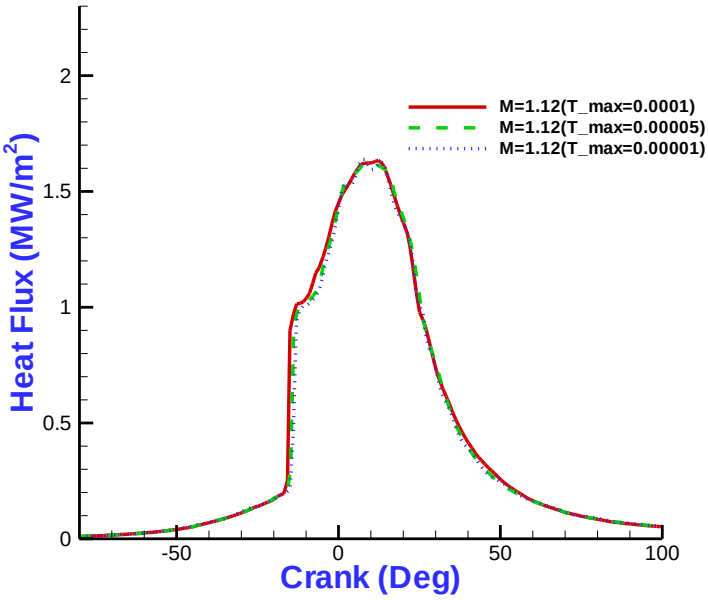

Figure 5. 3 Heat flux prediction for different maximum time steps

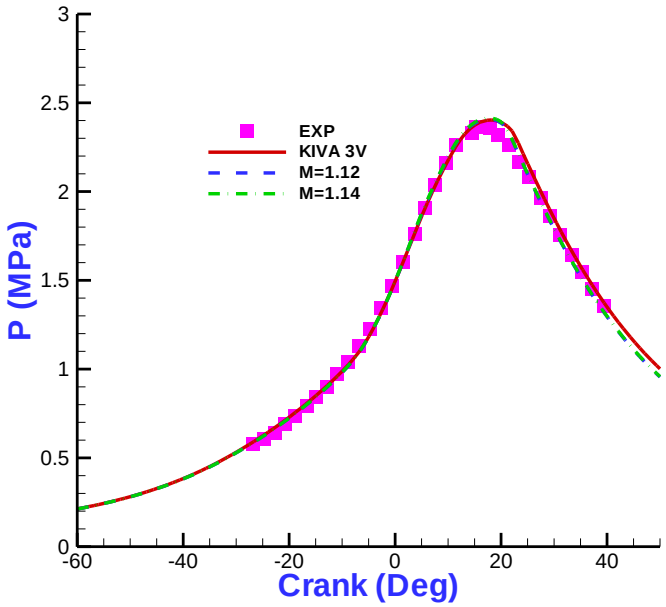

Figure 5. 4 Pressure trace for case 1

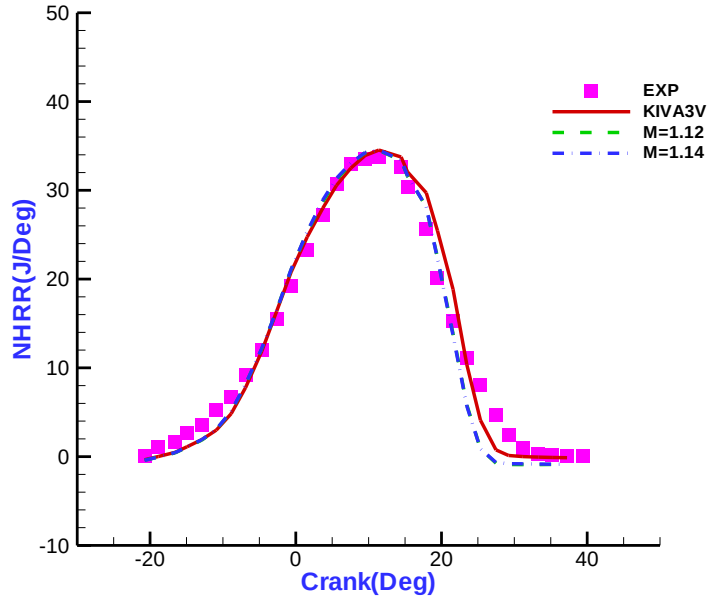

Figure 5. 5 Net heat release rate for case 1

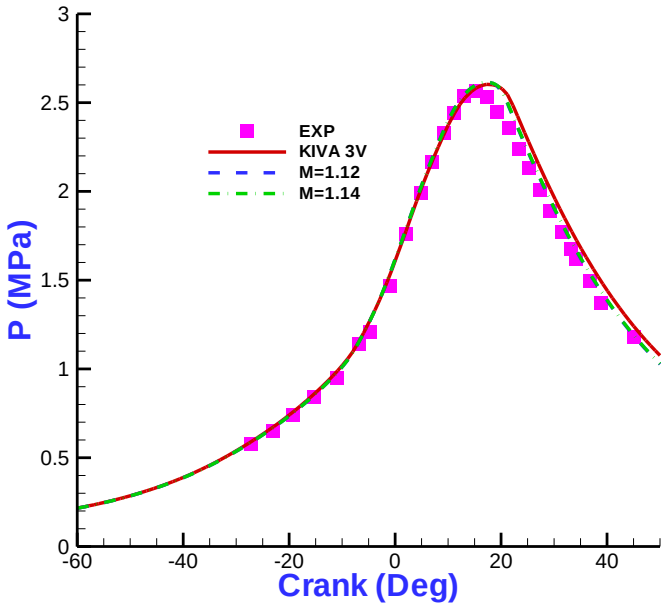

Figure 5. 6 Pressure trace for case 2

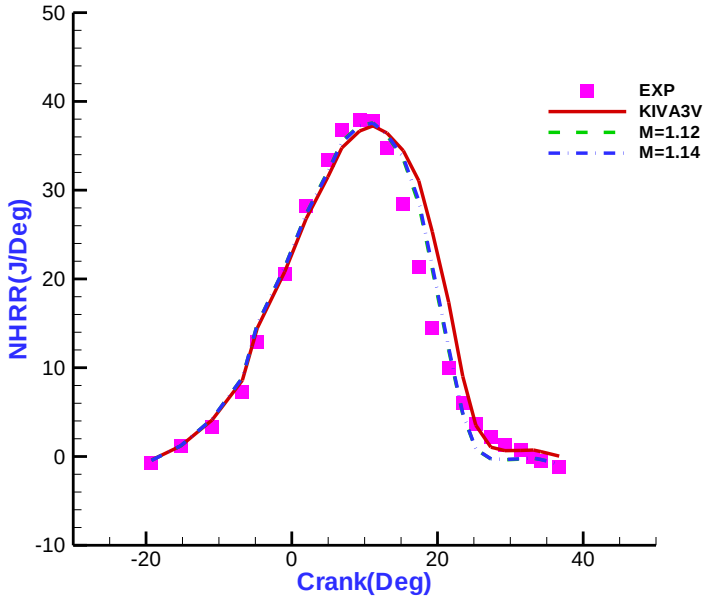

Figure 5. 7 Net heat release rate for case 2

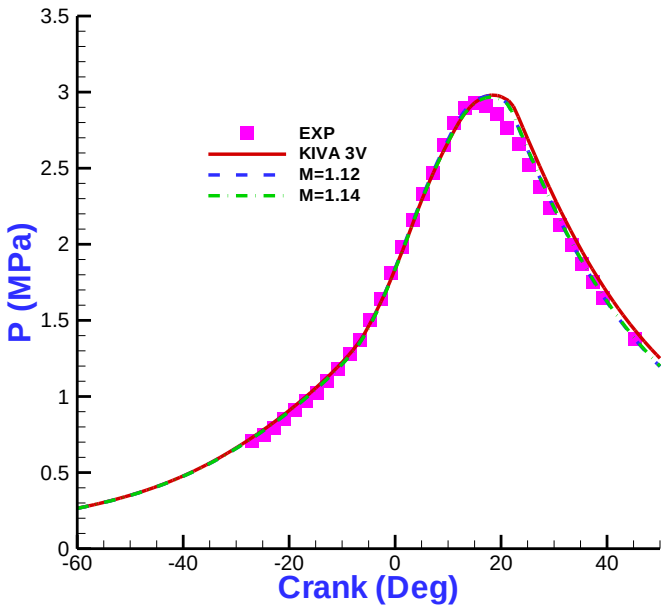

Figure 5. 8 Pressure trace for case 3

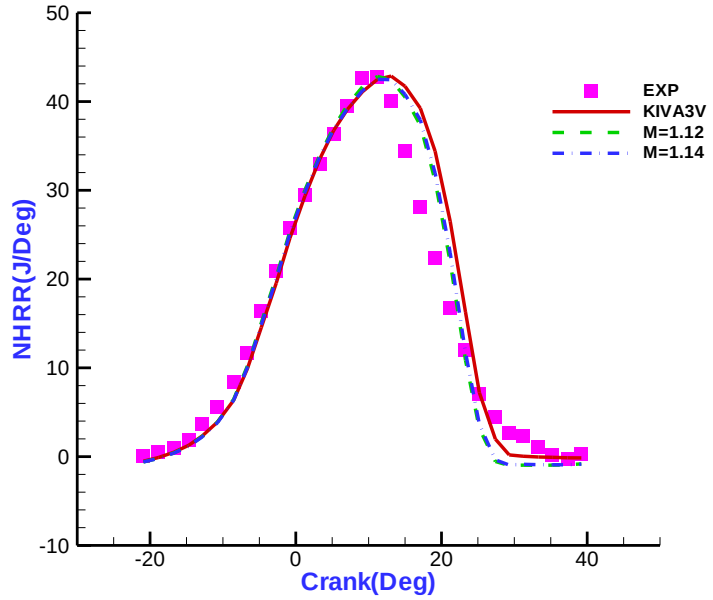

Figure 5. 9 Net heat release rate for case 3

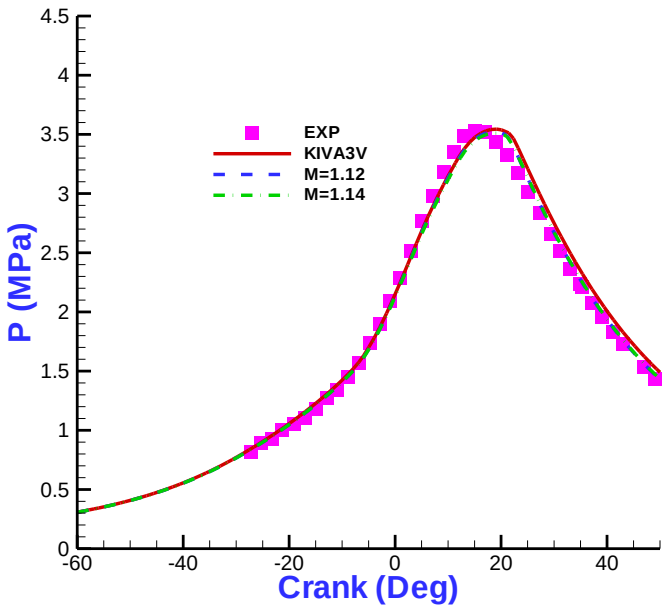

Figure 5. 10 Pressure trace for case 4

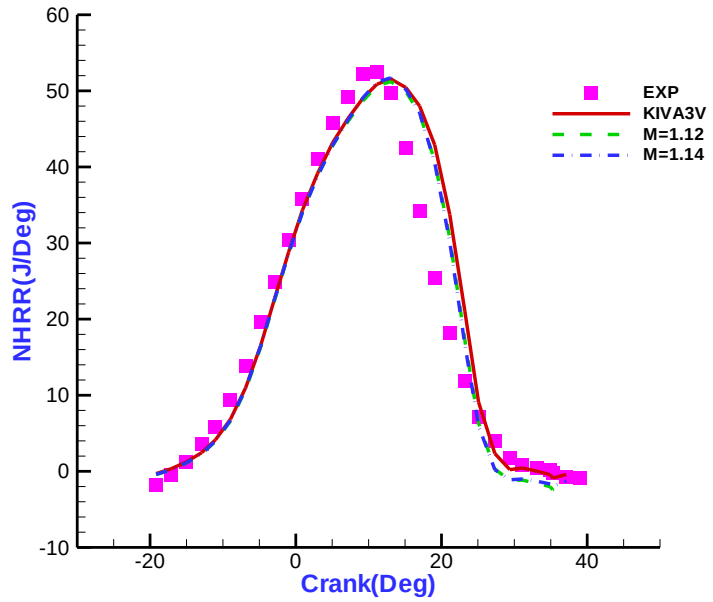

Figure 5. 11 Net heat release rate for case 4

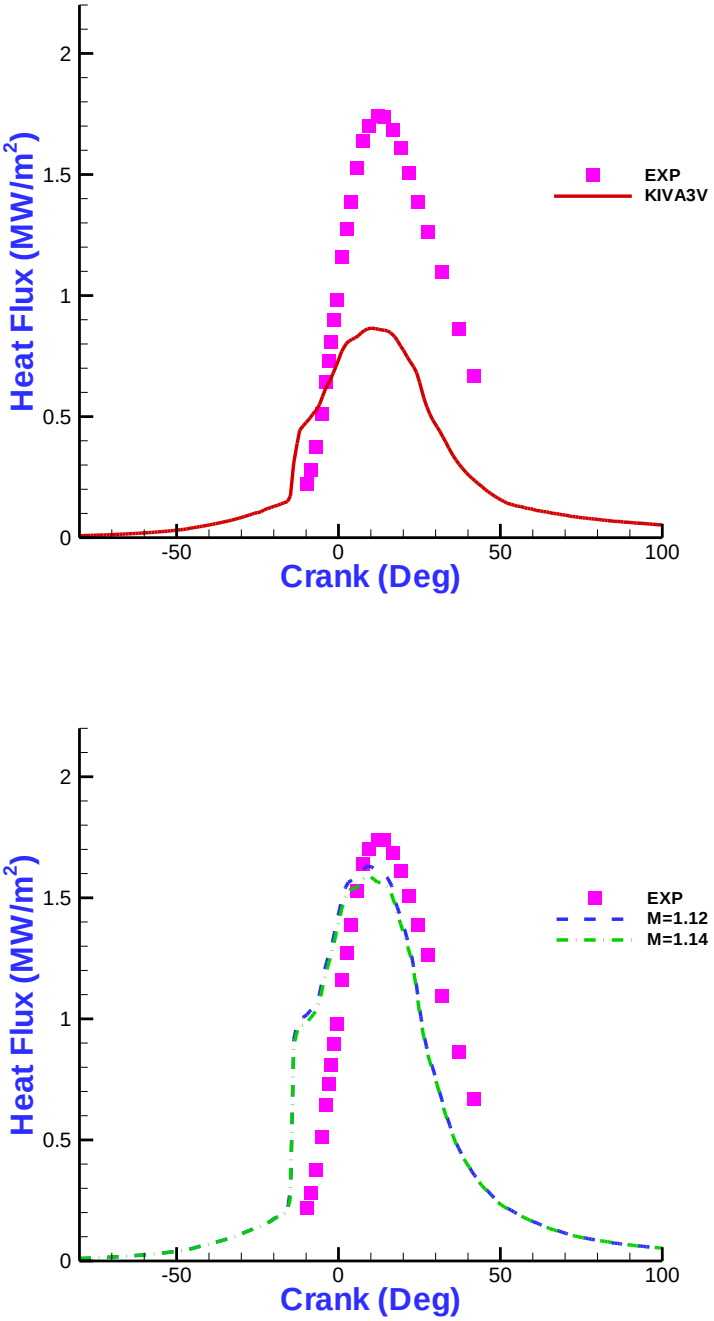

Figure 5. 12 Heat flux prediction for case 1

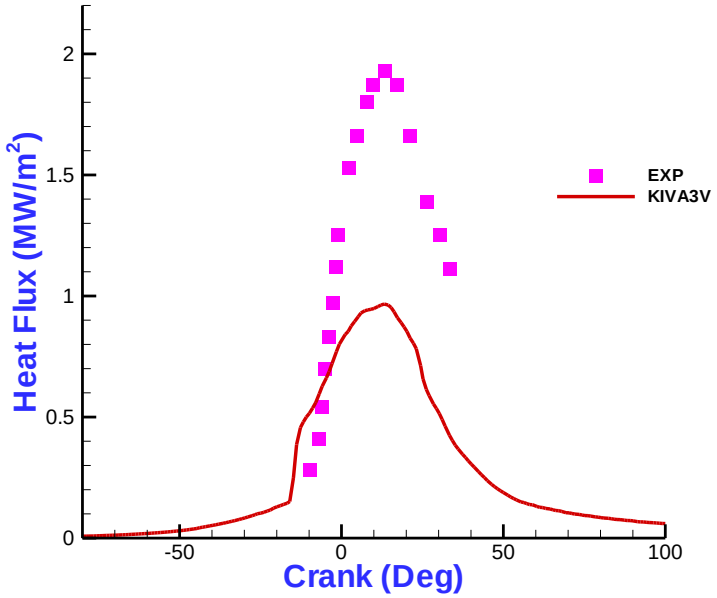

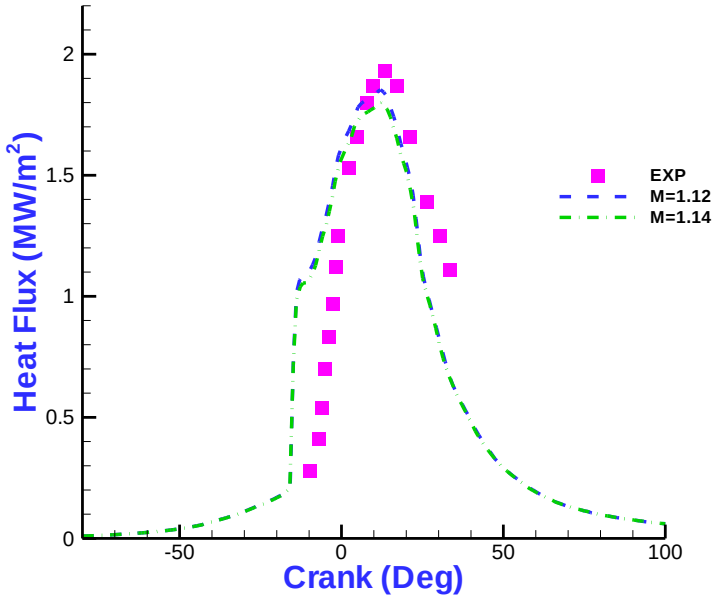

Figure 5. 13 Heat flux prediction for case 2

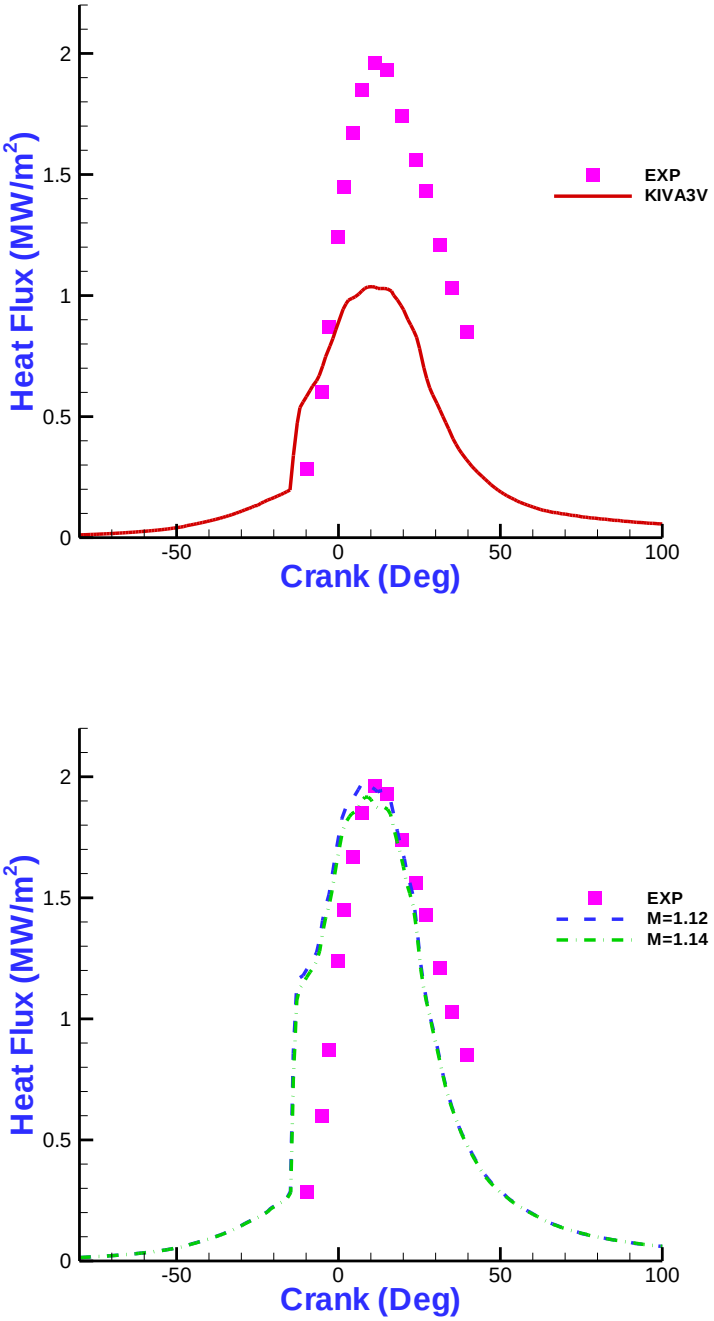

Figure 5. 14 Heat flux prediction for case 3

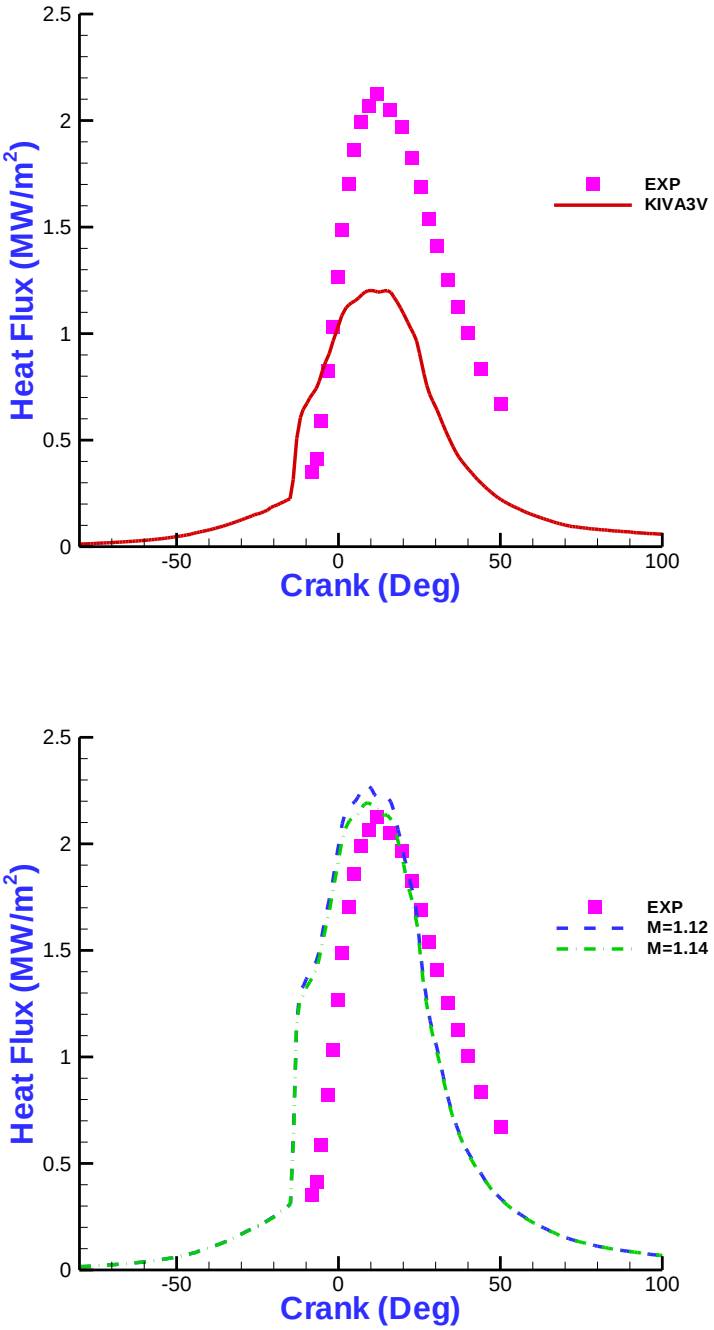

Figure 5. 15 Heat flux prediction for case 4

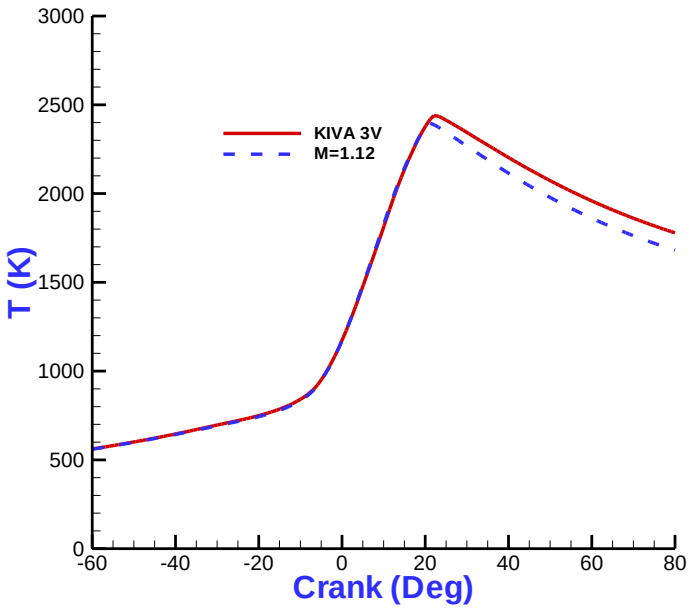

Figure 5. 16 Mean temperature for case 1

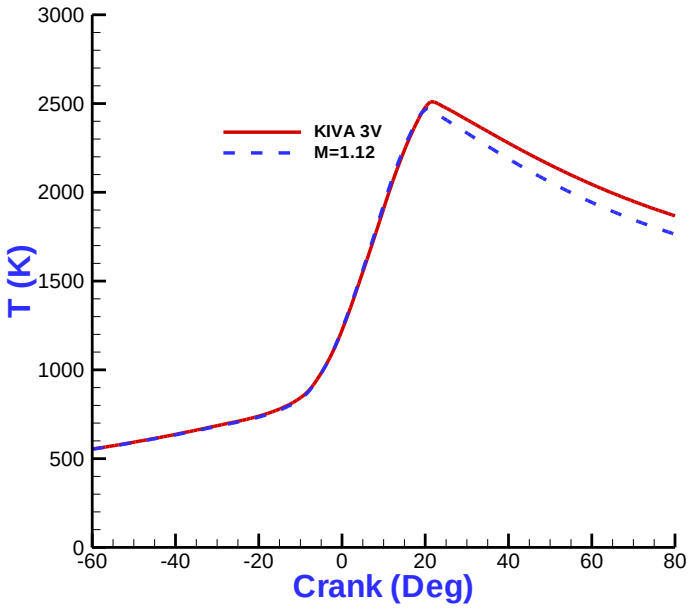

Figure 5. 17 Mean temperature for case 2

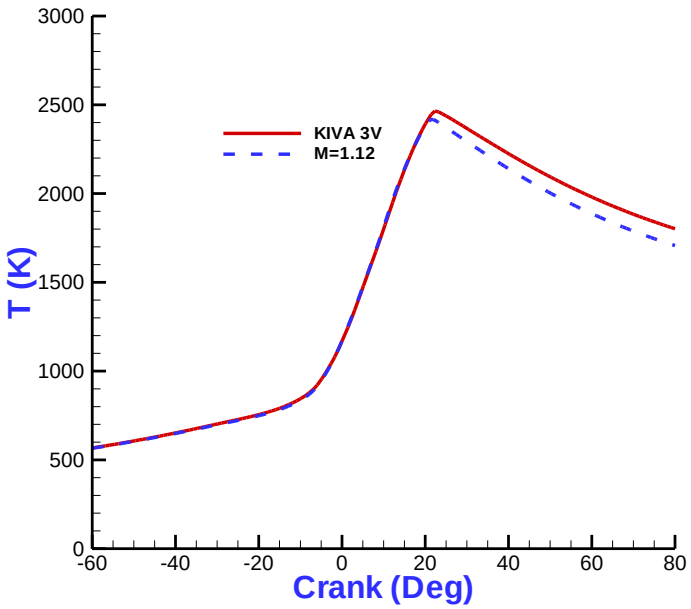

Figure 5. 18 Mean temperature for case 3

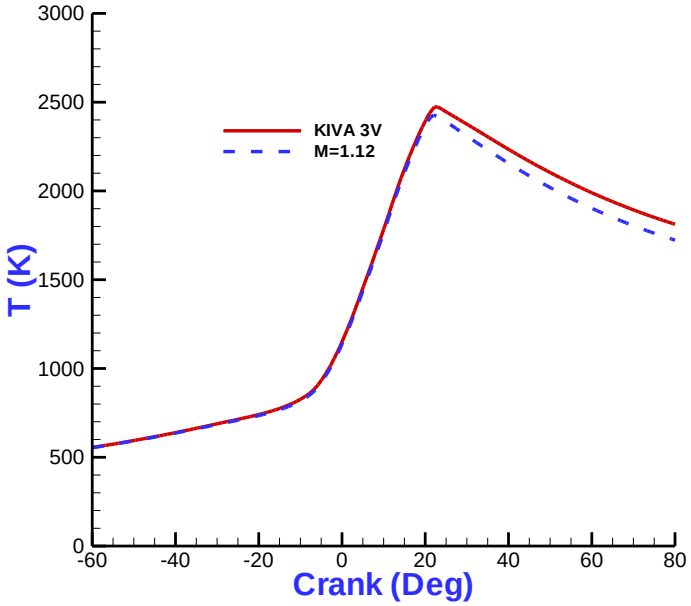

Figure 5. 19 Mean temperature for case 4

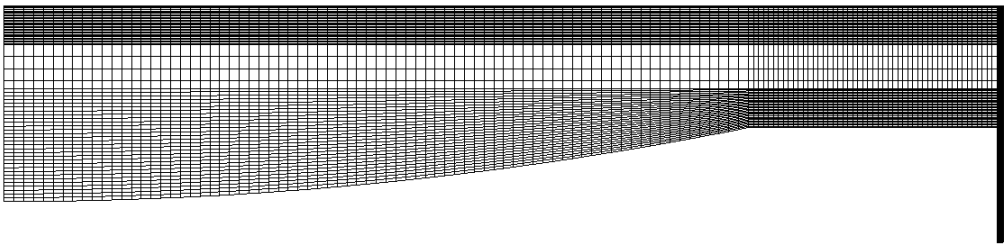

(a) Axis-symmetric mesh

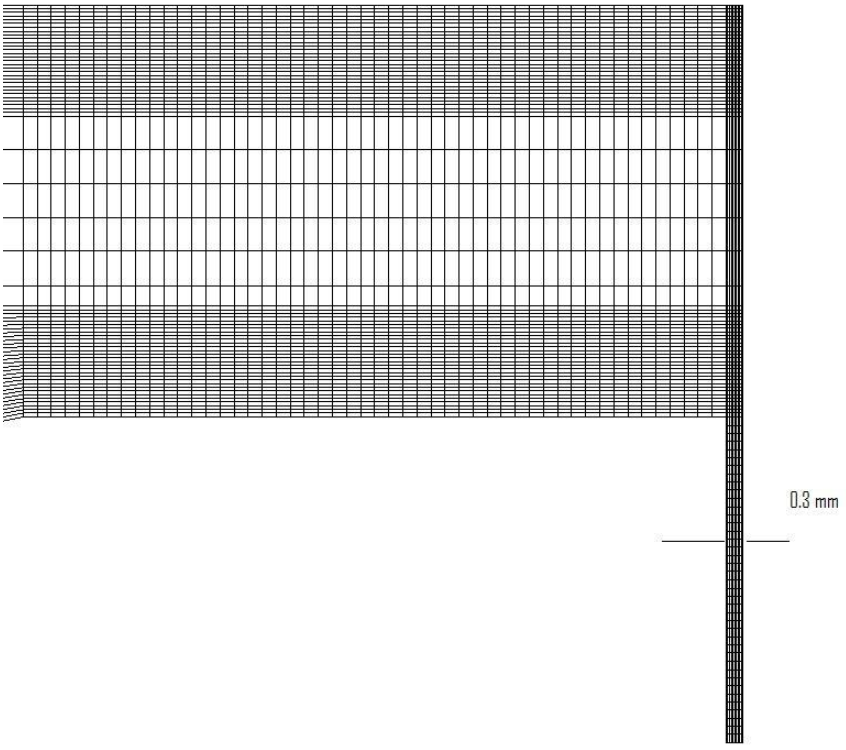

(b) Near crevice region

Figure 6. 1 The grids used for the calculation of HCCI cases at TDC

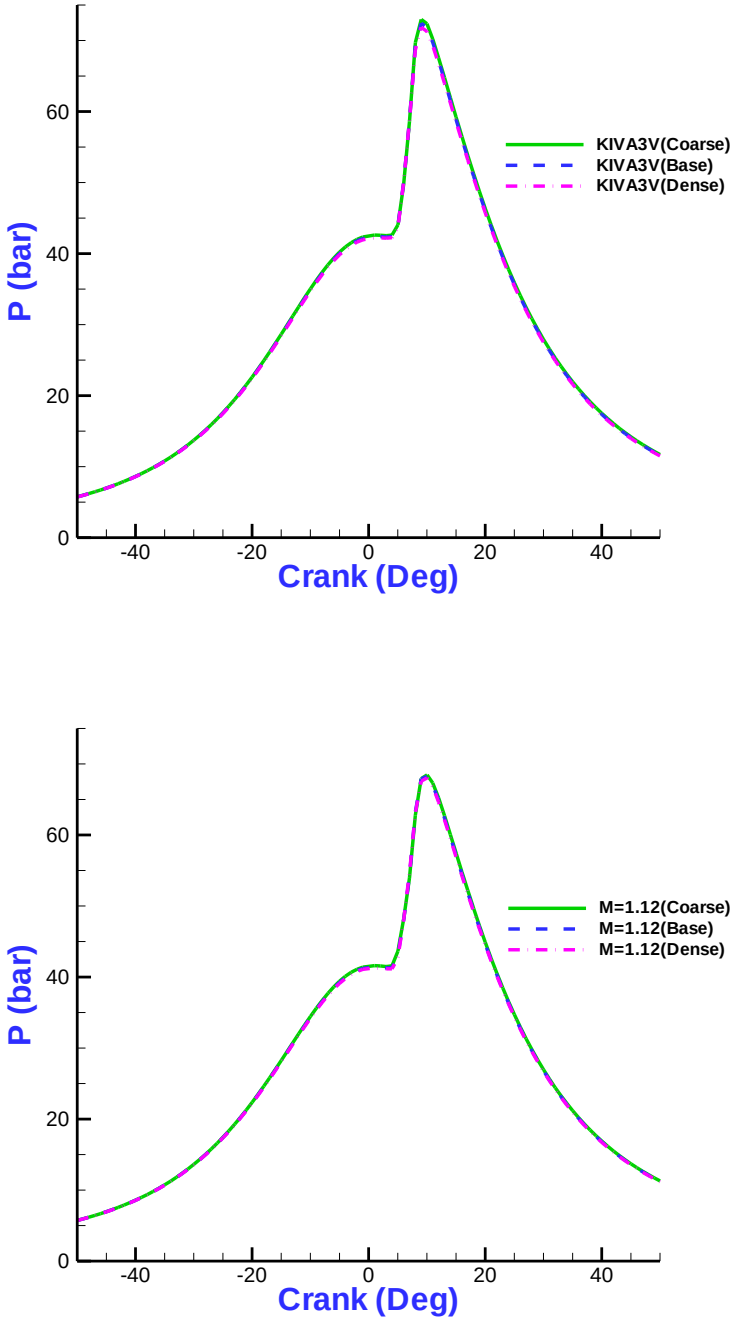

Figure 6. 2 Pressure trace prediction by different grid sets

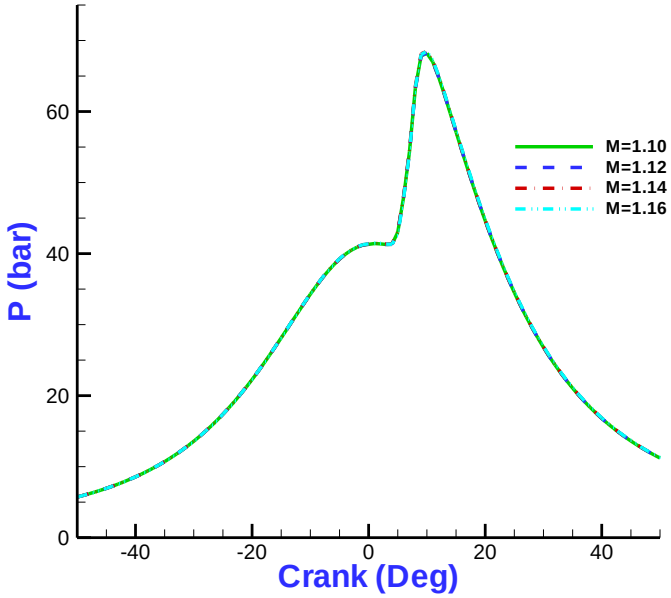

Figure 6. 3 Predicted pressure trace by different M values

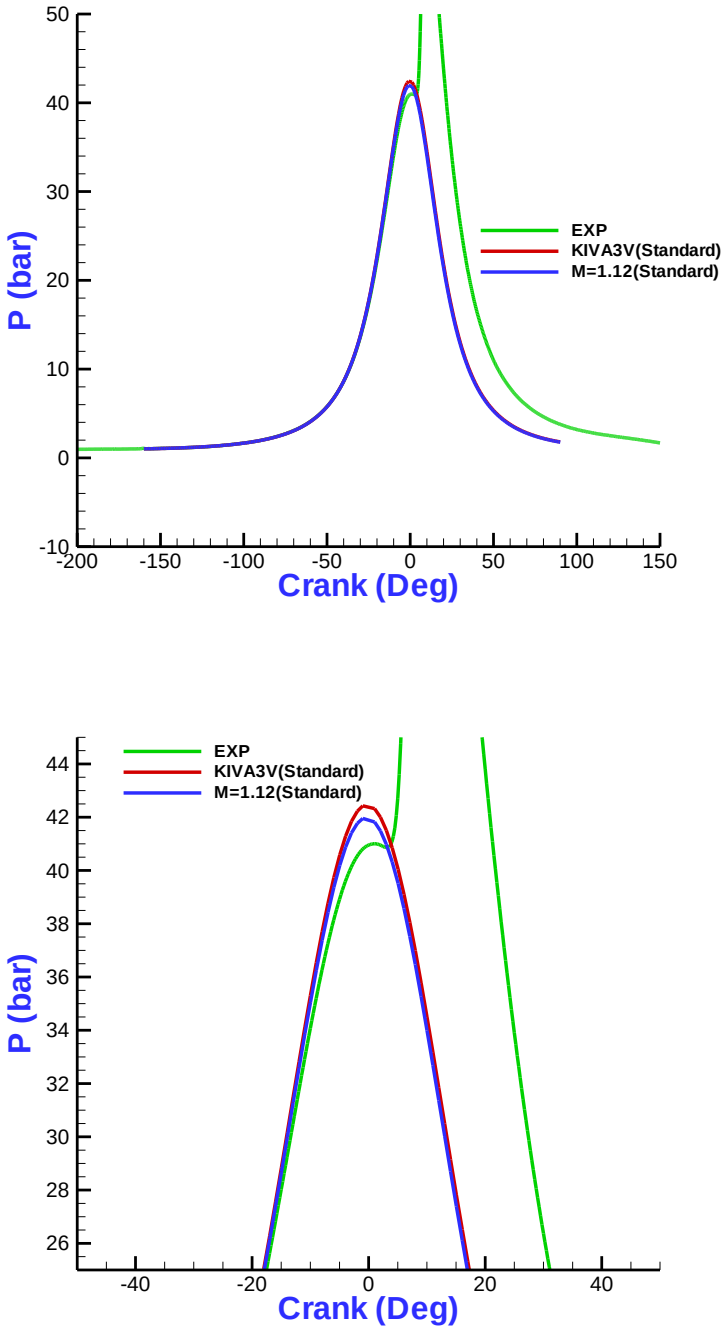

Figure 6. 4 Pressure trace of test case 1 with the standard *k*-*ε* model

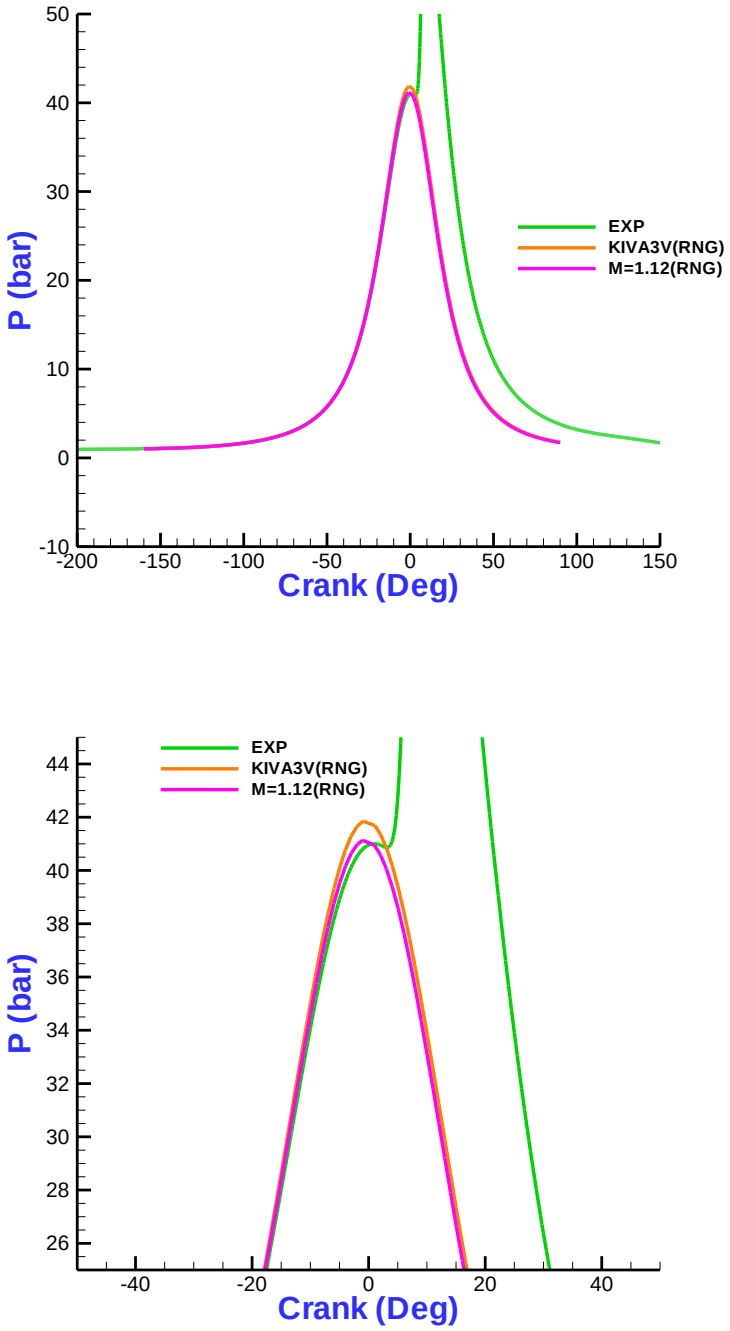

Figure 6. 5 Pressure trace of test case 1 with the RNG *k*-*ε* model

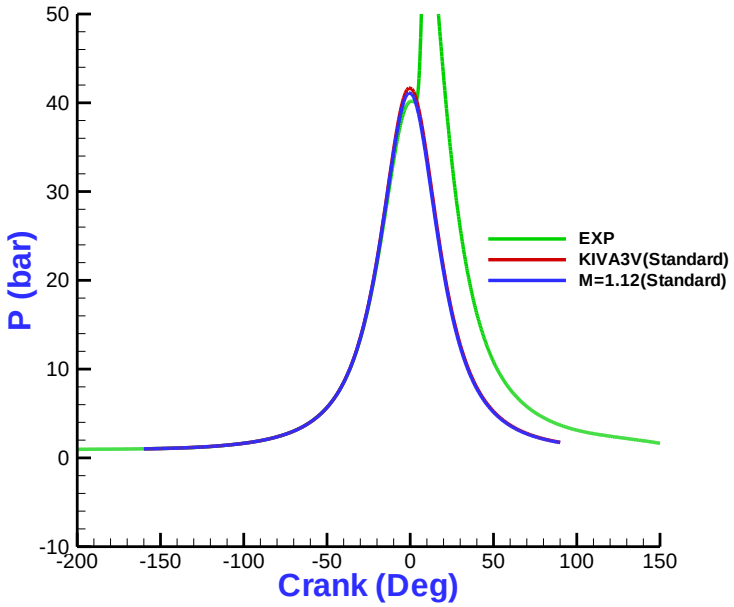

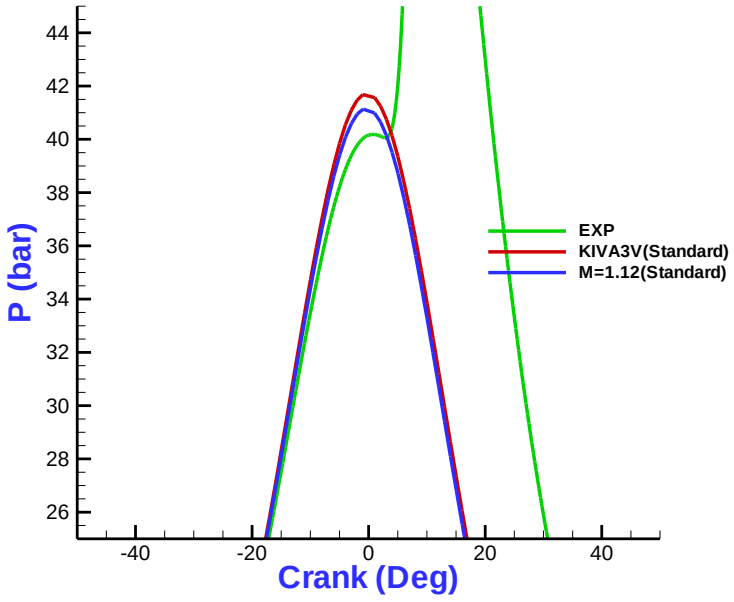

Figure 6. 6 Pressure trace of test case 2 with the standard *k*-ε model

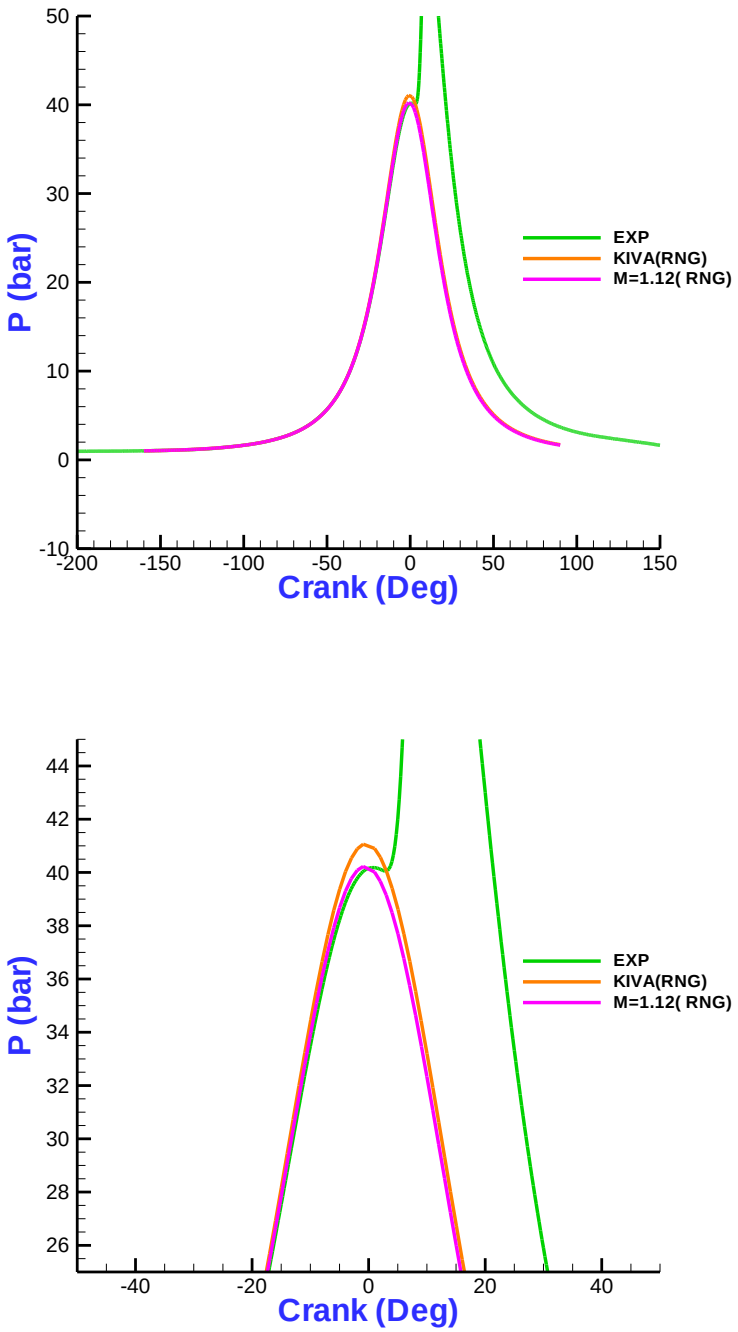

Figure 6. 7 Pressure trace of test case 2 with the RNG *k*-ε model

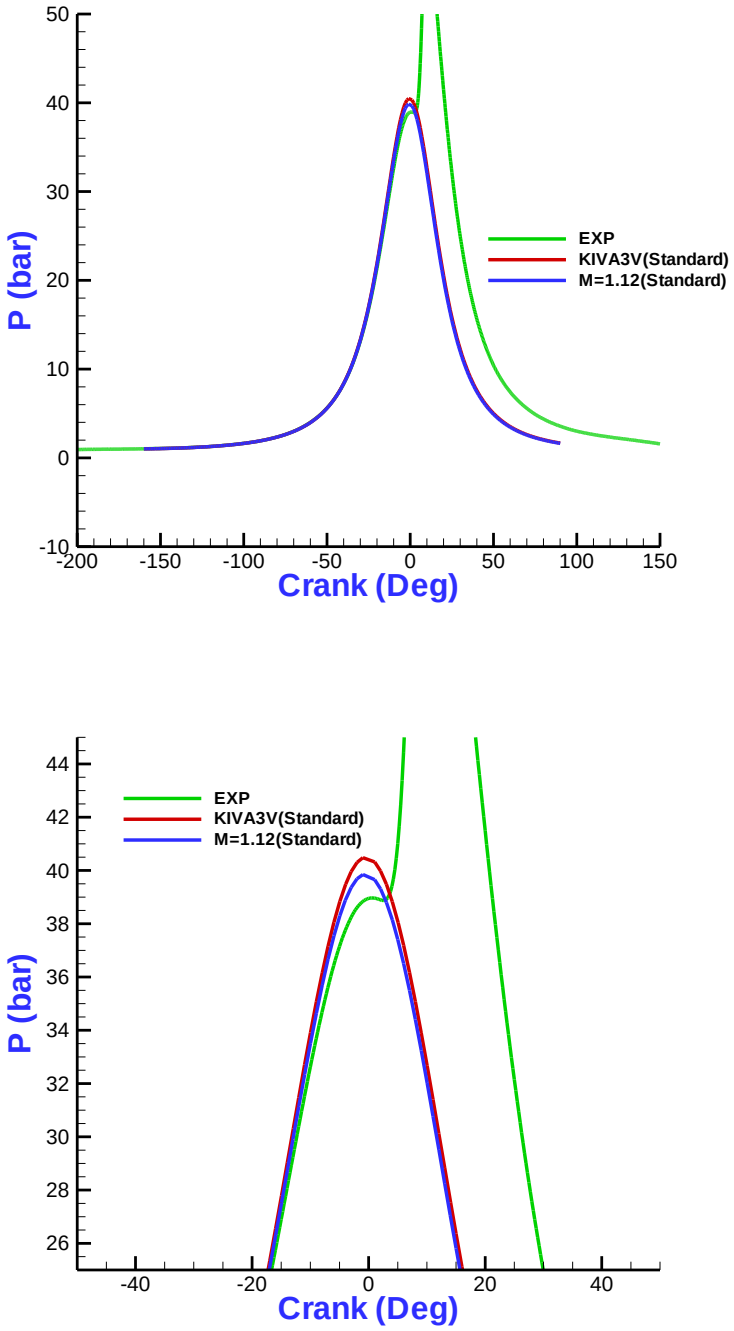

Figure 6. 8 Pressure trace of test case 3 with the standard *k*-*ε* model

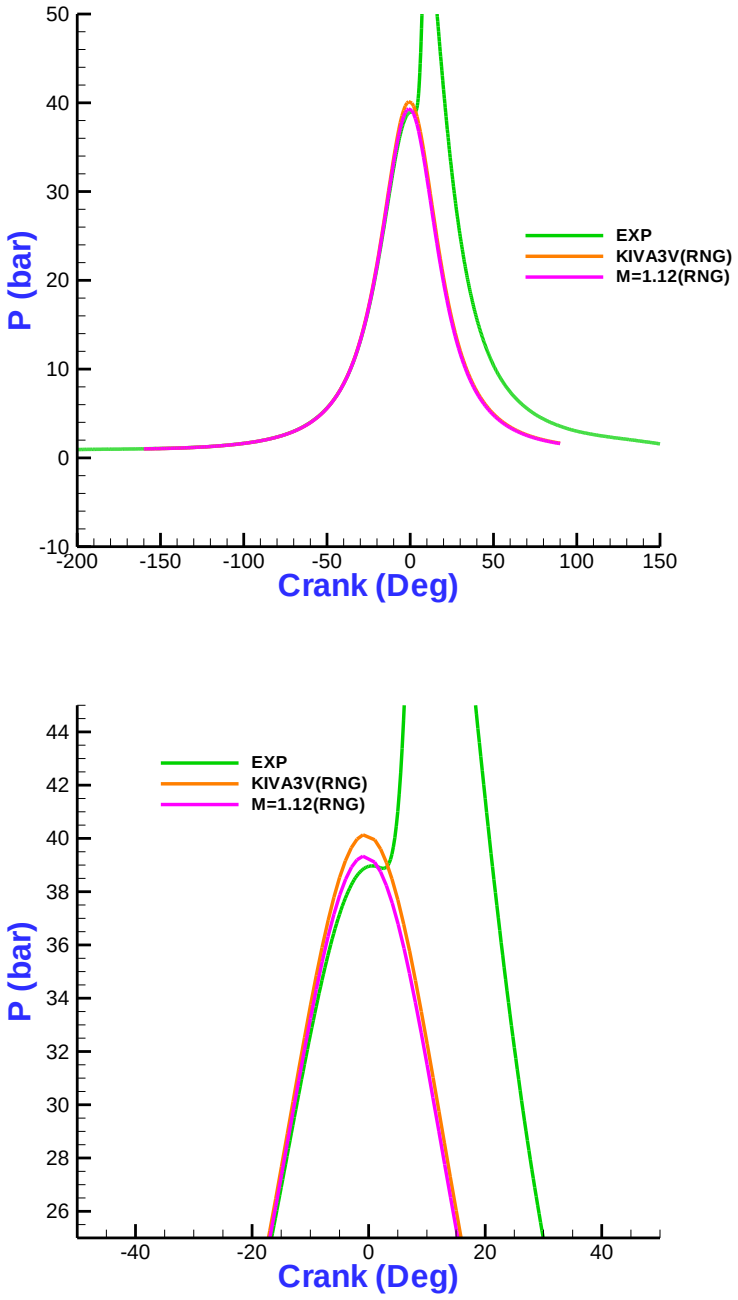

Figure 6. 9 Pressure trace of test case 3 with the RNG *k*-*ε* model

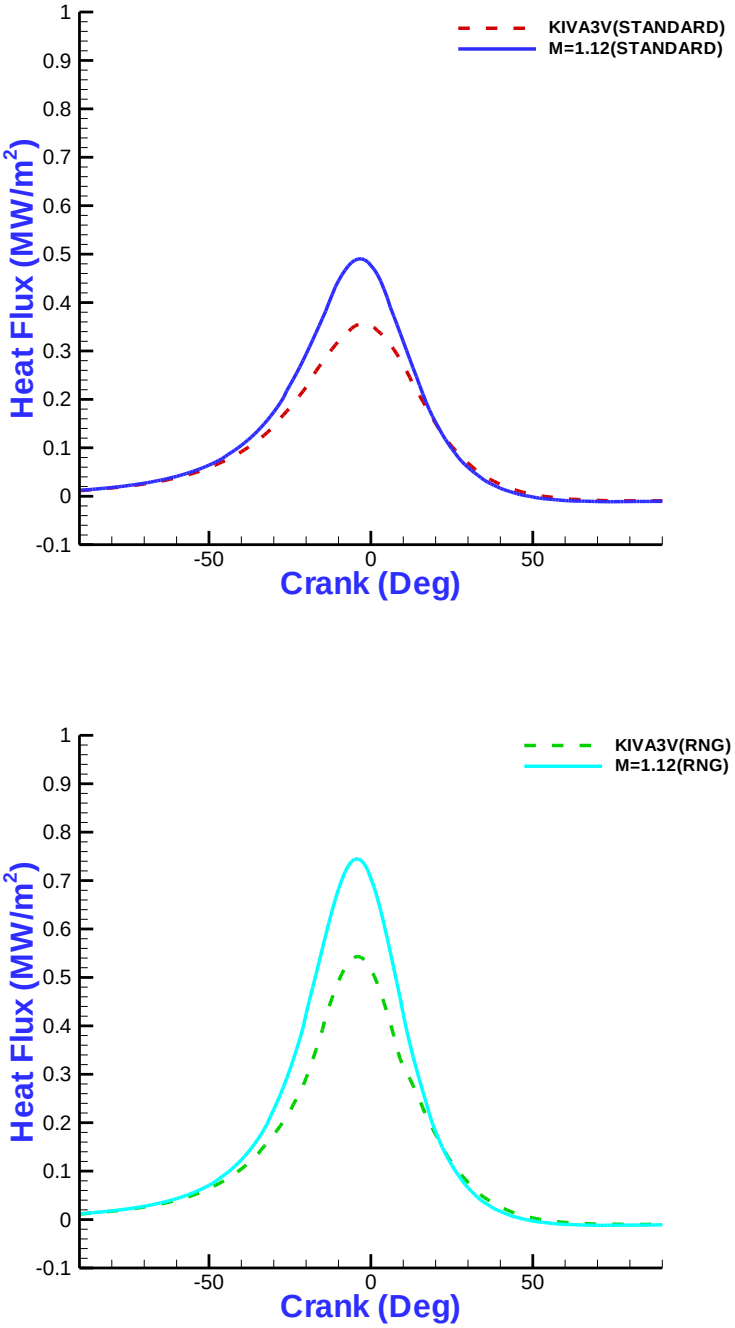

Figure 6. 10 Prediction of averaged heat flux of head surface for test case 1

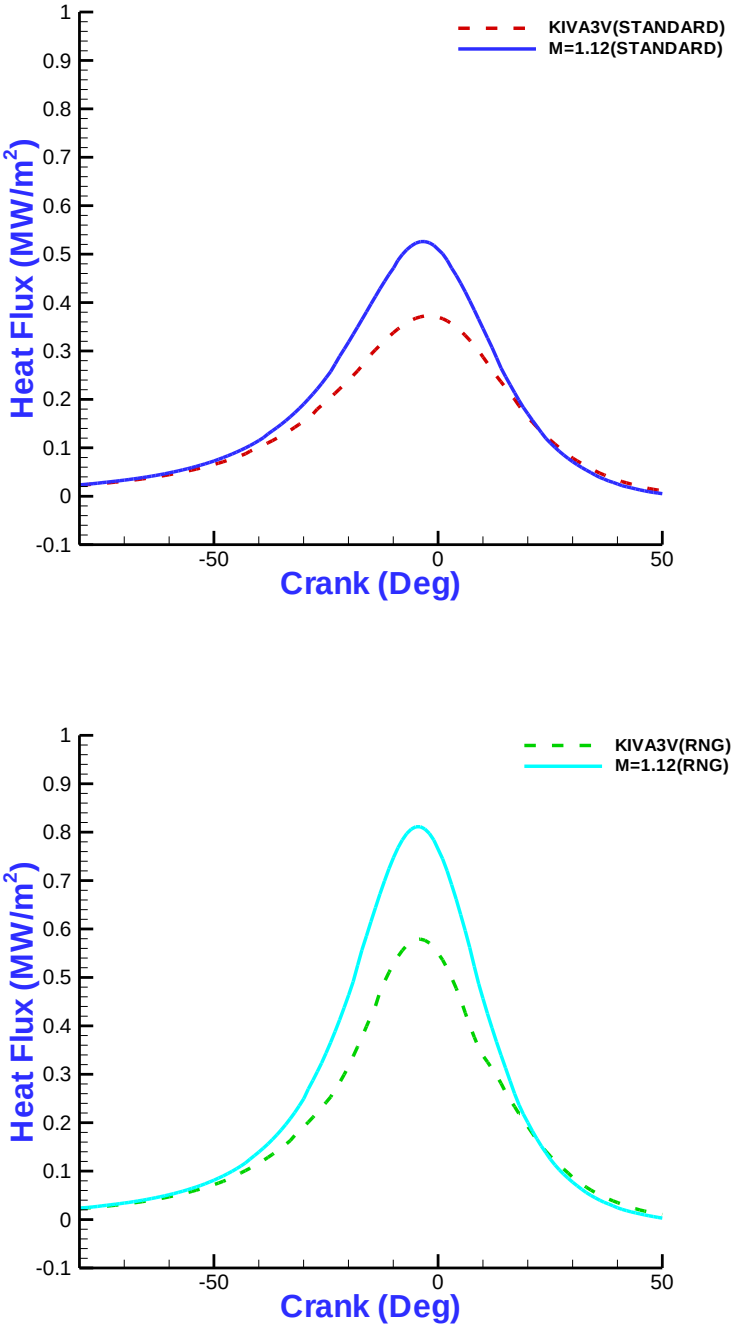

Figure 6. 11 Prediction of averaged heat flux of head surface for test case 2

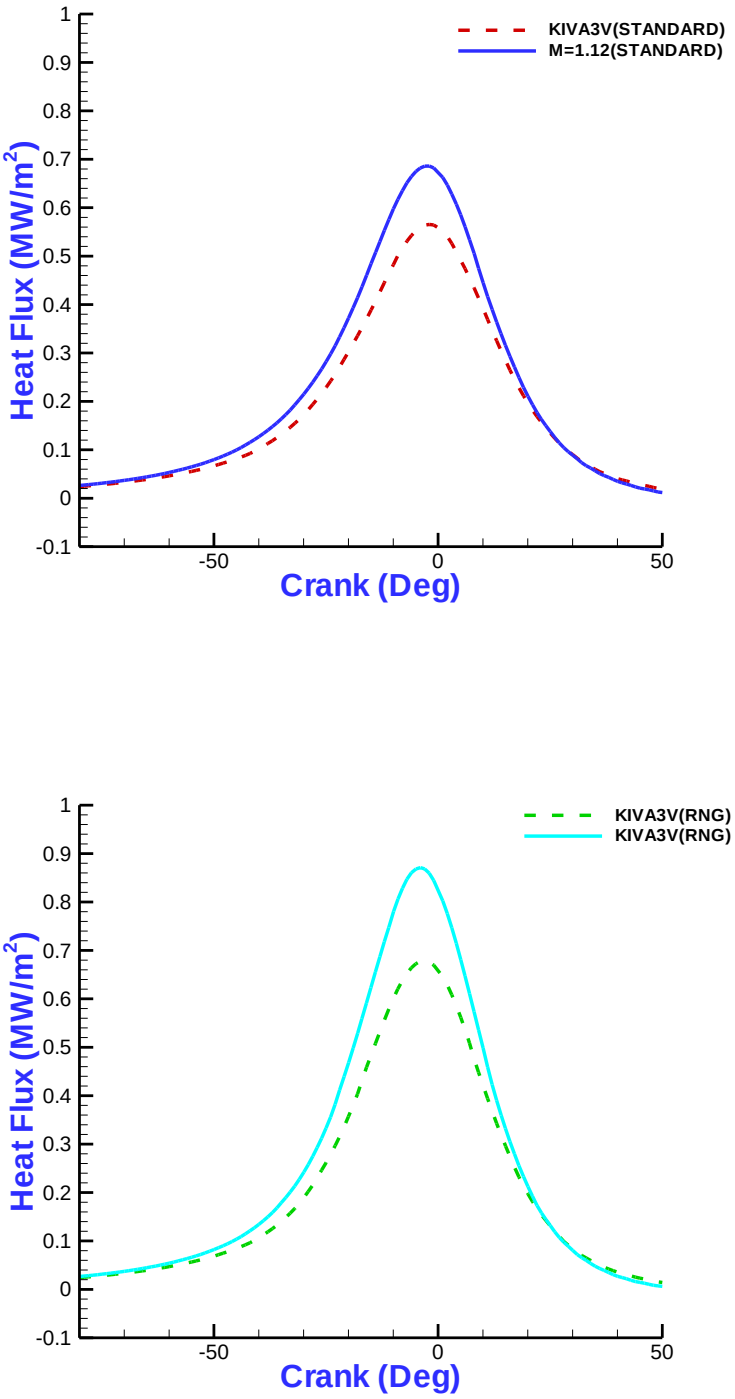

Figure 6. 12 Prediction of averaged heat flux of head surface for test case 3

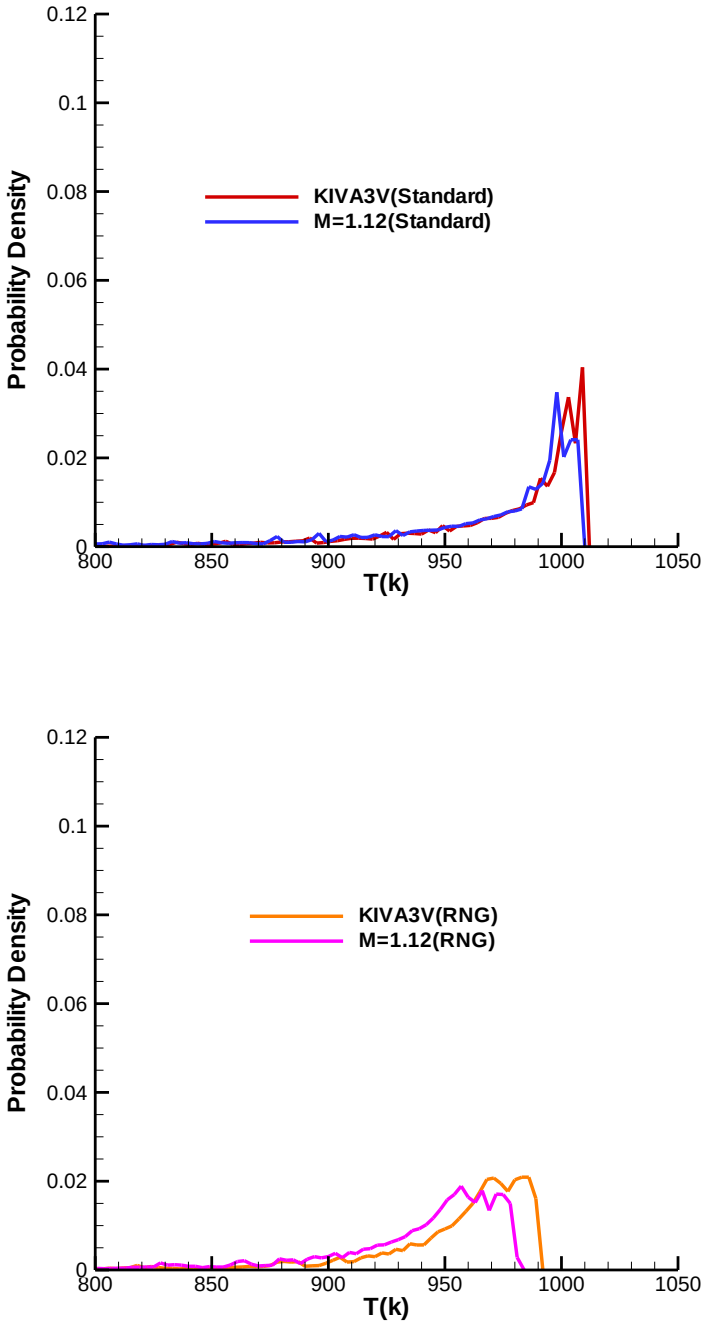

Figure 6. 13 Prediction of probability density of the charge temperature at 5 ATDC for test case 1

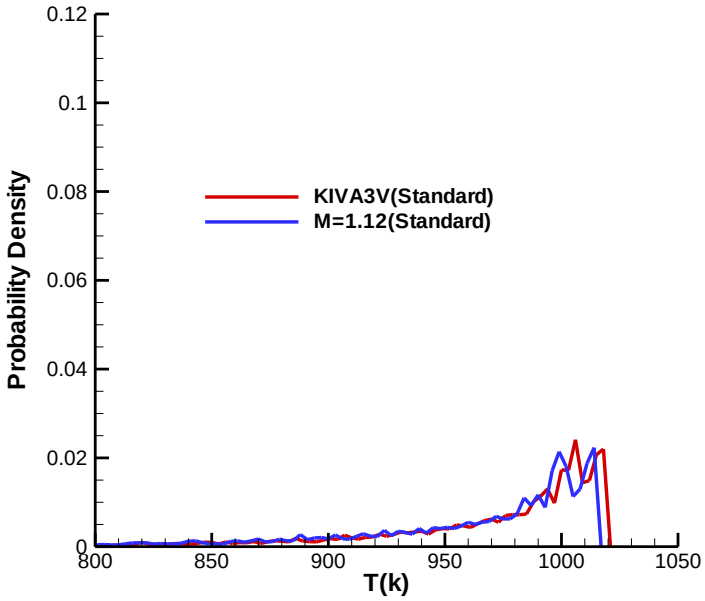

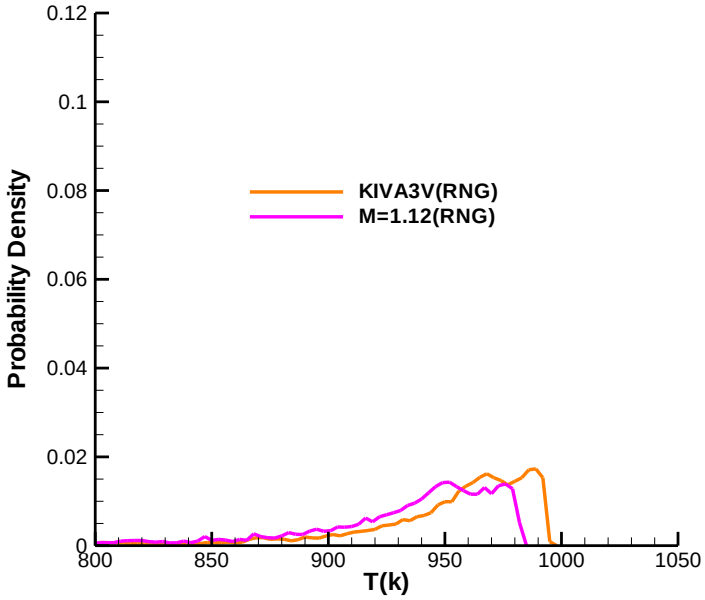

Figure 6. 14 Prediction of probability density of the charge temperature at 5 ATDC for test case 2

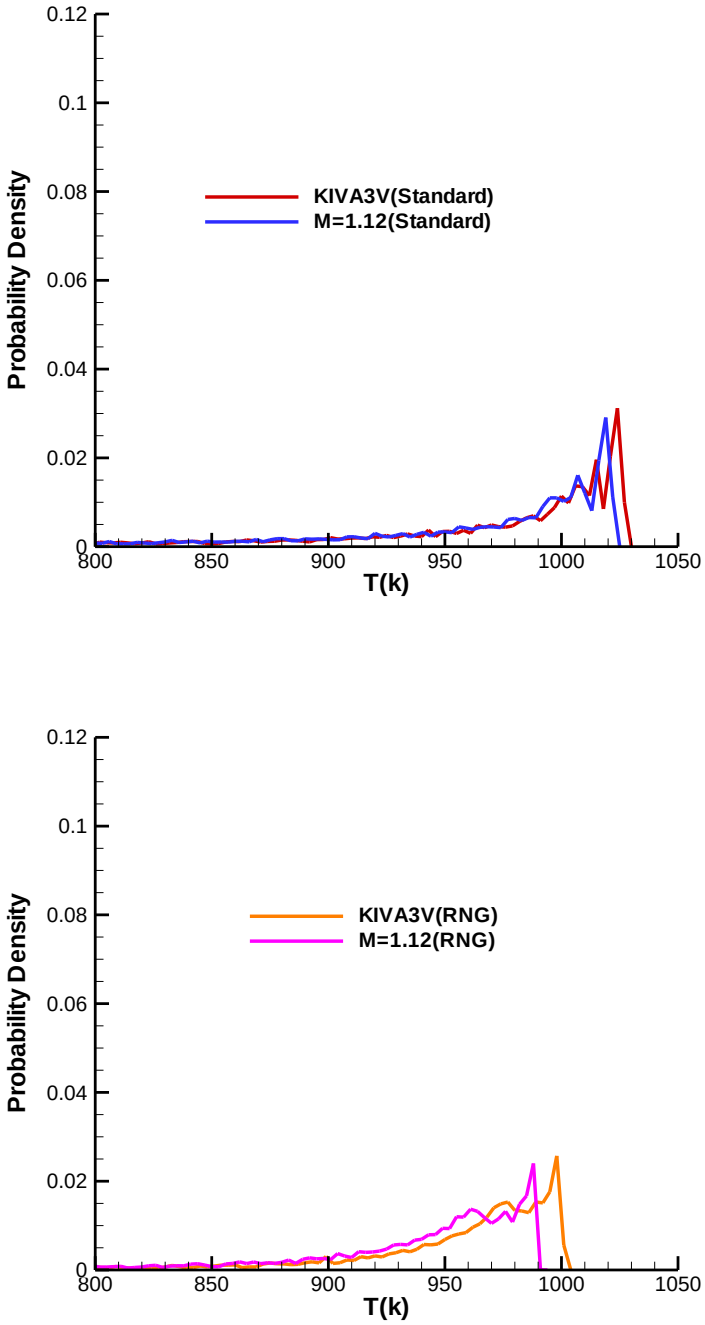

Figure 6. 15 Prediction of probability density of the charge temperature at 5 ATDC for test case 3

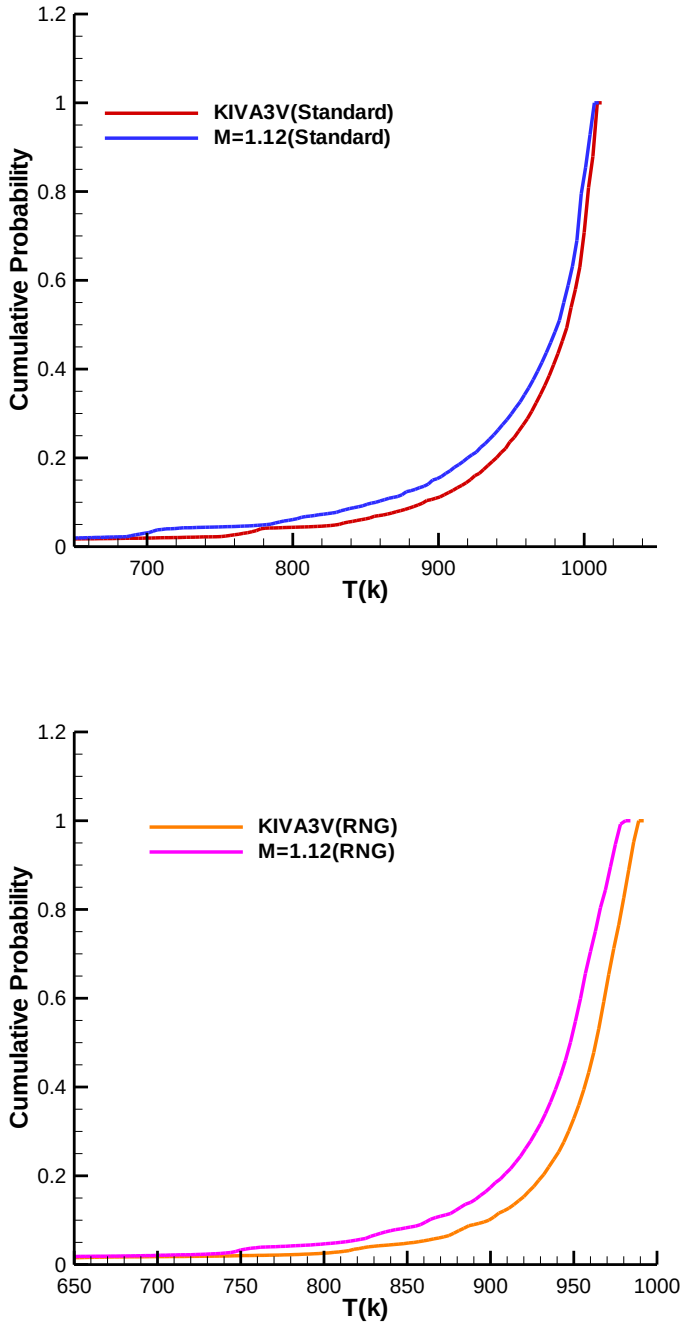

Figure 6. 16 Cumulative probability of the charge temperature at 5 ATDC for test case 1

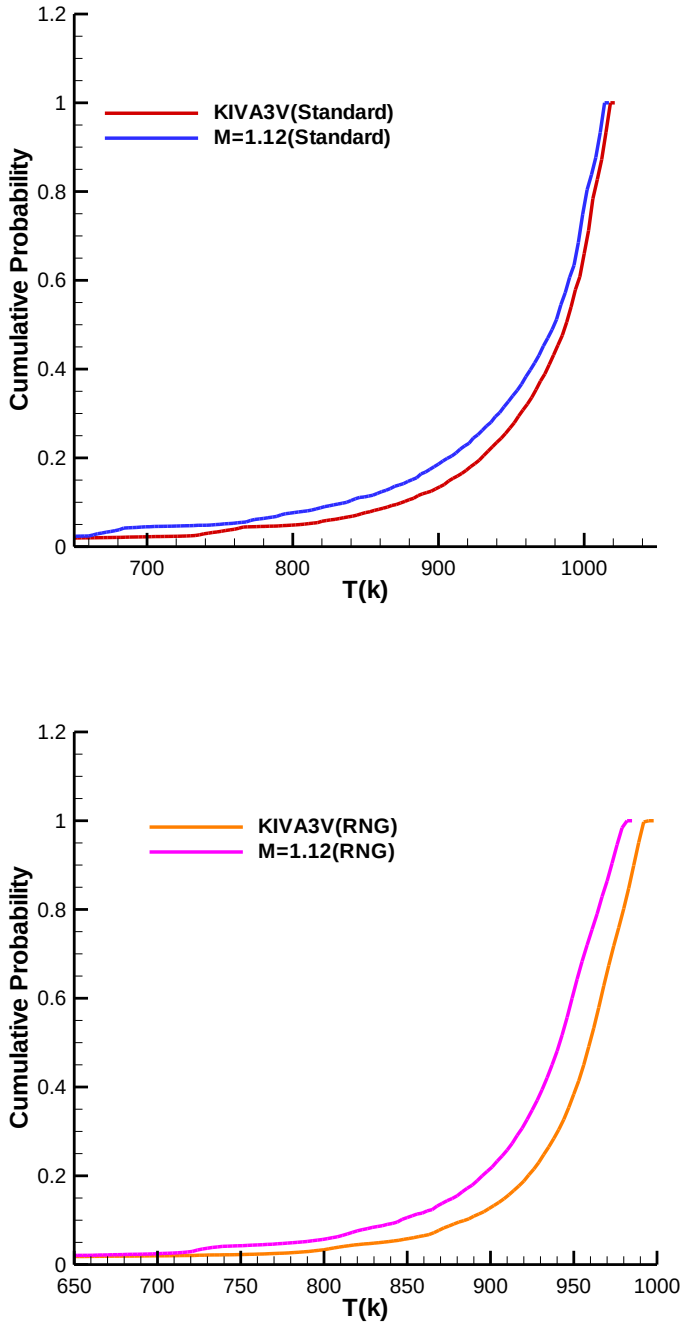

Figure 6. 17 Cumulative probability of the charge temperature at 5 ATDC for test case 2

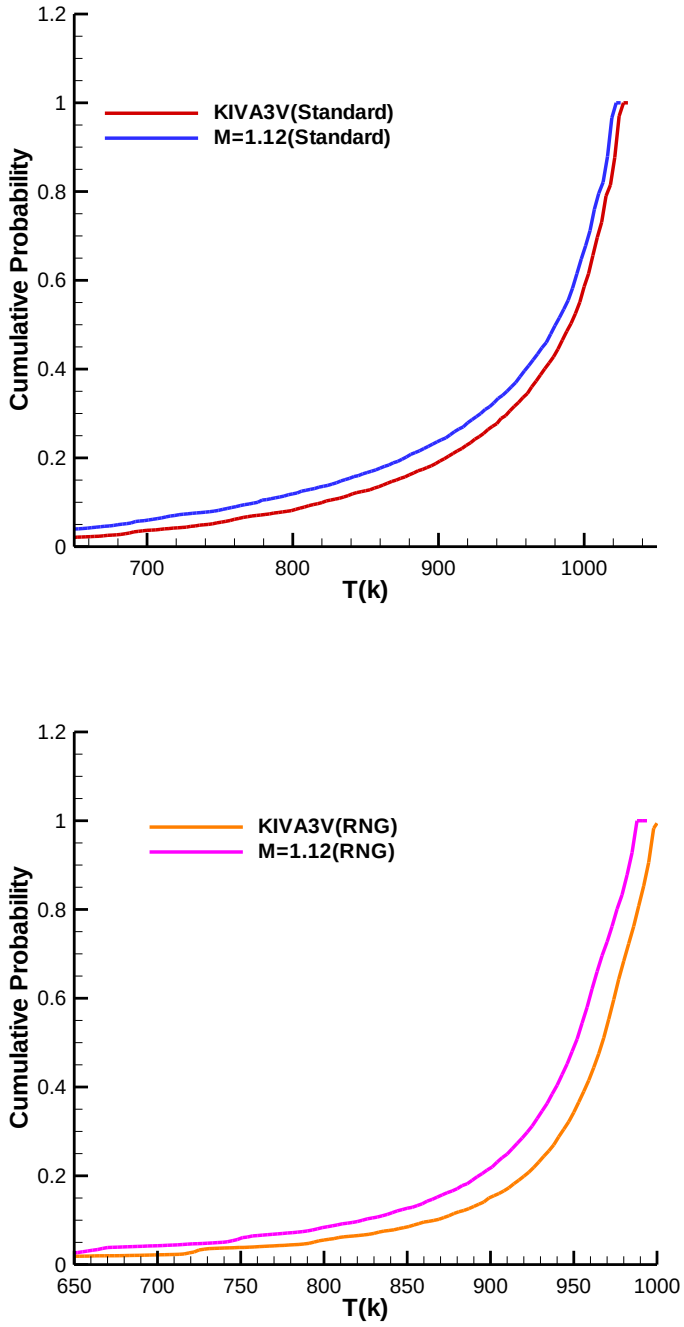

Figure 6. 18 Cumulative probability of the charge temperature at 5 ATDC for test case 3

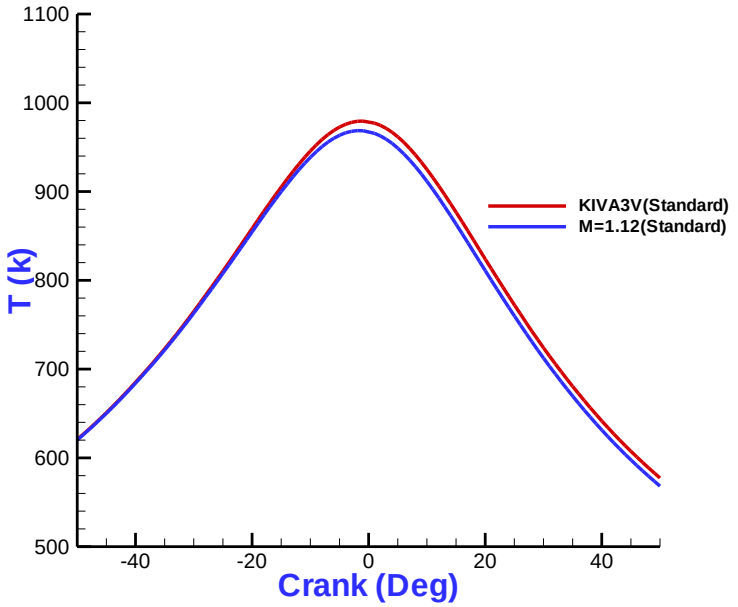

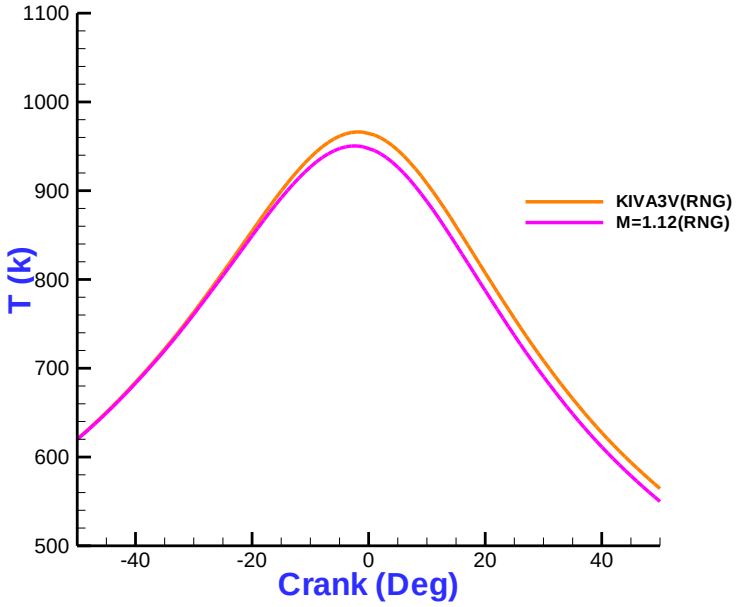

Figure 6. 19 Prediction of mean charge temperature for test case 1

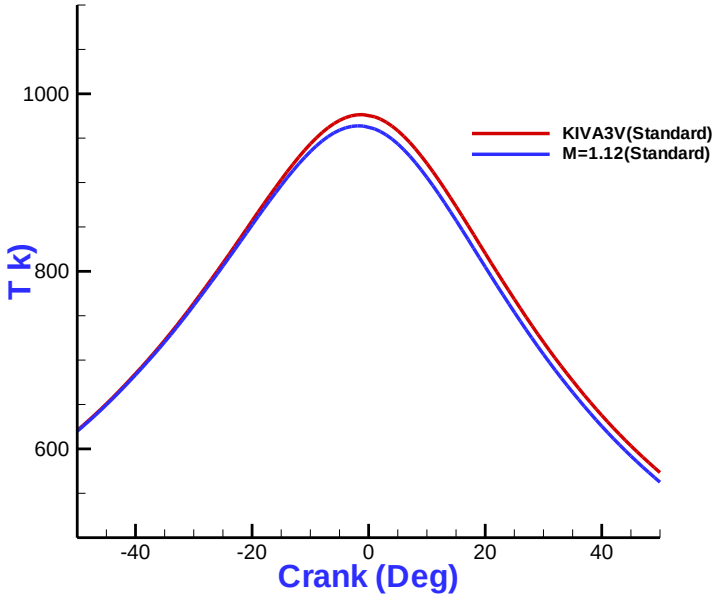

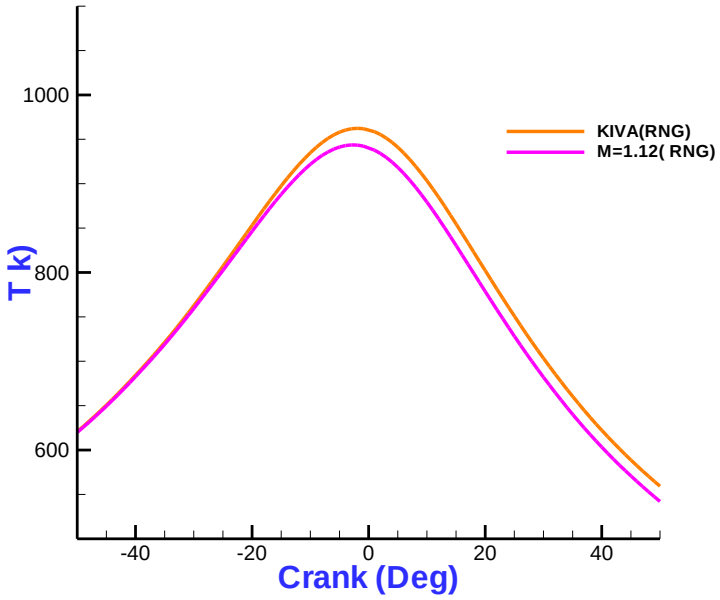

Figure 6. 20 Prediction of mean charge temperature for test case 2

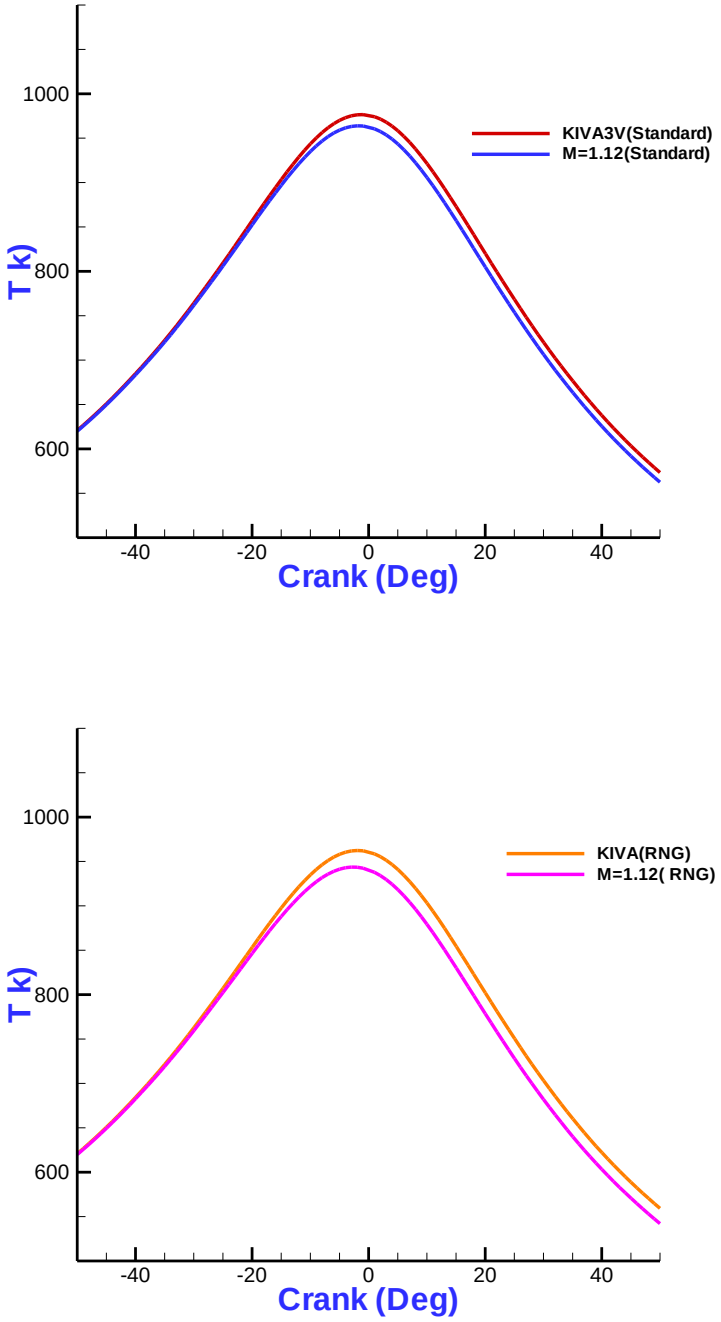

Figure 6. 21 Prediction of mean charge temperature for test case 3

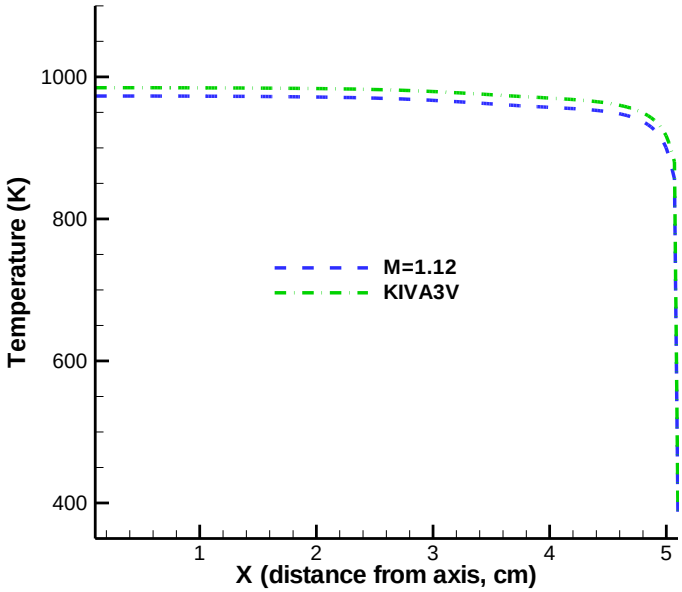
1000
800
600
400
Temperature (K)
M=1.12
KIVA3V
1
2
3
4
5
X (distance from axis, cm)

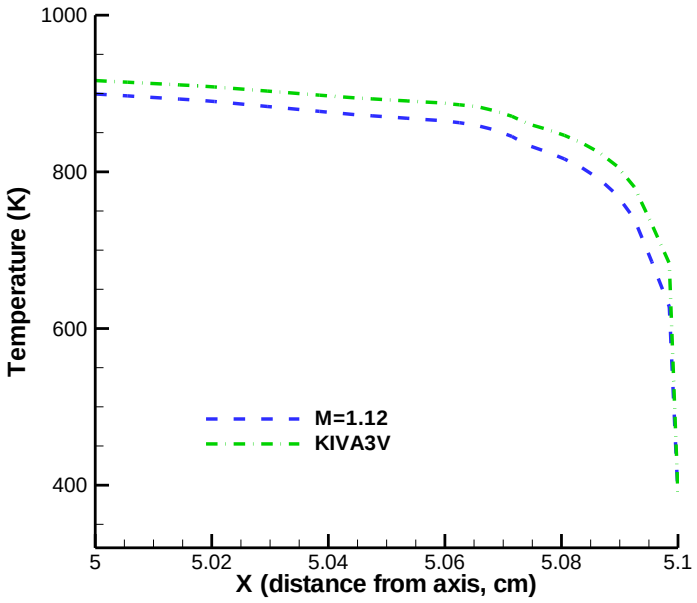
1000
800
600
400
Temperature (K)
M=1.12
KIVA3V
5
5.02
5.04
5.06
5.08
5.1
X (distance from axis, cm)

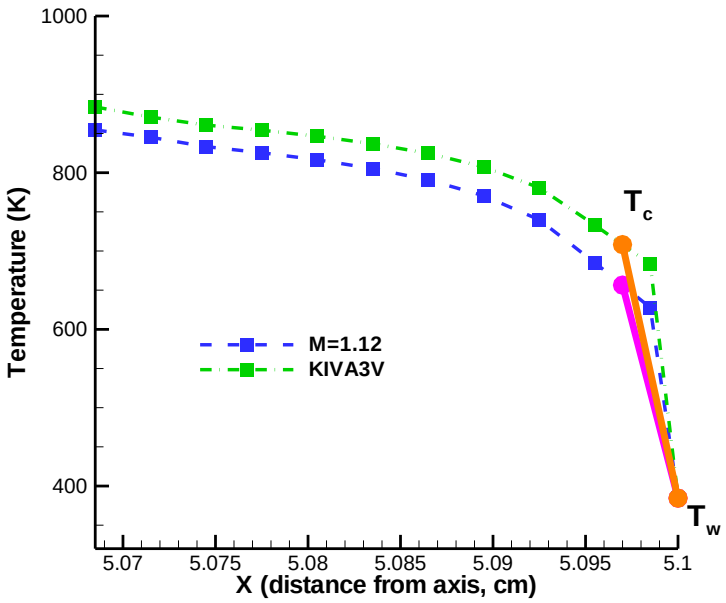

Figure 6. 22 Temperature profiles for the location of 3 mm below cylinder head at 5 ATDC (CASE 1)

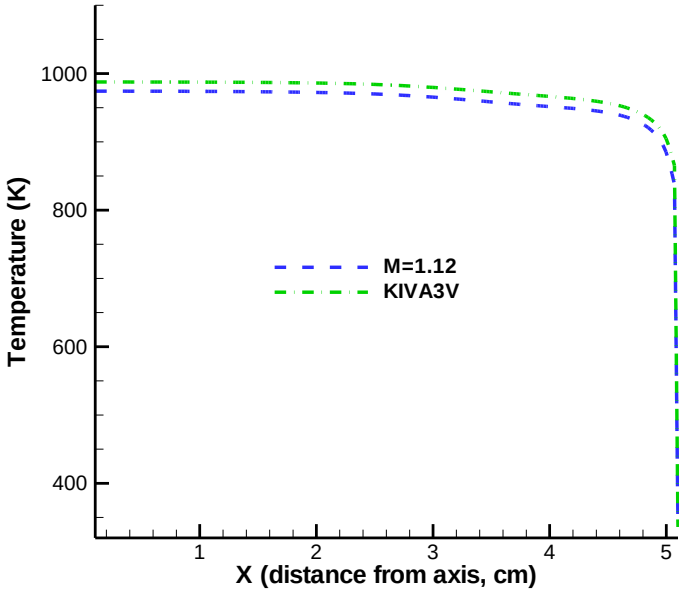

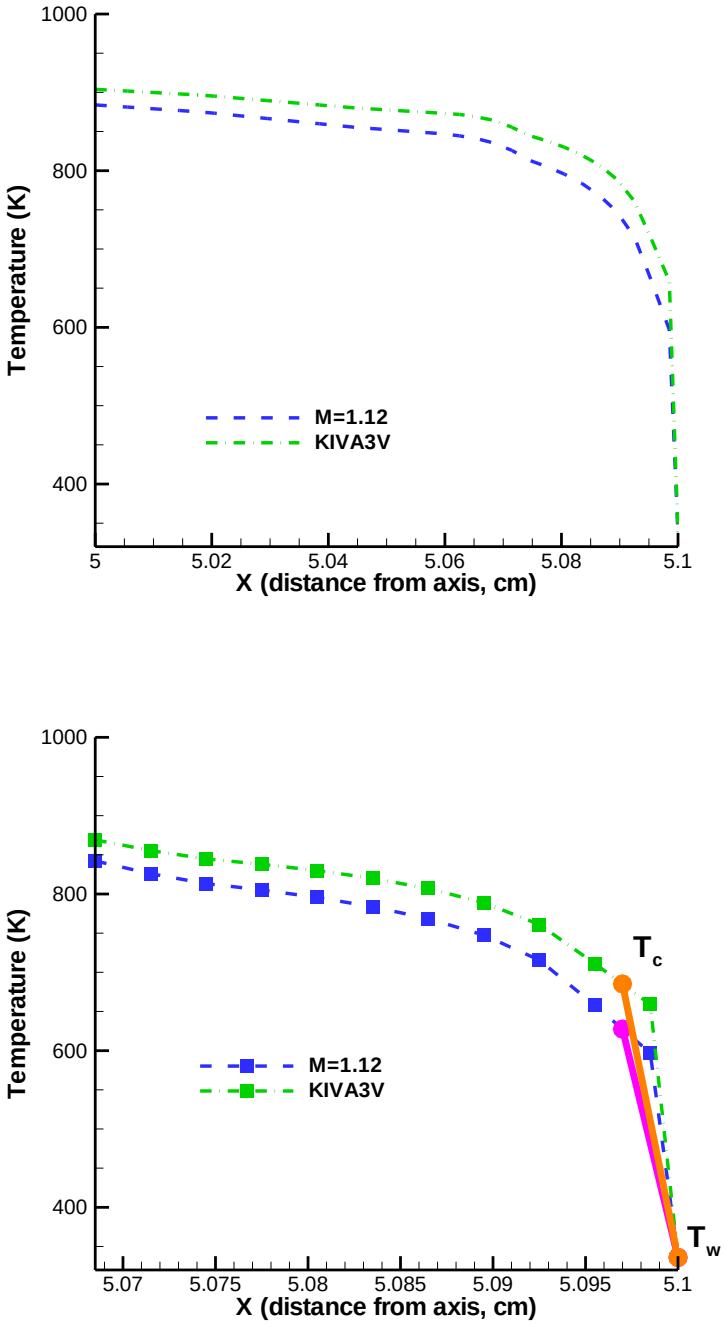

Figure 6. 23 Temperature profiles for the location of 3 mm below cylinder head at 5 ATDC (CASE 2)

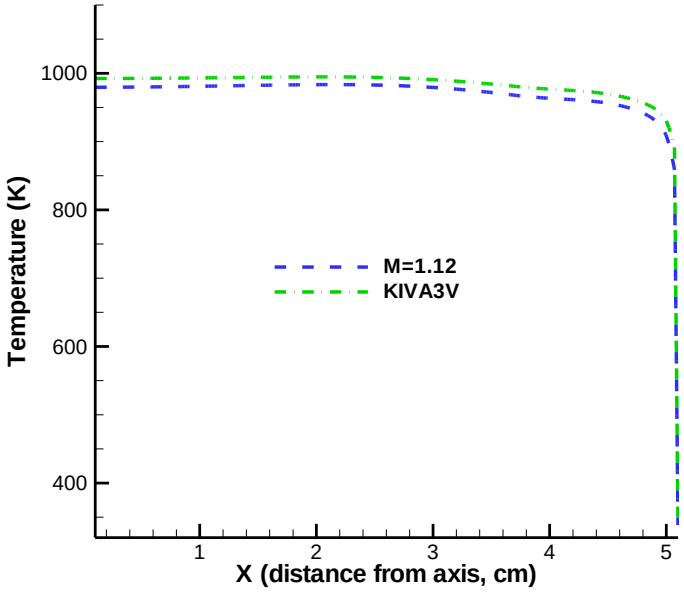
1000
800
600
400
Temperature (K)
M=1.12
KIVA3V
1
2
3
4
5
X (distance from axis, cm)

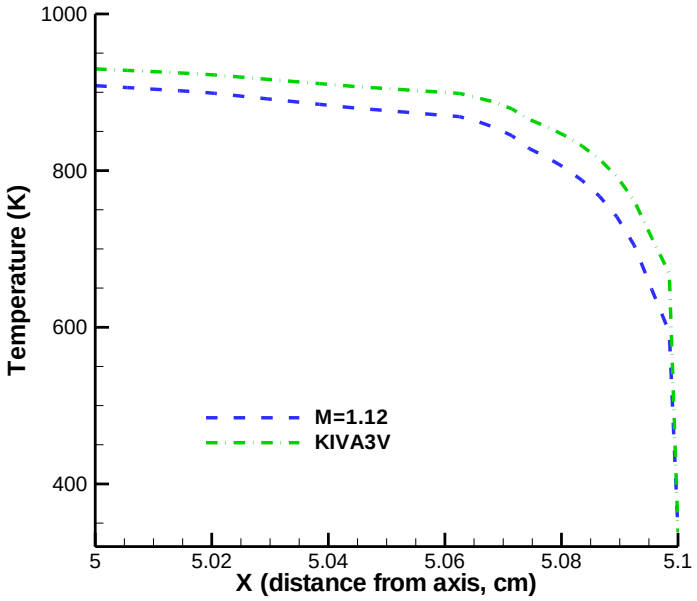
1000
800
600
400
Temperature (K)
M=1.12
KIVA3V
5
5.02
5.04
5.06
5.08
5.1
X (distance from axis, cm)

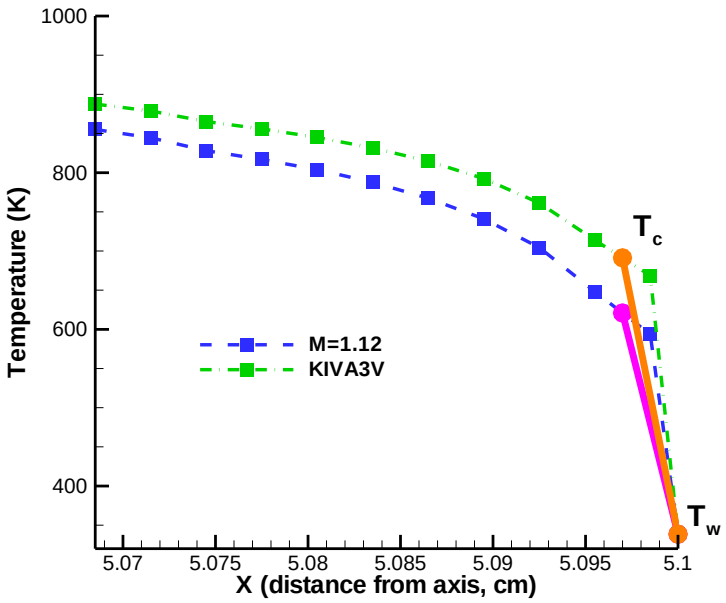

Figure 6. 24 Temperature profiles for the location of 3 mm below cylinder head at 5 ATDC (CASE 3)

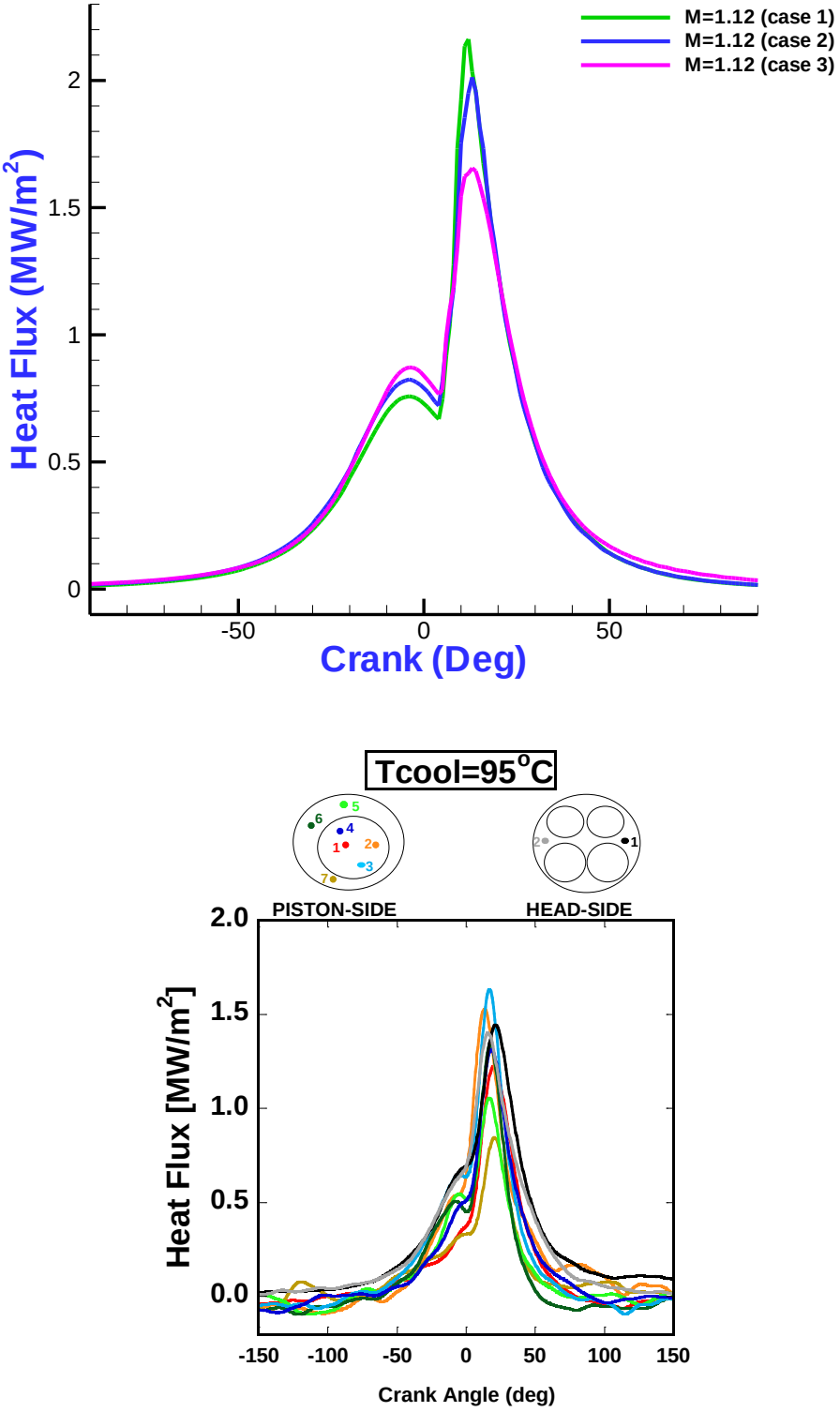

Figure 6. 25 Heat flux shape comparison to experimental data

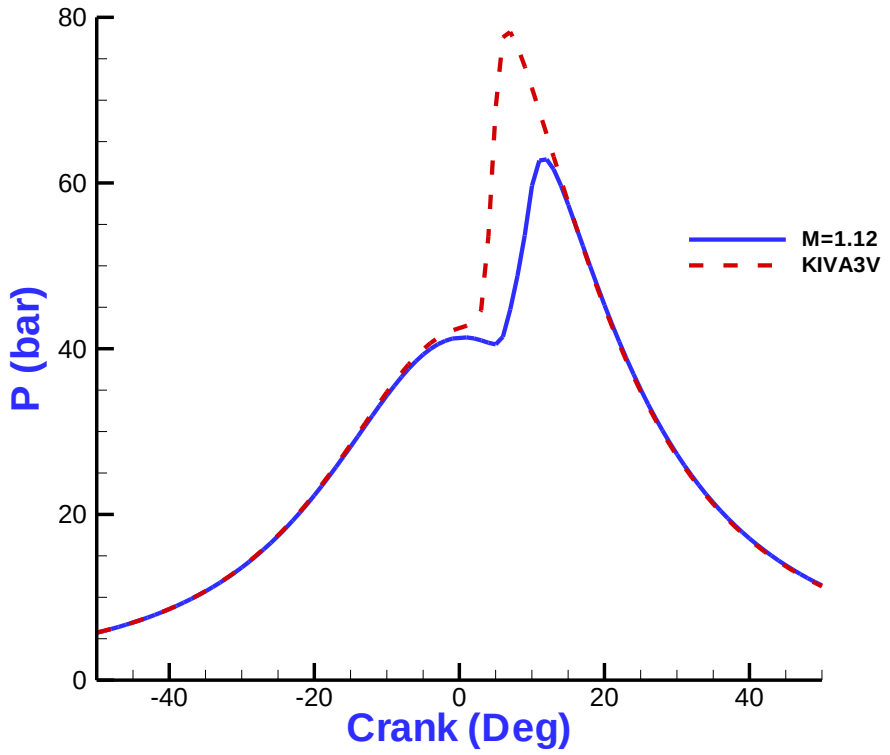

Figure 6. 26 Comparison of pressure trace prediction when the same initial charge temperature is used for each heat transfer model

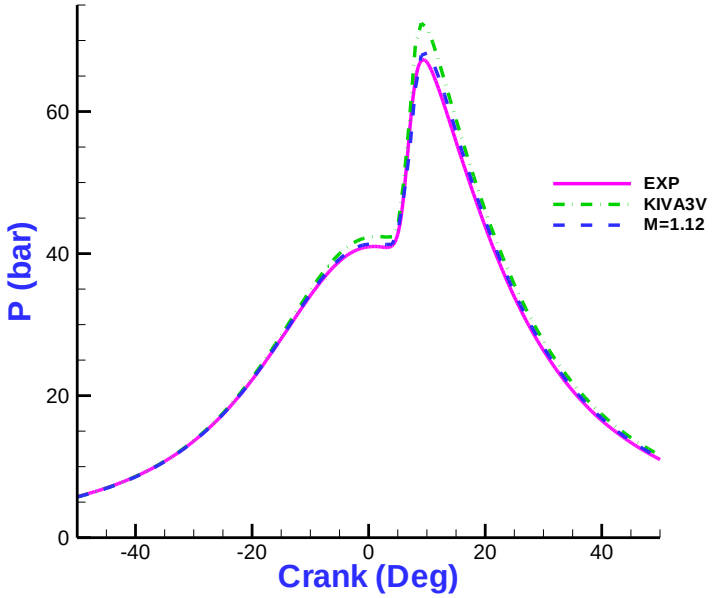

Figure 6. 27 Comparison of pressure trace for test case 1

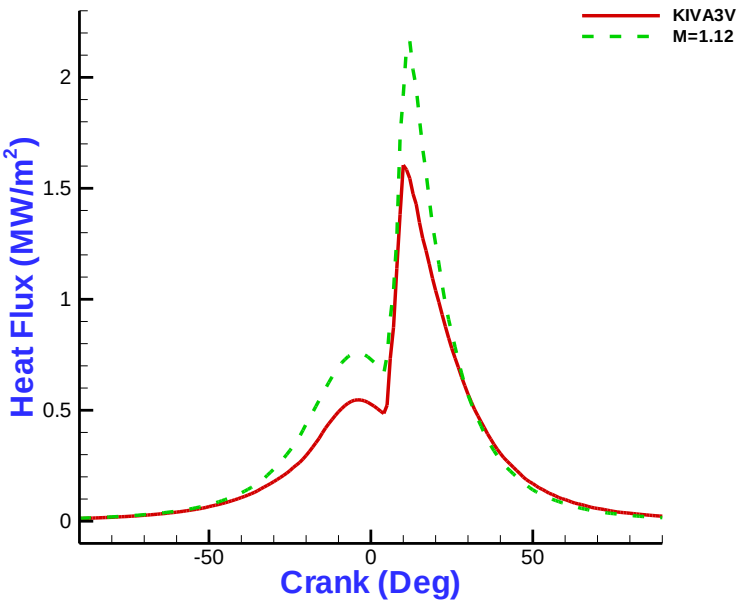

Figure 6. 28 Comparison of averaged heat flux of head surface for test case 1

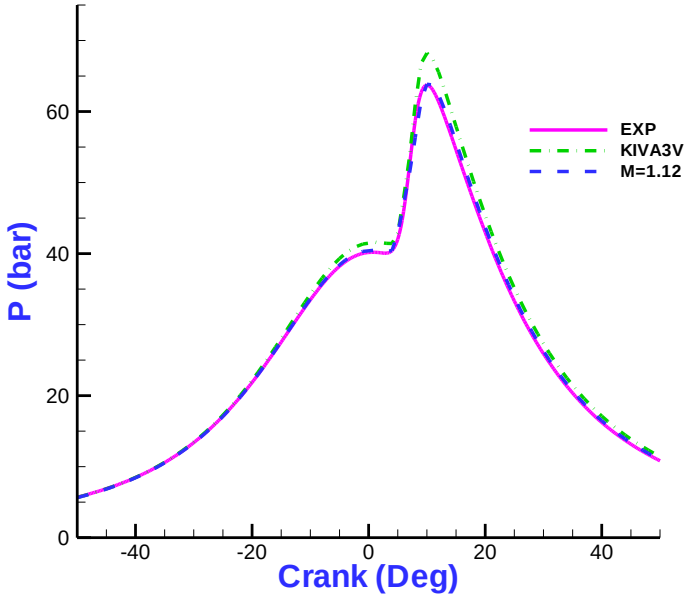

Figure 6. 29 Comparison of pressure trace for test case 2

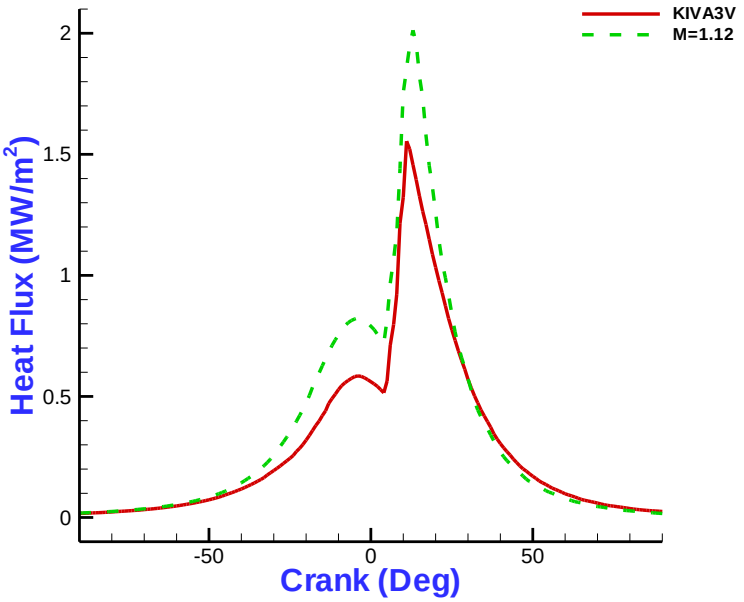

Figure 6. 30 Comparison of averaged heat flux of head surface for test case 2

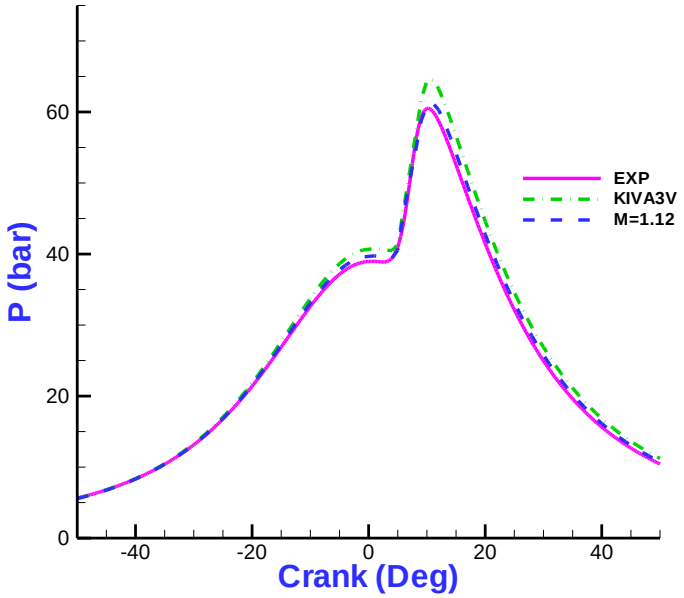

Figure 6. 31 Comparison of pressure trace for test case 3

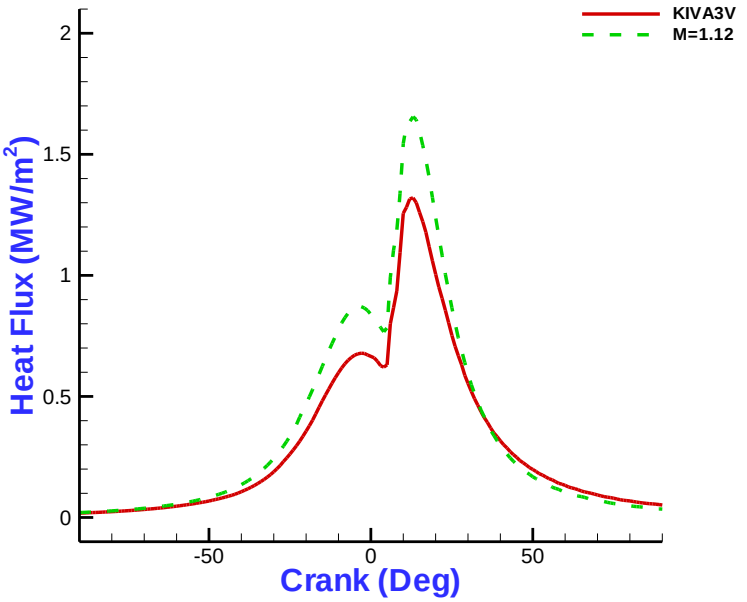

Figure 6. 32 Comparison of averaged heat flux of head surface for test case 3

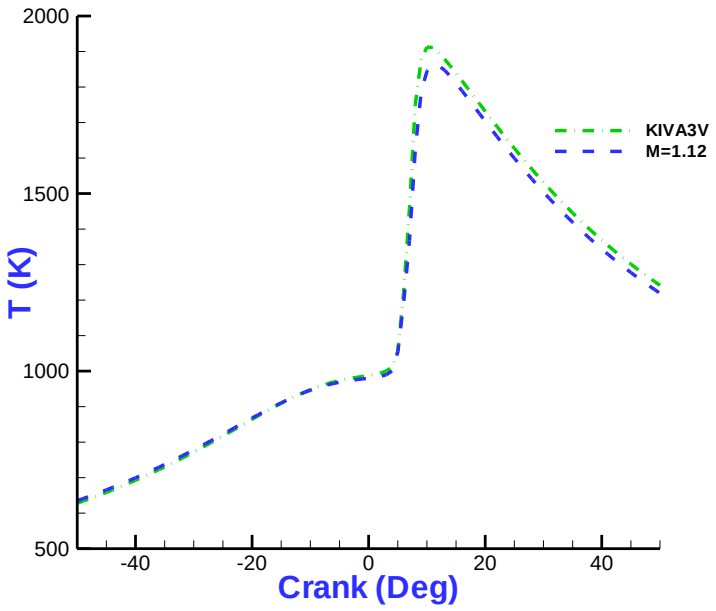

Figure 6. 33 Comparison of mean temperature for test case 1

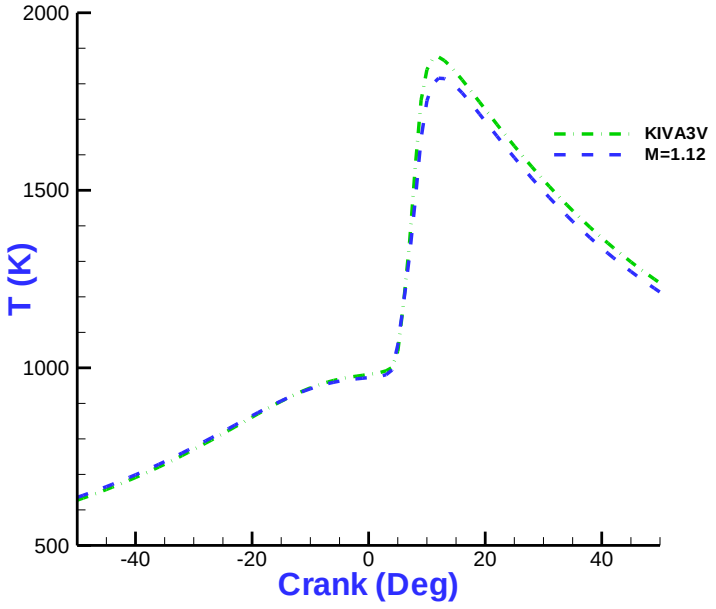

Figure 6. 34 Comparison of mean temperature for test case 2

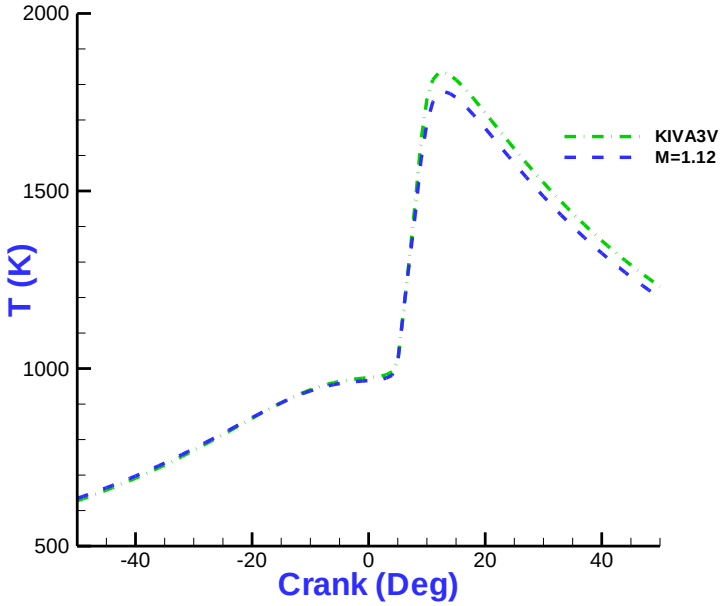

Figure 6. 35 Comparison of mean temperature for test case 3

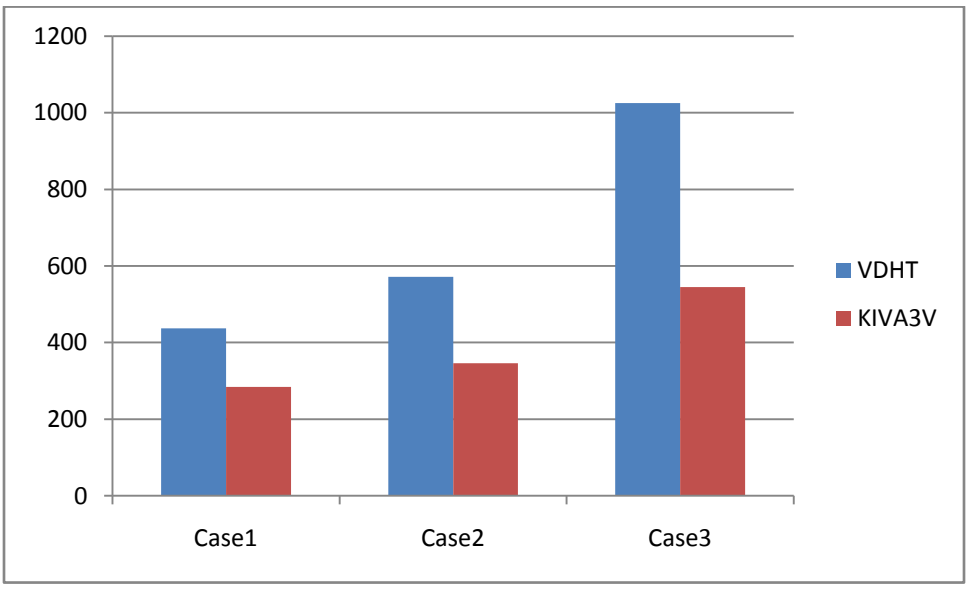

Figure 6. 36 Comparisons of CO emission predictions (PPM)

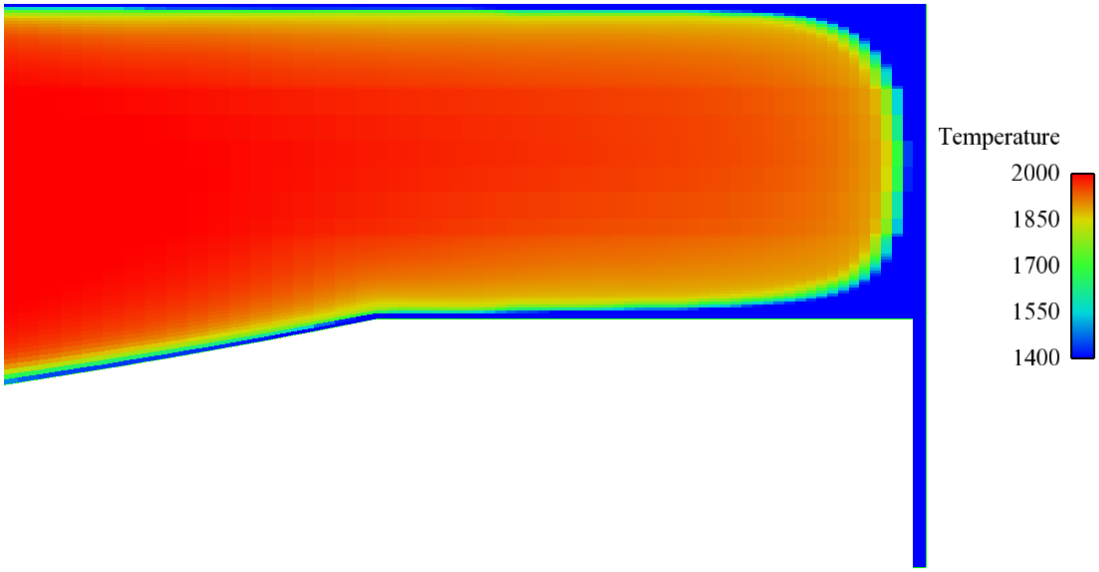

(a) VDHT

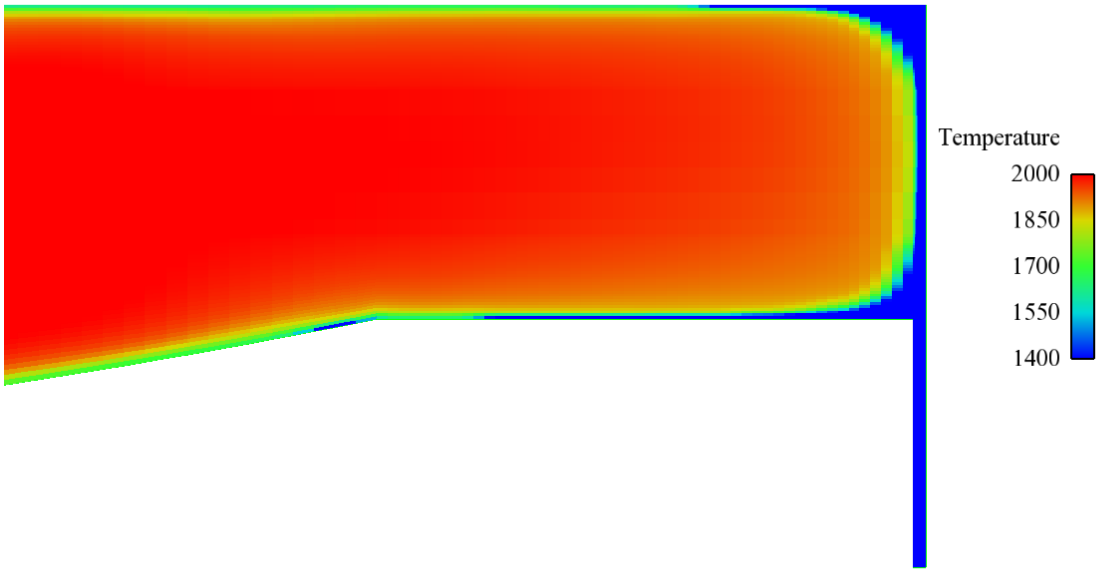

(b) KIVA3V

Figure 6. 37 Temperature distributions at 10 ATDC for case 1

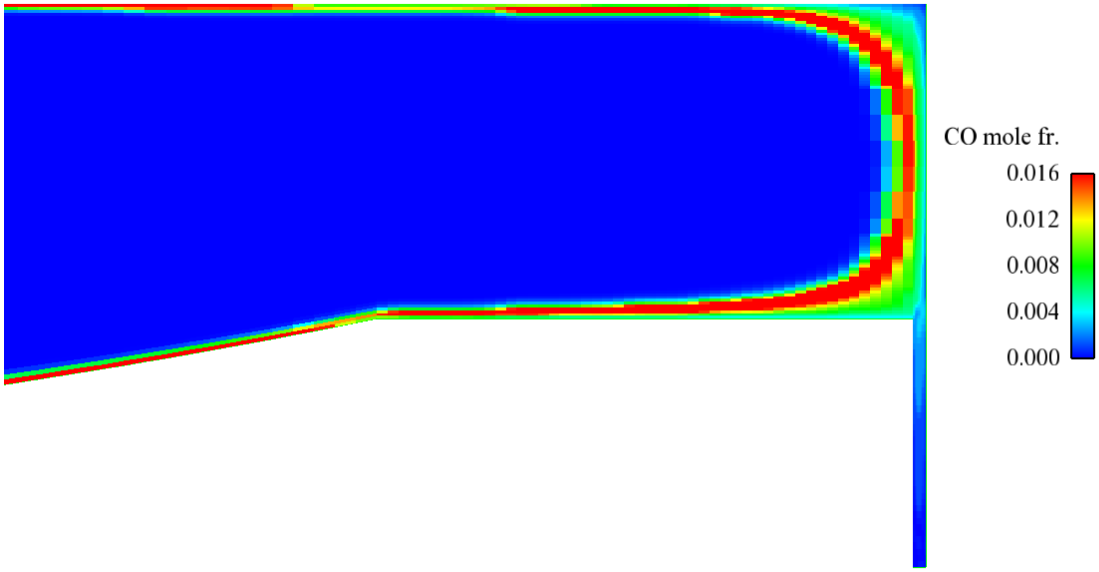

(a) VDHT

(b) KIVA3V

Figure 6. 38 CO distributions at 10 ATDC for case 1

BIBLIOGRAPHY

1. Myers, J. P., and Alkidas, A. C., “Effects of combustion chamber surface temperature on the exhaust emissions of a single-cylinder spark-ignition engine,” SAE paper 780642, 1978.

2. Willumeit, H. P., Steinberg, P., Otting, H., Scheibner, B., and Lee, W., "New Temperature Control Criteria for more Efficient Gasoline Engines," SAE Paper 841292, 1984.

3. Einaudi, G., and Mortara, W., "Engine Cooling Electronic Control System," SAE Paper 885085, 1988.

4. Couetouse, H., and Gentile, D., "Cooling System Control in Automotive Engines," SAE Paper 920788, 1992.

5. Guillemot, P., Gatellier, B., and Rouveirolles, B., “The influence of coolant temperature on unburned hydrocarbon emissions from spark ignition engine,” SAE paper 941692, 1994.

6. Russ, S., Kaiser, E. W., and Siegl, W. O., “Effect of cylinder head and engine block temperature on HC emissions from a single cylinder spark ignition engine,” SAE paper 952536, 1995.

7. Oude Nijeweme, D. J., Kok, J. B. W., Stone C. R., and Wyszynski, L., "Unsteady in-cylinder heat transfer in a spark ignition engine: experiments and modeling," *Proc Instn Mech Engrs*. Vol 215 Part D. 2001.

8. Stanglmaier, R. H., and Roberts, C. E., "Homogeneous Charge Compression Ignition (HCCI) : Benefits, Compromises, and Future Engine Applications," SAE Paper 1999-01-3682, 1999.

9. Sjoberg, M., Dec. J. E., Babajimopoulos, A., and Assanis, D. N., "Comparing Enhanced Natural Thermal Stratification against Retarded Combustion Phasing for Smoothing of HCCI Heat-release rate," SAE Paper 2004-01-2994, 2004.

10. Dec, J. E., Hwang, W., and Sjoberg, M., "An Investigation of Thermal Stratification in HCCI Engines Using Chemiluminescence Imaging," SAE 2006-01-1518, 2006.

11. Ock Taeck LIM, Hiroaki NAKANO, Norimasa IIDA, "The Research about the Effects of Thermal Stratification on n-Heptane/iso-Octane-Air mixture HCCI combustion using a Rapid Compression Machine," SAE Paper 2006-01-3319, 2006.

12. Dec. J. E., and Sjoberg, M., "A Parametric Study of HCCI Combustion – the Sources of Emissions at Low Loads and the Effects of GDI Fuel Injection," SAE 2003-01-0752, 2003.

13. Borman, G., Nishiwaki, K., "Internal-Combustion Engine Heat Transfer", *Prog Energy Combust Sci*, Vol. 13, 1987.

14. Woschni, G., "A Universally Applicable Equation for Instantaneous Heat Transfer Coefficient in the Internal Combustion Engine," SAE Paper 670931, 1967.

15. Annand, W. J. D., and Ma, T. H., "Instantaneous Heat transfer Rates to the Cylinder Head Surface of a Small Compression-Ignition Engine," *Proc Instn Mech Engrs*, Vol. 185, 1970-1971

16. Hohenberg, G. F., "Advanced Approaches for Heat Transfer Calculations," SAE Paper 790825, 1979.

17. Huber. K., Woschni, G., and Zeilinger, K., "Investigations on Heat Transfer in Internal Combustion Engines under Lowe Load and Motoring Conditions," SAE Paper 905018, 1990.

18. Han, S. B., Chung, Y. J., and Lee, S., "Empirical Formula for Instantaneous Heat Transfer Coefficient in spark-Ignition Engine," SAE Paper 972995, 1997.

19. Chen, K., and Karim, G. A., "Evaluation of the instantaneous unsteady heat transfer in a rapid compression – expansion machine," *Journal of Power and Energy* 212:5, 351-362, 1998.

20. Tsurushima, T., Kunishima, E., Asaumi, Y., Aoyagi, Y., and Enomoto, Y., "The Effect of Knock on Heat Loss in Homogeneous Charge Compression Ignition Engines," SAE Paper 2002-01-0108, 2002.

21. Chang, J., Guralp, O., Filipi, Z., Assanis, D. N., and Kuo, T. W., Najt, P., Rask, R., "New Heat Transfer Correlation for an HCCI Engine Derived from

Measurements of Instantaneous Surface Heat Flux," SAE Paper 2004-01-2996, 2004.

22. Krieger, R. B., and Borman, G. L., "The Computation of Apparent Heat Release for Internal Combustion Engines," ASME, Pap. 66-WA/DGP-4, 1966.

23. Poulos, S. G., and Heywood, J. B., "The effect of chamber geometry on spark-ignited engine combustion," SAE Paper 830334, 1983.

24. Morel, T., Fort, E., and Blumerg, P., "Effect of insulation strategy and design parameters on diesel heat rejection and performance," SAE Paper 850506, 1985.

25. Isshiki, N., and Nishiwaki, N., "Study on Laminar Heat Transfer of Inside Gas with Cyclic Pressure Change on an Inner Wall of a Cylinder Head," Proceedings of the 4th International Heat Transfer Conference, FC3.5, PP1-10, 1970.

26. Grief, R., Namba, T., and Nikanham, M., "Heat Transfer During Piston Compression Including Side Wall and Convection Effects," *Int. J. Heat and Mass Transfer*, Vol. 22, pp. 901-097, 1979.

27. James C. Keck., "THERMAL BOUNDARY LAYER IN A GAS SUBJECT TO A TIME Dependent Pressure," *Letters in Heat and Mass Transfer*, Vol. 8. pp 313-319, 1981.

28. Yang, J., and Martin, J. K., "Approximate Solution One-Dimensional Energy Equation for Transient, Compressible, Low Mach Number Turbulent Boundary Layer Flows," *Journal of Heat Transfer*, Vol. 111, pp 619-624, 1989.

29. Amsden, A. A., O'Rourke, P. J., and Butler, T. D., "KIVA-II: A Computer Program for Chemically reactive Flows with Sprays," Los Alamos National Laboratory, 1989.

30. Amsden, A. A., "KIVA-3V: A Block-Structure KIVA Program for Engines with Vertical or Canted Valves," Los Alamos National Laboratory, 1997.

31. Han, Z., and Reitz, R. D., "A temperature wall function formulation for variable-density turbulent flows with application to engine convective heat transfer modeling," *International journal of heat and mass transfer*, Vol. 40, No. 3, pp 613-625, 1997.

32. Fiveland, S. B., and Assanis, D. N., "Development of a Two-Zone HCCI Combustion Model Accounting for Boundary Layer Effects," SAE Paper 2001-01-1028, 2001.

33. Puzinauskas, P. and Borgnakke, C., "Evaluation and Improvement of an Unsteady Heat Transfer Model for Spark Ignition Engines," SAE Paper 910298, 1991.

34. Mark J. Jennings and T. Morel., "A Computational Study of Wall temperature Effects on Engine Heat Transfer," SAE Paper 910459, 1991.

35. K. Liu and R. H. Pletcher., "Compressibility and Variable Density Effects in Turbulent Boundary Layers," *Journal of Heat Transfer*, Vol, 129, pp 441-447, 2007.

36. White, F. M., and G. H. Christoph, "A Simple Theory for the Two-Dimensional Compressible Turbulent Boundary Layer," *Journal of basic Engrg*., Vol 7. pp. 465-470, 1972.

37. Park, Hee Jun, Assanis, Dennis. N., and Jung, Dohoy, "Development of an In-Cylinder Heat Transfer Model with Compressibility Effects on Turbulent Prandtl Number, Eddy Viscosity Ratio and Kinematic Viscosity Variation," SAE Paper 2009-01-0702, 2009.

38. Pope, S. B., "Turbulent Flows," Cambridge, 2001.

39. Reitz, R. D., "Assessment of Wall Heat Transfer Models for Premixed-Charge Engine Combustion Computations," SAE 910267, 1991.

40. Diana, S., Gigilo, V., Police, G., Bella, G., and Cordiner, S.,"Heat Transfer Evaluation in 3D Computations of Premixed SI Engines," SAE 972876, 1997.

41. Papageorgakis, G. C., "Turbulence Modeling of Gaseous Injection and Mixing in DI engines," Ph.D. Thesis, University of the Michigan, 1997.

42. Speziale, C. G., "On Non-linear k-l and k-ε models of turbulence," *J. Fluid Mech*. Vol. 179, pp. 459-475, 1987.

43. Germano, M., Piomeli, U., Moin, P., and Cabot, W. H., "A Dynamic Subgrid-Scale Eddy Viscosity Model," *Phys. Fluids* A, Vol. 3. Pp. 1760-1765, 1991.

44. Yakhot, V., and Orszag, S. A., "Renormalization group analysis of turbulence. I. Basic Theory," *J. Sci. Comput*. 1, 3, 1986.

45. Vanzieleghem, B. P., "Combustion Modeling For Gasoline Direct Injection Using KIVA-3V," Ph.D, Thesis, University of the Michigan, 2004.

46. Spalding, D. B., "Mixing and Chemical Reactions in Steady Confined Turbulent Flames," 13th Symposium (International) on Combustion, P. 649, The Combustion Institute, 1971.

47. Magnussen, B. F., and Hjertager, B. H., "On Mathematical Modeling of Turbulent Combustion with Special Emphasis on Soot Formation and Combustion," 16th Symposium on Combustion, P 719, The combustion Institute, 1976.

48. Cant, R. S., Pope, S. B., and Bray, K. N., "Modelling of flamelet surface to volume ratio in turbulent premixed combustion," 23nd Symposium on Combustion, P. 809-815, The Combustion Institute, 1990.

49. Boudier, P., Henriot, S., Poinsot, T., "A Model for Turbulent Flame Ignition and Propagation in Spark Ignition Engines," 24th Symposium on Combustion, P. 503-510, The Combustion Institute, 1992.

50. Meneveau, C., and Poinsot, T., "Stretching and Quenching of Flamelets in Premixed Turbulent Combustion," *Combustion and Flame* 86, 311-332, 1991.

51. Duclos, J. M., and Veynante, D., "A Comparison of Flamelet Models for Premixed Turbulent Combustion," *Combustion and Flame* 95, pp 101-117, 1993.

52. Poinsot, T., Veynante, and D., Candel, S., "Quenching processes and premixed turbulent combustion diagrams," *Journal of Fluid Mechanics*, 228, 561-606, 1991.

53. Abdel-Gayed R. G., Bradley, D., Hamid, M. N., and Lawes, M., "Lewis number effects on turbulent burning velocity," Twentieth Symposium (International) on Combustion, pp. 505-511, The Combustion Institute, Pittsburgh, 1984.

54. Metghalchi, M., and Keck, J. C., "Burning Velocities of Mixtures of Air with Methanol, Isooctane, and Indolene at High Pressure and Temperature," *Combustion and Flame* 48, pp 191-210, 1982.

55. Babajimopoulos, A., Assanis, D. N., Flowers, D. L., Aceves, S. M., and Hessel, R. P., "A fully coupled computational fluid dynamics and multi-zone model with detailed chemical kinetics for the simulation of premixed charge compression ignition engines," *International Journal of Engines Research*. Vol. 6, pp 497-512, 2005.

56. Onishi, S., Jo, S. H., Shoda, K., Jo, P. D., and Kato, S., "Active thermo-atmosphere combustion (ATAC) –a new combustion process for internal combustion engines," SAE paper 790501, 1979.

57. Noguchi, M., Tanaka, Y., Tanaka, T., and Takeuchi, Y., "A study on gasoline engine combustion by observation of intermediate reactive products during combustion," SAE paper 790840, 1979.

58. Iida, N., "Combustion analysis of methanol-fueled active thermo-atmosphere combustion (ATAC) engine using a spectroscopic observation," SAE paper 940864. 1994.

59. Hultqvist, A., Christenen, M., Johansson, B., Richeter, M., Nygren J., and Alden, M., "HCCI combustion process in a single cycle high-speed fuel tracer LIF and chemiliuminescence imaging," SAE paper 2002-01-0424, 2002.

60. Aceves, S. M., Flowers, D. L., Westbrook, C. K., Smith, J. R., Pitz, W., Dibble, R., Christensen, M., and Johansson, B., "A multi-zone model for prediction of HCCI combustion emission," SAE paper 2000-01-0327, 2000.

61. Aceves, S. M., Flowers, D. L., Martinez-Frias, J., Smith, J. R., Westbrook, C. K., Pitz, W. J., Dibble, R., Wright, R. F., Akinyemi, W. C., and Hessel, R. P., "A sequential fluid-mechanics chemical-kinetic model of propane HCCI combustion," SAE paper 2001-01-3612, 2002.

62. Aceves, S. M., Martinez-Frias, J., Flowers, D. L., Smith, J. R., Dibble, R., Wright, J. F., and Hessel, R. P., "A decoupled model of detailed fluid mechanics followed by detailed chemical kinetics for prediction of iso-octane HCCI combustion," SAE paper 2001-01-3612, 2001.

63. Flowers, D., Aceves, S., Martinez-Frias, J., Hessel, R., and Dibble, R., "Effects of mixing on hydrocarbon and carbon monoxide emissions prediction for isooctane HCCI engine combustion using a multi-zone detailed kinetics solver," SAE paper 2003-01-1821, 2003.

64. Reynolds, W. C., "Computation of Turbulent Flows," *A. Rev. Fluid Mech*. 8, 183, 1976.

65. Yakhot, V., and Orsazg, S. A., "Renormalization group analysis of turbulence, I, Basic Theory," *J. Sci. Comput*. 1, 1, 1996.

66. Kays, W. M., 'Turbulent Prandtl number-where are we?" ASME *J. Heat Transfer* 116, 284, 1994.

67. Alkidas, A. C., "Heat Transfer Characteristics of a Spark-Ignition Engine," *Journal of Heat Transfer* VOL 102, 189-193, 1980.

68. Alkidas, A. C., and Myers, J. P., "Transient Heat-Flux Measurements in the Combustion Chamber of a Spark-Ignition Engine," *Journal of Heat Transfer*, Vol 104, 62-67, 1982.

69. Abraham, J., Bracco, F. V., and Reitz, R. D., "Comparison of Computed and Measured Premixed Charge Engine Combustion," *Combustion and Flame* 60, pp 309-322, 1985.

70. Heywood, J. B., "Internal Combustion Engine Fundamentals," 1988.

71. Persson, H., Hildingsson, L., Hultqvist, A., Johansson, and B., Ruebel, J., "Investigation of Boundary Layer Behavior in HCCI Combustion using Chemiluminescence Imaging," SAE 2005-01-3729, 2005.

72. Paul. M. Najt and David E. Foster, "Compression-Ignited Homogeneous Charge Combustion," SAE Paper 830264, 1983.

73. Thring, R. H., "Homogeneous Charge Compression-Ignition (HCCI) Engines," SAE Paper 892068, 1989.

74. Taro Aoyama, Yoshiaki Hattori and Junichi Mizuta, “An Experimental Study on Premixed - Charge Compression Ignition Gasoline Engine,” SAE Paper 960081 1996.

75. Thomas III W. R., and Timothy, J. C., “Homogeneous Charge Compression Ignition of Diesel Fuel,” SAE Paper 961160, 1996.

76. Taro Aoyama, Yoshiaki Hattori and Junichi Mizuta, “An Experimental Study on Premixed- Charge Compression Ignition Gasoline Engine,” SAE Paper 960081 1996.

77. Magnus Christensen, Bengt Johanson, PerAmneus and Fabin Mauss, “Supercharged Homogeneous Charge Compression Ignition,” SAE Paper 980787, 1998.

78. Tetsuya Igarashi, Norimasa Iida, “Auto Ignition and Combustion of DME and n-Butane / Air Mixtures in Homogeneous Charge Compression Ignition Engine,” SAE Paper 2000-01-1832, 2000.

79. Sjöberg, M., and Dec, J. E., "An Investigation of the Relationship between Measured Intake Temperature, BDC Temperature, and Combustion Phasing for Premixed and DI HCCI Engines," SAE Paper 2004-01-1900, 2004.

80. Mack, H., Bogin, G., Chen, J. Y., and Dibble, R. W., “Multicylinder Engine Control Using Turbo / Supercharging: Modeling and Experiments,” LTC University Consortium Meeting, Sandia National Laboratory, 2007.

81. Chang, J., Filipi, Z., Assanis, D., Kuo, T. W., Najt, P., and Rask., R., "Characterizing the thermal sensitivity of a gasoline homogeneous charge compression ignition engine with measurements of instantaneous wall temperature and heat flux," International Journal of Engine Research, Vol 6. Pp 289-309, 2005.

82. Hessel, R. P., Foster, D. E., Aceves, S. M., Davisson, M. L. Espinosa-Loza, F., Flowers, D. L., Pitz, W. J., Dec, J. E., Sjoberg, M. and Babajimopoulos A., "Modeling Iso-octane HCCI Using CFD with Multi-Zone Detailed Chemistry; Comparison to Detailed Speciation Data Over a range of lean Equivalence Ratios," SAE Paper 2008-01-0047, 2008.

83. Aceves, S. M., Flowers, D. L., Espinosa-Loza, F., Martinez-Frias, J., Dibble, R. W., Christensen, M., Johansson, B., and Hessel, R. P., "Piston-Liner Crevice Geometry Effect on HCCI Combustion by Multi-Zone Analysis," SAE paper 2002-01-2869, 2002.